THERMAL MANAGEMENT OF SOLID OXIDE FUEL CELLS
BY FLOW ARRANGEMENT

A THESIS SUBMITTED TO
THE GRADUATE SCHOOL OF NATURAL AND APPLIED SCIENCES
OF
MIDDLE EAST TECHNICAL UNIVERSITY

BY

FIRAT ŞEN

IN PARTIAL FULFILLMENT OF THE REQUIREMENTS
FOR
THE DEGREE OF MASTER OF SCIENCE
IN
MECHANICAL ENGINEERING

JULY 2012

Approval of the thesis:

**THERMAL MANAGEMENT OF SOLID OXIDE FUEL CELLS
BY FLOW ARRANGEMENT**

Submitted by **FIRAT ŞEN** in partial fulfillment of the requirements for the degree of **Master of Science in Mechanical Engineering, Middle East Technical University** by;

Prof. Dr. Canan Özgen   _____
Dean, Graduate School of **Natural and Applied Sciences**

Prof. Dr. Süha Oral   _____
Head of Department, **Mechanical Engineering**

Assoc. Prof. Dr. İlker Tarı   _____
Supervisor, **Mechanical Engineering Dept, METU**

Examining Committee Members:

Assoc. Prof. Dr. Derek K. Baker   _____
Mechanical Engineering Dept., METU

Assoc. Prof. Dr. İlker Tarı   _____
Mechanical Engineering Dept., METU

Assist. Prof. Dr. Ahmet Yozgatlıgil   _____
Mechanical Engineering Dept., METU

Assist. Prof. Dr. Tuba Okutucu Özyurt   _____
Mechanical Engineering Dept., METU

Dr. Sadig Kuliyev   _____
Researcher, Vestel Defense Industries

Date: 24.07.2012

I hereby declare that all information in his document has been obtained and presented in accordance with academic rules and ethical conduct. I also declare that, as required by these rules and conduct, I have fully cited and referenced all material and results that are not original to this work.

Name, Last name : Fırat Şen

Signature   :

ABSTRACT

THERMAL MANAGEMENT OF SOLID OXIDE FUEL CELLS
BY FLOW ARRANGEMENT

Şen, Fırat

M.Sc., Department of Mechanical Engineering

Supervisor: Assoc. Prof. Dr. İlker Tarı

July 2012, 114 pages

Solid oxide fuel cell (SOFC) is a device that converts the chemical energy of the fuel into the electricity by the chemical reactions at high temperatures (600-1000°C). Heat is also produced besides the electricity as a result of the electrochemical reactions. Heat produced in the electrochemical reactions causes the thermal stresses, which is one of the most important problems of the SOFC systems. Another important problem of SOFCs is the low fuel utilization ratio. In this study, the effect of the flow arrangement on the temperature distribution, which causes the thermal stresses, and the method to increase the fuel utilization, is investigated.

An SOFC single cell experimental setup is developed for Cross-Flow arrangement design. This setup and experimental conditions are modeled with Fluent[®]. The experimental results are used in order to validate and verify the model. The model results are found to capture with the experimental results closely. The validated model is used as a reference to develop the models for different flow arrangements and to investigate the effect of the flow arrangement on the temperature distribution. A method to increase the SOFC

fuel utilization ratio is suggested. Models for different flow arrangements are developed and the simulation results are compared to determine the most advantageous arrangement.

ÖZ

KATI OKSİT YAKIT HÜCRELERİNİN AKIŞ AYARLAMASIYLA ISIL YÖNETİMİ

Şen, Fırat

Yüksek Lisans, Makina Mühendisliği Bölümü

Tez Yöneticisi: Doç. Dr. İlker Tarı

Temmuz 2012, 114 sayfa

Katı oksit yakıt pilleri (KOYP), yüksek sıcaklıklarda (600-1000°C) yakıtın kimyasal enerjisini elektrokimyasal reaksiyonlarla elektrik enerjisine çeviren sistemlerdir. Elektrokimyasal reaksiyonlar sonucu elektrik enerjisinin yanında ısı enerjisi de üretilmektedir. Bu sayede KOYP sistemlerinin verimi yüksek olmaktadır. Elektrokimyasal reaksiyon sonucu açığa çıkan ısı enerji verimini arttırmasının yanında KOYP sistemlerinin en büyük problemlerinden biri olan termal strese de neden olmaktadır. KOYP sistemlerinin diğer bir problemi ise düşük yakıt kullanım oranıdır. Bu çalışmada KOYP gaz akış kanal tasarımlarının termal stresi yaratan sıcaklık dağılımına olan etkisi incelenmiş ve yakıt kullanım oranını arttırmaya yönelik çalışmalar yapılmıştır.

Çapraz gaz akış kanalı tasarımı için KOYP tek hücre test düzeneği oluşturulmuştur. Deneyde kullanılan tasarım ve çalışma koşulları Fluent$^{®}$ ile modellenmiştir. Deney sonuçları ile model sonuçları karşılaştırılarak model doğrulanması yapılmıştır. Modelin deney sonuçları ile yakın değerler verdiği görülmüştür. Doğrulanan model referans alınarak farklı tasarımlar için modeller oluşturulmuş ve akış kanalı tasarımının sıcaklık dağılımına olan etkisi

incelenmiştir. KOYP yakıt kullanım oranını arttırmaya yönelik yakıt geri besleme yöntemi önerilmiştir. Farklı tasarımlar için yakıt geri besleme modelleri oluşturularak karşılaştırmalar yapılmıştır.

Anahtar Kelimeler: KOYP, Modelleme, CFD, Akış Düzenlemesi, Sıcaklık Dağılımı

To My Parents

ACKNOWLEDGEMENTS

TABLE OF CONTENTS

LIST OF TABLES

LIST OF FIGURES

FIGURES

LIST OF SYMBOLS

x, y, z	Cartesian coordinates
ΔG	Change in molar Gibbs free energy [J/kg]
ΔG^0	Change in molar Gibbs free energy at standard pressure
ΔH	Enthalpy change [J/kg]
ΔS	Entropy change [J/kg.K]
ΔV_{act}	Activation polarization [V]
ΔV_{con}	Concentrations polarization
ΔV_{ohm}	Ohmic polarization
c_i	Concentration of species [mole/m^3]
$D_{T,i}$	Thermal diffusion coefficient
$D_{i,j}$	Diffusion coefficient
$D_{i,j,eff}$	Effective binary diffusion coefficient [m^2/s]
F	Faraday constant [96500C/mole]
$\vec{F}$	External body force
h	Enthalpy
I	Current [A]
i	Current density [A/m^2]
i$_{exc}$	Exchange current density [A/m^2]
i_{exc}^a	Anode exchange current density
i_{exc}^c	Cathode exchange current density
i_{lim}^a	Anode limited current density
i_{lim}^c	Cathode limited current density
$i_{0,ref}$	Exchange current density at reference condition

J_i	Diffusion flux [mole/m^{2}s]
M_i	Molecular weight [kg/mole]
$\vec{n}$	Unit normal vector of the boundary walls
W_{elec}^{max}	Maximum electrical work [W]
P	Pressure [Pa]
Q	Heat generation
R	Universal gas constant [J/mole.K]
R_i	Rate of production [kg/m^{3}s]
S_m	Additional mass source
S_i	Additional species source
S_h	Volumetric source or sink of energy
T	Temperature [T]
t	Time
V	Potential difference [V]
V_{cell}	Actual cell voltage
$V_{theoretical}$	Theoretical voltage
$\vec{v}$	Velocity vector
Y_i	Mass fractions
α	Charge transfer coefficient
α_a	Anode charge transfer coefficient
α_c	Cathode charge transfer coefficient
σ	Electrical conductivity [1/ohm.m]
ε	Porosity
ς	Tortuosity
η_{act}	Activation loss
η_{ohmic}	Ohmic resistance
ϕ	Electrical potential [V]

ρ	Density [kg/m^3]
$\vec{\tau}$	Stress tensor
μ_{fuel}	Fuel utilization factor
χ_j	Mole fraction
γ_j	Concentration exponent for species j
$(N-1)$	Number of species

LIST OF ABBREVIATIONS

AFC   Alkaline Fuel Cell

APU   Auxiliary Power Unit

ASR   Area Specific Resistance

CFD   Computational Fluid Dynamics

CTE   Coefficient of Thermal Expansion

DMFC   Direct Methanol Fuel Cell

FDE   Finite Difference Equation

FEA   Finite Element Analysis

MCFC   Molten Carbonate Fuel Cell

MOLB   Mono-Block Layers Built

OCV   Open Circuit Voltage

PAFC   Phosphoric Acid Fuel Cell

PEMFC   Proton Exchange Membrane Fuel Cell

PEN   Positive Electrode-Electrolyte-Negative Electrode

PES   Porous Electrode Supported

PCFC   Protonic Ceramic Fuel Cell

SAFC   Sulfuric Acid Fuel Cell

SOFC   Solid Oxide Fuel Cell

TPB   Three Phase Boundary

TUI   Text User Interface

UDF   User Defined Function

UDS   User Defined Scalar

CHAPTER 1

INTRODUCTION

In recent years, energy has become the most important and challenging aspect of our existence due to its high usage in our daily lives and in an industry. To supply this high demand on energy, more interest and effort are put into developing improved energy generation methods because of fast depletion of natural resources and more importantly harmful effects of burning fuels on nature. These concerns over the consumption of fossil fuels make the research in using alternative fuels as an energy source inevitable.

At first sight, only clean and renewable energy sources such as solar and wind energy seems to solve above concerns in a long term but in the mean time, more efficient and less polluting energy conversion devices can be very helpful. For that purpose fuel cells are appealing.

As the energy usage and pollution increases, popularity of clean and renewable energy production methods increases. With high efficiency in energy conversion and ability to operate from mili-Watt to Mega-Watts, a Solid Oxide Fuel Cell (SOFC) receives much more attention. Beside this, it has ability to be used in stationary and mobile applications.

1.1   Type of Fuel Cells

A fuel cell is a device that converts the chemical energy from a fuel into the electricity through a chemical reaction with the oxygen or another oxidizing agent. Based on their working temperature and type of the fuel used as an energy source, there are mainly eight type of fuel cells, which are:

- Solid Oxide Fuel Cell (SOFC)

- Alkaline Fuel Cell (AFC)

- Direct Methanol Fuel Cell (DMFC)

- Phosphoric Acid Fuel Cell (PAFC)

- Molten Carbonate Fuel Cell (MCFC)

- Proton Exchange Membrane Fuel Cell (PEMFC)

- Protonic Ceramic Fuel Cell (PCFC)

- Sulfuric Acid Fuel Cell (SAFC)

The main characteristics of major fuel cells and comparisons between them are given in Table 1.1.

Table 1.1 Comparison of fuel cell technologies [1]

Types of Fuel Cell	Electrolyte	Operating Temperature	Fuel	Oxidant	Efficiency
Alkaline (AFC)	Potassium hydroxide (KOH)	50-200°C	Pure hydrogen or hydrazine	O_2/Air	50-55%
Direct methanol (DMFC)	polymer	60-200°C	liquid methanol	O_2/Air	40-55%
Phosphoric acid (PAFC)	Phosphoric acid	160-210°C	Hydrogen from hydrocarbons and alcohol	O_2/Air	40-50%
Sulfuric acid (SAFC)	Sulfuric acid	80-90°C	Alcohol or impure hydrogen	O_2/Air	40-50%
Proton-exchange membrane (PEM)	Polymer, proton-exchange membrane	50-80°C	Less pure hydrogen from hydrocarbons or methanol	O_2/Air	40-50%
Molten carbonate (MCFC)	Molten salt such as nitrate, sulphate, carbonates...	630-650°C	Hydrogen, carbon monoxide, natural gas, propane, marine diesel	CO_2/O_2/Air	50-60%
Solid oxide (SOFC)	Ceramic as stabilized zirconia and doped perovskite	600-1000°C	Natural gas or propane	O_2/Air	45-60%
Protonic ceramic (PCFC)	Thin membrane of barium cerium oxide	600-700°C	Hydrocarbons	O_2/Air	45-60%

Fuel cells are different from batteries in that, they require a constant source of fuel and oxygen to run, but they can produce the electricity continuously for as long as these inputs are supplied. Also, fuel cells are known as a direct energy conversion devices and are inherently more efficient because they directly convert the chemical energy in a fuel to the electrical energy by eliminating the intermediate stages of the thermal energy (heat from combustion) and the

mechanical energy (e.g. turbine run on hot gasses or steam) as in conventional electrical power plants [2].

Among the fuel cells, a PEMFC and an SOFC are the most popular ones for both the research and the market. Being suitable for cars and mass transportation, the PEMFC's are investigated more and well developed. On the other hand, the SOFC being an electricity generating device has become more important due to their fuel flexibility (carbon-based fuels e.g. natural gas), high efficiency and clean and quiet operation.

1.2   Solid Oxide Fuel Cell (SOFC)

Several devices are invented for conversion of a chemical fuels directly into an electrical power. The SOFCs are the most efficient ones with about 60% for combined cycles.

Osamu Yamamoto [4] says that "In 1839, Sir William Grove reported the principle of fuel cell operation firstly whereas using the ceramic started with Nernst at 1899 by discovering the solid oxide electrolyte. Nernst and his colleagues in Gottingen proposed the basic idea and materials at the end of the nineteenth century. Over 100 years later considerable advances in theory and experiment are made [3]. The first ceramic fuel cell study started with Baur at 1937, which works at $1000^{o}C$".

The SOFCs operate at high temperatures and employ the ceramics as the main functional elements of the cell. Each cell is composed of an anode and a cathode separated by a solid impermeable electrolyte. These three zones together are called the Positive Electrode-Electrolyte-Negative Electrode, the PEN. A schematic of the Solid Oxide Fuel Cell (SOFC) is shown in Figure 1.1
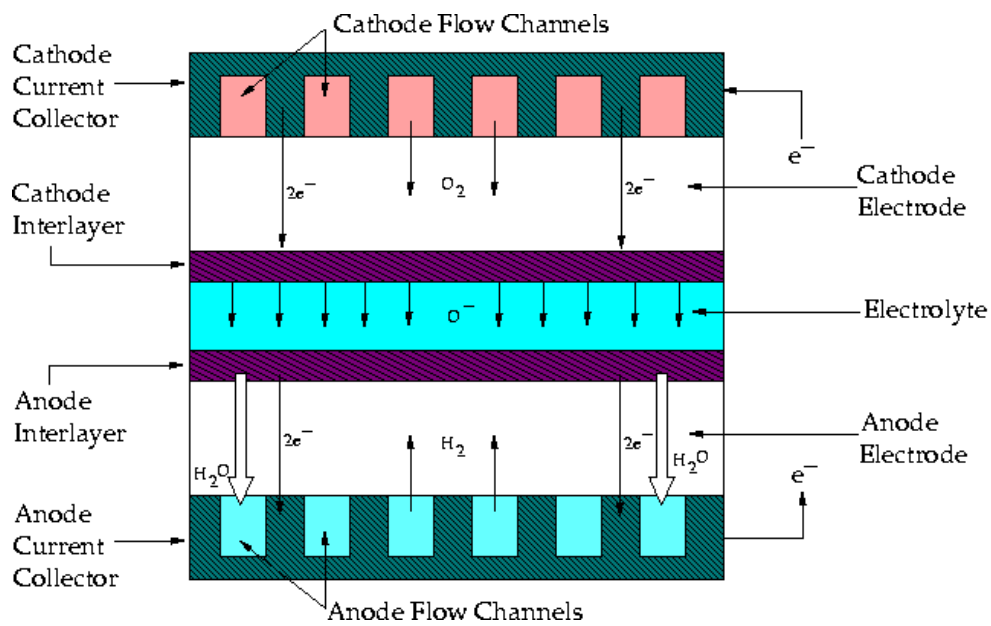
Figure 1.1 Schematic of a Solid Oxide Fuel Cell [5]

In an SOFC, a fuel (mainly pure hydrogen or syngas, which is a gas mixture rich in hydrogen) is supplied to the electrically conducting porous ceramic anode and an oxidant is supplied to the electrically conducting porous cathode. These electrically conducting porous anode and cathode are attached on each sides of an ionically conducting ceramic electrolyte. The electrochemical reactions occur at the catalyst layers, the anode/electrolyte and the cathode/electrolyte gas interfaces, which are also known as the Three Phase Boundaries (TPBs).

At the cathode/electrolyte gas interface, oxygen is reduced to the oxygen ions. The oxygen ions are conducted through the oxygen vacancies in the electrolyte to the anode side. At the anode/electrolyte gas interface, the oxygen ions react with the hydrogen to form the water. From this reaction, the electrons are released and the heat is produced. These electrons travel through an external circuit to a load and back to the cathode electrode to complete the circuit.

One of the biggest advantages of SOFCs is their high efficiency, which is not thermodynamically restricted by the Carnot efficiency [6-12]. As a result, most of the chemical energy of the fuel can be converted into the electricity and heat

in an SOFC operation. On the other hand, main disadvantage of SOFC is its low fuel utilization which decreases the efficiency SOFC system.

1.2.1 Design Configurations of SOFCs

In an SOFC, an interconnector also called as a bipolar plate, contains gas flow channels formed on its surface. The gas flow channels are used to distribute the gasses along the anode and the cathode electrodes. There exist three major design configurations of the SOFCs, which are:

- Monolithic,
- Tubular and
- Planar

The monolithic design configuration as shown in Figure 1.2, is difficult to manufacture, which is the main disadvantage of this design, so, it is not developed beyond the research.
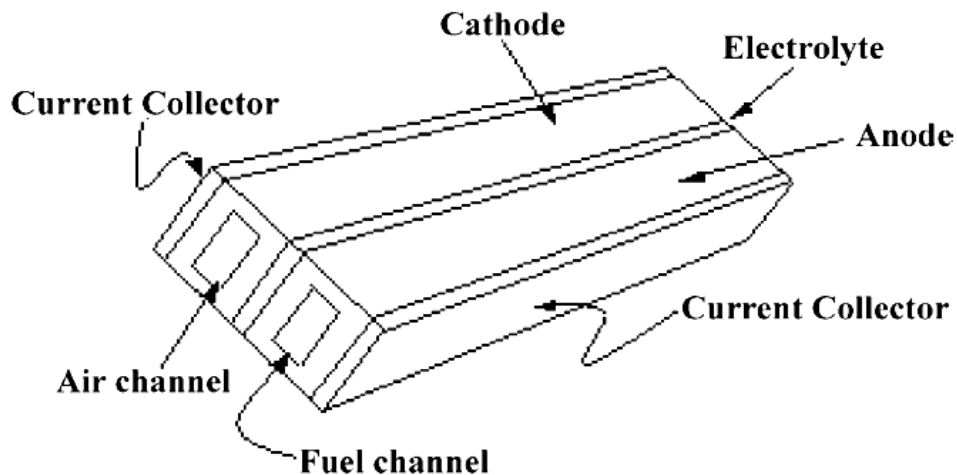
Figure 1.2 Monolithic SOFC design configuration [13]

The tubular design configuration shown in Figure 1.3, is the most popular. It is also difficult to manufacture and it has the lowest power density, when compared with the other design configurations. On the other hand, it is advantageous in the gas sealing during a stacking the cells.
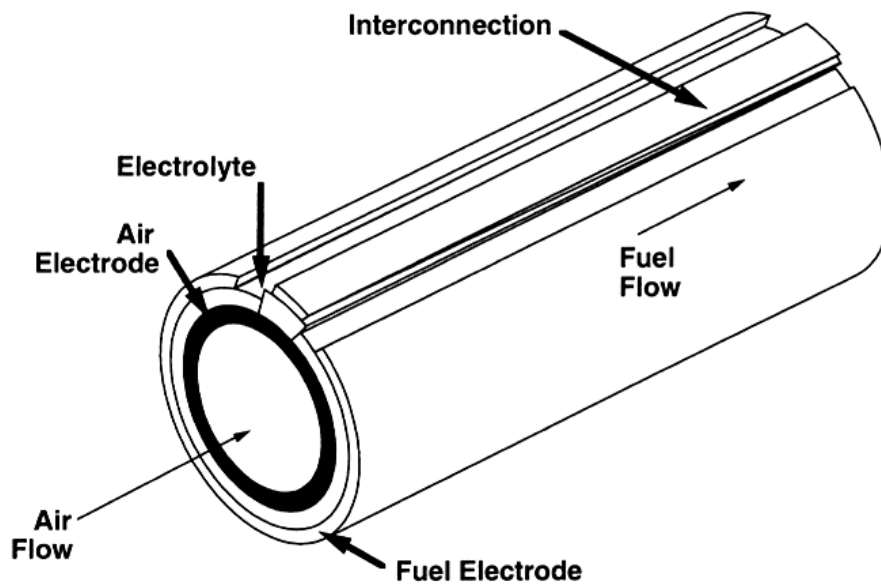
Figure 1.3 Tubular SOFC design configuration [14]

The planar SOFC design configuration gives the maximum power density, which cannot be reached with the other configurations. It is also easy to manufacture. When planar configuration is compared with the tubular design, although an interconnector fabrication cost is high, a system production cost is low because the planar design has higher service lifetime. Therefore, in recent years, the planar design configuration attracts research mostly in the two forms, which are the flat and the radial configurations and they are shown in Figure 1.4 and Figure 1.5 respectively.
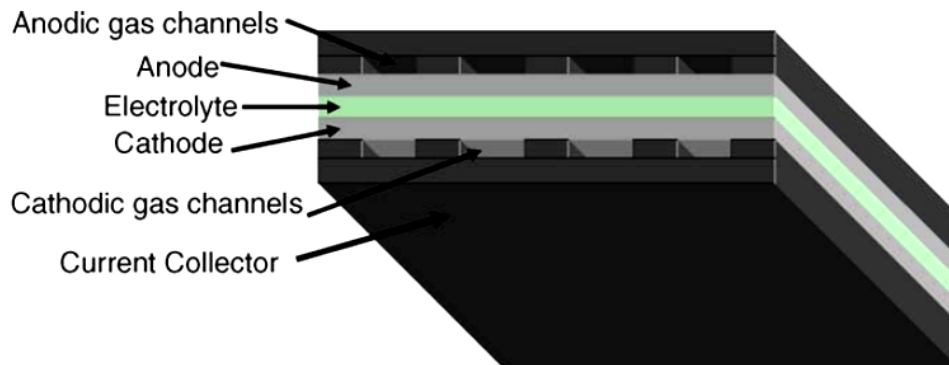
Figure 1.4 Flat planar SOFC design configuration [15]
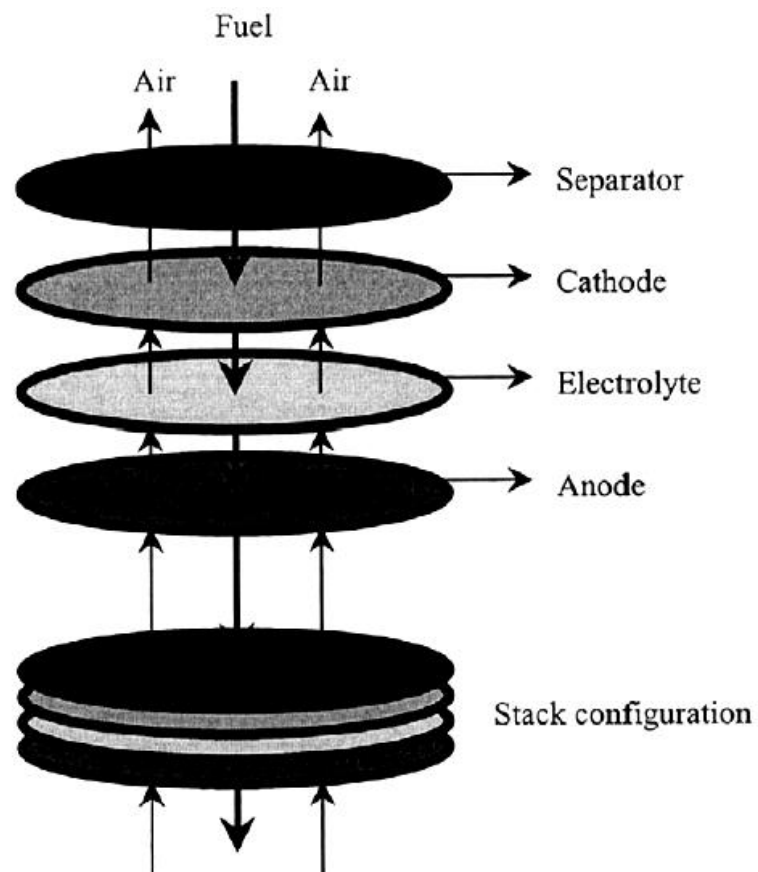
Figure 1.5 Radial planar SOFC design configuration [1]

Today, these two types of designs become more popular due to the main advantage of the planar type design in the gas sealing and the main advantage of flat the plate design in the ease of manufacturing.

8

1.2.2 PEN Configuration for Planar Design

The PEN is the electricity generating component of the SOFC and it works between 600-1000°C. For a planar SOFC design, the PEN can be produced either an electrode supported or an electrolyte supported. These possible configurations are shown in Figure 1.6. In view of SOFC mechanical stability, the electrolyte supported PEN's are less susceptible to mechanical failure than the electrode supported PEN's, which has higher weight related problems due to the thick electrodes.
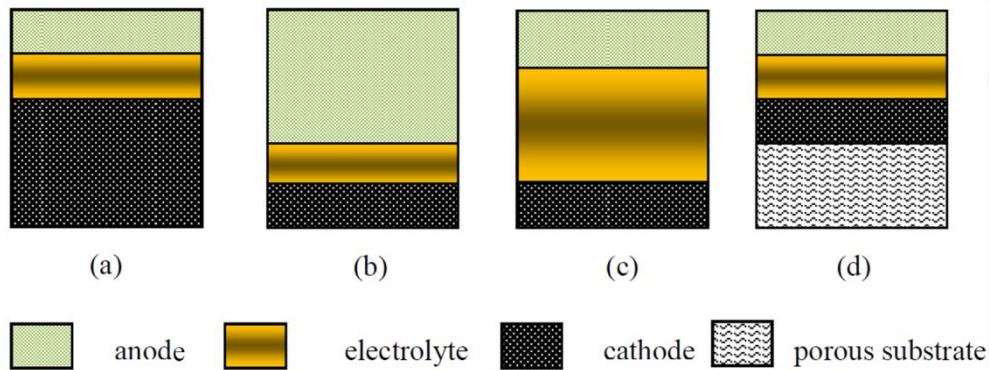
Figure 1.6 SOFC PEN structure configurations (a) cathode supported (b) anode supported (c) electrolyte supported (d) porous substrate supported [6]

To increase the mechanical stability of a PEN an idea of supporting the two electrodes with a new material is developed. But this increases the complexity in the porous substrate supported design, which is unacceptable.

1.2.3 SOFC Stacking

An SOFC gas flow channels distribute the fuel and the oxidant to the electrode surfaces. They are manufactured on the interconnector surfaces, which affect the durability and the performance of SOFCs. Mostly, three different flow arrangements for the flat-planar design are used in the SOFC stacks, which are Co-Flow, Cross-Flow and Counter-Flow arrangements, as shown in Figure 1.7.
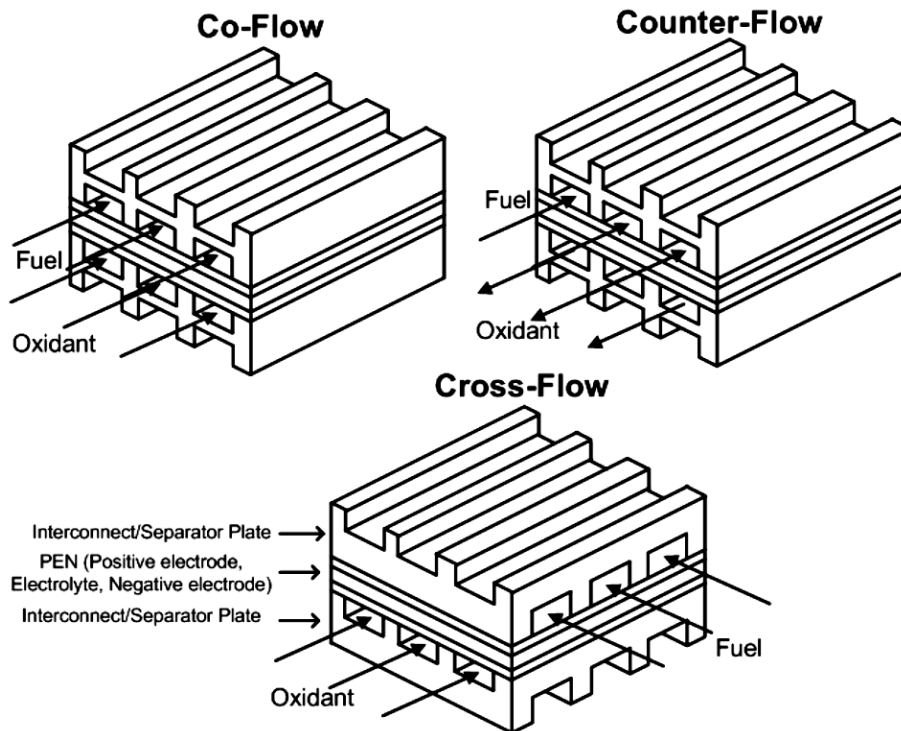
Figure 1.7 Different flow arrangements for flat-planar SOFC design [25]

When stacking the cells, the same interconnector plays a role in transferring the electrons from the anode side of a cell to the cathode side of another cell. At the two ends of the stack, the top or bottom interconnectors are the positive and the negative poles.

Usually a single cell of SOFC produces usable power at voltages between 0.5V-0.9V. Because of this fact, a large number of cells stacked upon each other in a serial manner, as shown in Figure 1.8. More power can be generated at a desired voltage with this arrangement.
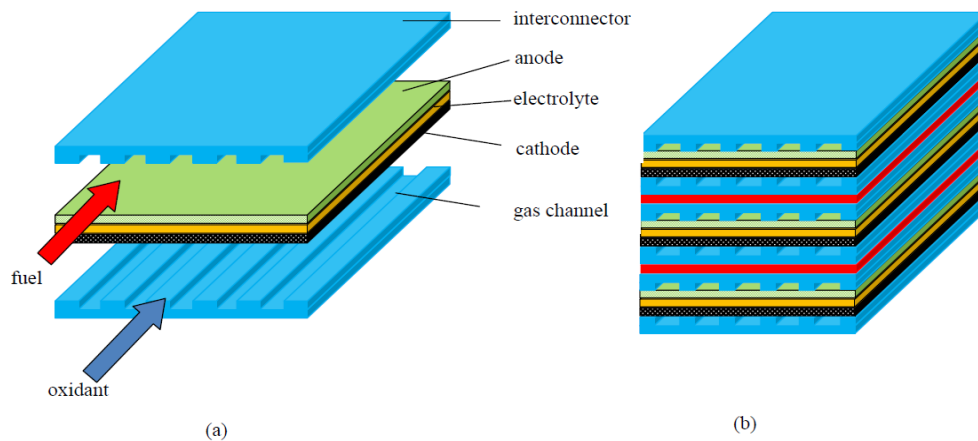
Figure 1.8 (a) SOFC single cell (b) SOFC stack with 3 cells [6]

1.3 Objectives

The main problem of an SOFC stack is its short life time, compared to the other conventional energy conversion methods. This makes the SOFC unfavorable. One of the main reasons of this problem is the thermal stresses due to the temperature gradients formed by heat generation in a steady state operation. These temperature gradients cause some SOFC components to fail which increases maintenance expenses in final products.

Although there are many experimental and theoretical studies for the high temperature SOFCs, there are few studies available regarding the problem mentioned above. Therefore, the objective of this study is:

1. To develop experimentally validated and verified a single cell SOFC mathematical model.
2. To use this model as a reference to develop the new and different gas flow channel designs for the interconnector and setup a mathematical models for a single cell.
3. To consider recycling the anode exhaust for the different gas flow channel designs.

1.4   Thesis Outline

In Chapter 2, literature survey is given. In Chapters 3 and 4, an SOFC working principle and the validating and verifying the SOFC model with an experiment are given. Then in Chapter 5, improvements in an SOFC stack are explained. Summary of the findings and recommendations for future works are explained in Chapter 6.

CHAPTER 2

LITERATURE SURVEY

Related to the SOFCs, because of their high working temperatures, temperature dependent properties and brittle structure of a PEN, there are crucial problems to be solved. One of the most important problems is the temperature gradient due to the heat generation from the electrochemical reactions.

During operation of SOFCs, temperature gradients appearing in the cell components will grow with temperature dependent parameters of a PEN. These temperature gradients cause cell components to be exposed to the thermal stresses which is mainly the result of the different Coefficient of Thermal Expansions, CTE, of components. Thermal stresses cause to cracks in a PEN structure, which will result in failure of the SOFC. Therefore, in literature, the main focus of an SOFC research is on the thermal management of an SOFC single cell or stacks as well as their performance.

As discussed earlier, the experimental setup for investigating an SOFC is difficult and expensive so many studies are based on modeling of an SOFC to investigate critical parameters. These modeling studies differ in the geometry, a PEN structure and size of an SOFC single cell or a stack to identify unresolved problems. So, literature survey can be categorized into two parts as cell and stack level modeling relevant to this thesis study.

2.1 Cell Level Modeling

In literature, cell level modeling studies are mainly focused on the effect of parameters (e.g. thickness and porosity of electrodes) of the PEN and the

design of the interconnectors on the performance of a cell under various operating conditions. These modeling studies include zero, one or multidimensional approaches depending on the type of problem investigated. Bovea et al. [26] studied the requirements of an SOFC mathematical model for a system simulation. They aimed in guiding future research for an SOFC improvements and optimizations by reviewing most significant SOFC models and the possibility of their use in a macro-model with different assumptions made when adapting micro-model equations to a macro-model. In micro scale, models behavior of individual SOFC components are focused, while in macro scale models, all operation behaviors of the SOFCs are investigated. They concluded with performing quantitative analysis for differences between different assumptions and estimated reliability of the model. On the other hand, in their second study Bovea et al. [27] say that zero dimensional approximations, in which gas composition variation is neglected, may lead to inaccurate results. So, they developed an analytical, one dimensional model by integrating the local equations defined in Part 1 of his study. In that model, changes in gas composition is assumed to be significant in outlet direction only,

There are 2-D studies based on the effects of an electrode and an electrolyte thickness and their porosity on the cell performance. Bariza et al. [28] studied effect of the electrode and electrolyte thickness on the temperature increment attributed to the chemical reactions and the irreversibilities. Junxiang et al. [29] in their study, investigated heterogeneous electrode properties, which includes various nonlinear distributions in a general sense according to the porous electrode features as well as linear functionally graded porosity distribution. They performed extensive numerical analysis to elucidate various heterogeneous porous electrode property effects on the cell performance. Results indicate that, the cell performance is strongly dependent on the porous microstructure distributions of the electrodes.

Besides the 1-D and 2-D simulations, the 3-D simulations are very important in predicting SOFC performance, optimizing the interconnector design, studying the effect of some parameters on the performance of an SOFC. Yakabe et al. [30] studied a different approach in which an electric current flow and a chemical and a thermo-fluid phenomena were carried out in a consecutive repetition and then the results of both calculations were correlated each other, which made it possible to simulate the diagonal electric current in the electrolyte. In addition, the effects of the geometry of the cell components on the cell performance were considered perfectly in the calculation. From this study, it can be concluded that the diagonal flow of the electric current appears in the electrolyte when there is a large distribution of the electromotive force. In this thesis study, the electrolyte is not fully defined that is, it is defined as a wall with a certain thickness, which is between the anode and the cathode electrodes. Because of this assumption, current path along the diagonal of the electrolyte should not be examined. Also, affect of the diagonal current path on the temperature distribution in the electrolyte thickness and diagonal direction due to an ohmic heating, should not be examined. Furthermore, the heat generated as a result of the electrochemical reaction is arbitrarily assumed to be distributed equally to the anode and the cathode electrodes. So, the affect of the heat transfer rate from the anode and the cathode electrodes due to the electrochemical reaction and comparison of the affect of this rate with an ohmic heating due to the diagonal current path on the temperature gradient, should not be completely distinguished. Actually, for a PEN, the most critical region in view of mechanical stability and electrochemical performance is the electrolyte.

As discussed earlier, the temperature gradient plays a very important role in both the performance and lifetime of an SOFC. So it is investigated in lots of studies. Yunzhen et al. [31] studied the temperature distributions, variations of reaction species and current densities of mono-block layers built (MOLB)-type SOFC under the different working conditions for Co-Flow and Counter-Flow

cell designs. The results show that, Co-Flow design has more uniform temperature and current density distribution. Also, an interesting result is that, the average temperatures of the PEN (positive/electrolyte/negative) and the current densities rise when the flow rate or the hydrogen mass fraction in the fuel is increased. However, the average temperatures of the PEN decrease with increasing the delivery rate of the air, from which it is observed that the design of the cathode side gas flow channels are important in the cell performance and the optimum flow rate of the air for the SOFC operation and an experimental setup should be used. The same result is also concluded by Zuopeng et al. [32] for the anode supported planar SOFC and the suggestions for improved cell designs are discussed. They also concluded with an interesting result that the most critical region in view of electrical performance in the interconnector is where the cathode is directly connected to the separator plate with no air channel in between. In such a region, the local current density and electrical potential are recorded, which results in a local minimum power production. In addition, highest temperature gradients are seen in this region. So, from this study, it can be regarded that, simplifications in the model geometry are very important depending on the expectations from the study and should be thought carefully.

Recknagle et al. [33] studied three dimensional model geometries to simulate the Cross-Flow, Co-Flow and Counter-Flow interconnector designs. When these three interconnector designs compared, the results show that, similar fuel utilizations are achieved for a given average cell temperature. However, the temperature distributions, which largely determine the thermal stresses during operation, are dependent on the interconnector design. Co-Flow design has the most uniform temperature distribution and the smallest temperature gradient thus offers a thermo-structural advantage over the other flow cases, as shown in Figure 2.1.

| (a) Cross-Flow | (b) Co-Flow | (c) Counterflow |
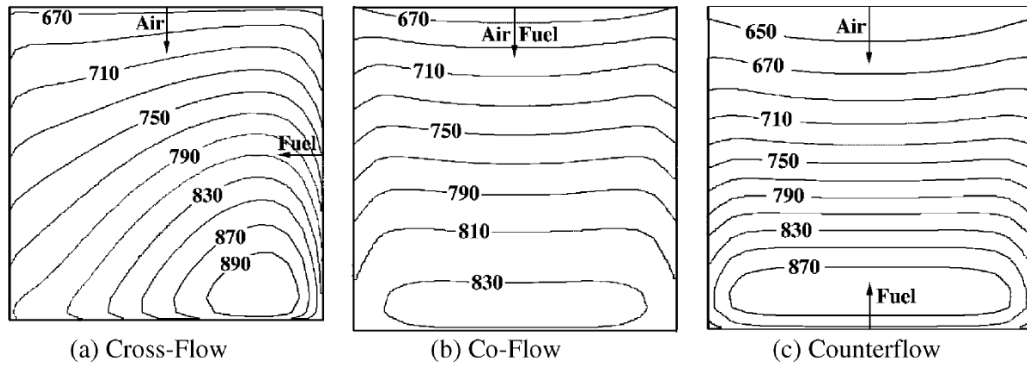
Figure 2.1 Temperature distributions on the cell active area for (a) Cross-Flow, (b) Co-Flow and (c) Counter-Flow arrangements [33]

The similar study with [33] is also investigated by Achenbach [34], Mitsunori Iwata et al. [35] and Christoph Stiller et al. [36]. Achenbach [34] investigated three flow arrangements and concluded with the same temperature profiles with [33], while Mitsunori Iwata et al. [35] studied only Cross-Flow arrangement and concluded with the same temperature profile with [33] and [34]. This profile is such that, the temperature is highest near the fuel inlet and the air outlet. For Cross-Flow arrangement, all the three studies [33-35], agree in the reason for the type of a temperature profile, which is, since the air flow rate is much larger than the fuel flow rate, larger convection heat of the air flow determines the temperature distribution. The similar results are also discussed in studies of MOLB-type SOFC [31] and the anode supported planar SOFC [32]. Although, the same result with above for Co-Flow and Counter-Flow arrangements can also be concluded from Christoph Stiller et al. [36], a slightly different temperature profile is obtained for the Cross-Flow arrangement, which is shown in Figure 2.2. It is observed that, the maximum temperature occurs at the air outlet and nearly midpoint of the fuel inlet and outlet. The different results, in studies through [33-36], can easily be attributed to the flow rate of the air and ratio of the air flow to the fuel, which is emphasized in these studies. Also, a valuable reason can be argued that the PEN electrochemical parameters, as well as mechanical properties, are very important in the SOFC modeling result.
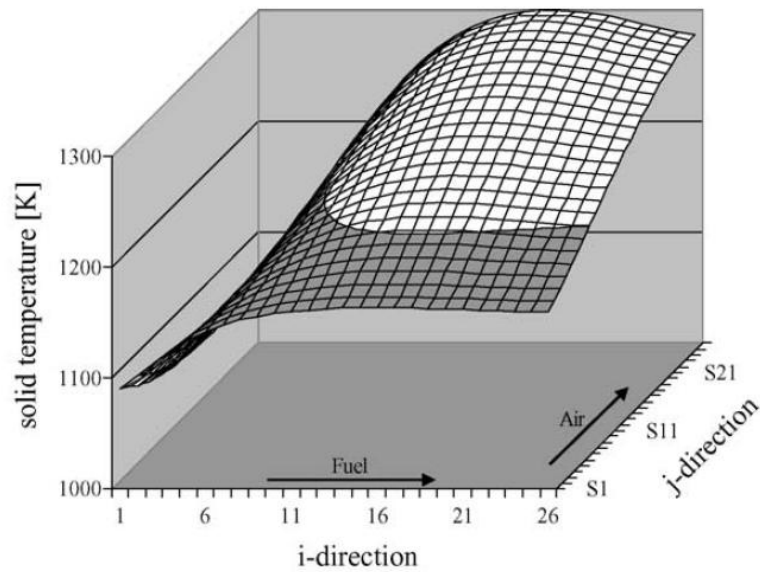
Figure 2.2 Temperature distributions on the cell active area for Cross-Flow arrangement [36]

In literature, there are also several studies for the different type of the PEN configuration. Yuzhang Wang et al. [37] studied simulating the steady state electrochemical characteristics and the multi-species/heat transport to simulate the variation of species concentrations, a temperature distribution, a potential and a current density for two types of a Porous-Electrode-Supported (PES) SOFC in Co-Flow pattern. These two type of cells use the same material and manufacturing process but they are differ in the gas flow channel design and electrolyte as shown in Figure 2.3. The results show that, type-II PES-SOFC has better performance than type-I. Also it is concluded that, the fuel and air are heated up continuously through the flow channel and the maximum temperature of these gases occur at the end of the anode near the electrolyte. This result, agrees with the results obtained by [31-36] and should be taken into account in studying the SOFC model results.
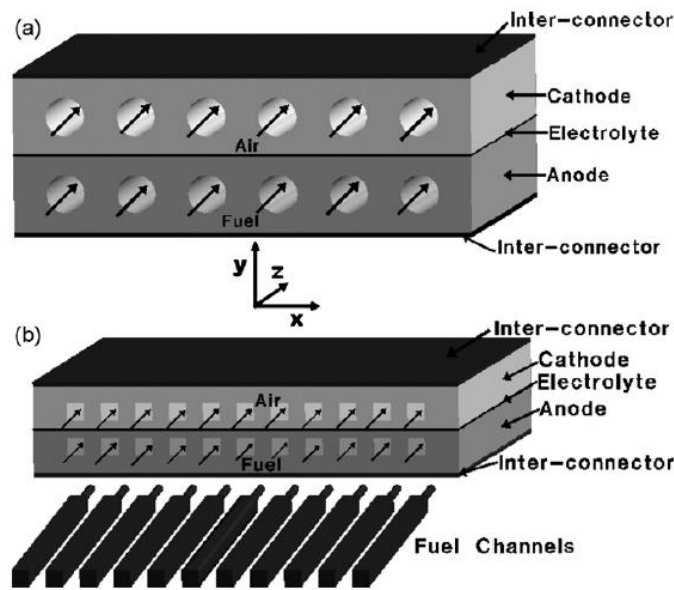
Figure 2.3 Schematic views of two types of planar PES-SOFC: (a) type-I (b) type-II [37]

As discussed above, in study of [32], simplifications done in the model geometries, to make the model easier and decrease the solution time, affects the model results. The main simplification done in model geometry is leaving out of count the SOFC components and some parts of these components. That is, only the gas flow channels are included in the solution domain, which assumes that the fuel and air coming from the feed headers/manifolds are equally distributed to the fuel and air corresponding gas flow channels in contact with the anode and cathode surface of the PEN respectively. So, this brings the necessity of developing and optimizing the feed headers. Related to this issue, Hong Liu et al. [38] proposed a novel designs for general applications in the fuel cells and the fuel processing reactors and studied them numerically using Fluent® and validated the model experimentally. Another important study in this issue is conducted by Huang et al. [39]. In this paper, the flow uniformity in various interconnectors and its influence to the cell performance of an SOFC is investigated both numerically and experimentally. Four different designs are developed and an experimental setup is developed as shown in Figure 2.4.
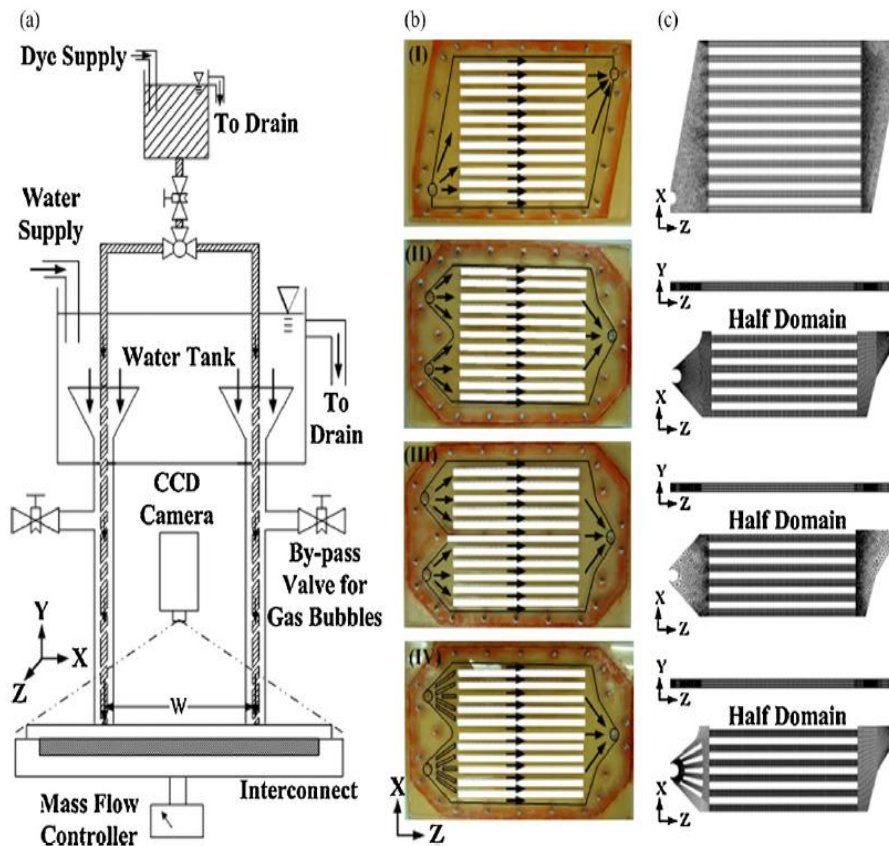
Figure 2.4 (a) Schematic of the hydraulic platform for flow visualizations and velocity measurements, (b) Four different designs, (c) Corresponding four numerical models [39]

The numerical results and the experimental setup for this study show that, improvement on the flow uniformity in the interconnectors can effectively remove the local hot spots on the PEN and increase the peak power density of the single-cell stack at least up to 11%. Also, suggestions for the fuel and air Reynolds Number, by considering the achievement of a reasonably good power density, while remaining an economic fuel utilization rate and having a smaller temperature gradient are discussed, importance of which is discussed above.

Another important parameter related with SOFC performance and the temperature homogeneity is the cathode/interconnect contact area and electrical collecting pins size, which is investigated by Grondin et al. [40]. The results show that, increasing the contact area decreases the power density of a cell and

20

also decreases the temperature gradient. Also, better homogeneity on the temperature and increase in the power density is achieved with a decreasing collecting pins size. Decrease in a collecting pin sizes will result in a decrease in a cross section of the air flow channels and increase in the velocity of the air besides the convective heat transfer coefficient at the cathode side, which is similar to conclusions obtained through [31-38].

2.2   Stack Level Modeling

The SOFC stack is composed of two or more cells arranged in a series manner in view of electrical connection. In literature, an SOFC stack is investigated for the temperature distribution, the gas flow uniformity for each cell, the thermal stresses as a result of temperature gradient. Lockett et al. [41] investigated 20-cell micro-tubular SOFC stack and a CFD model of this system using the commercial code Fluent® 6.0 to be compared with the experimental results in further studies to obtain a first approximation to the temperature and flow distributions.

In literature, there are also several important studies investigating the transient behavior of stack. He et al. [42] studied Molten Carbonate Fuel Cell (MCFC) stack in a 3D and presented the transient three dimensional model, which is capable of doing the transient calculations. With this model, it is possible to investigate the response of the stack to the sudden changes in the load, which gives a good idea about the time dependent response of the stack temperatures and the current distributions for Cross-Flow arrangement. Since most of studies investigated the steady state behaviors, with this study, the effect of this assumption can be analyzed.

In the cell level modeling section, importance of the model geometry simplifications generally on feed headers, are discussed. When modeling stacks, beside feed headers, simplifications of the gas manifolds are also done in the geometry to decrease the solver time. The results obtained with this assumption assumes that, all of the cells in the stack, gets the same amount of

the fuel and the air, which is different in a real situation as discussed in the study by Boersma et al. [43]. They suggested a useful tool for the flow distribution for the fuel cell stacks. Also, the results show that, at 38% height of the stack height receives a flow that is equal to the average flow, and about 25% of the cells receives less than the average flow, while the rest receives more are obtained. A similar study related to field, is done by Haruhiko et al. [44]. They investigated the relationships between the gas-flow uniformity in the planar direction, the gas-flow uniformity in the stacking direction, and the cell performance in Co-Flow type MCFC. A comparison is made for the effect of the uniformity of these two types of gas flows. Results show that, the gas-flow uniformity in the planar direction have 2 or 10 times more effect than the gas-flow uniformity in the stacking direction on the cell performance, which reveals the fact that, it is important to achieve the gas-flow uniformity in the stacking direction in order to attain the designed cell performance. By making into account this conclusion, Joonguen et al. [45] studied the characterization of an electrochemical reaction and a thermo-fluid flow in the metal-supported SOFC stacks with six cells with various manifold designs and concluded with the effect of the manifold designs on the current density and the temperature distribution. This phoneme was also studied by Bi et al. [46] and showed that, the ratio of the outlet manifold width to the inlet manifold width, which has a suitable value of larger than 1, is the key design parameter that affects the flow uniformity,. These results, which are obtained through [43-46], reveal the fact that, to obtain better and reliable stack model results, both the gas manifold and the feed headers must be included in the model geometry.

Several studies are available in literature concerned with the thermal issues of an SOFC in stack level beside the cell level. Koeppel et al. [47] studied the effect of various design changes on the temperature distribution and uniformity for a tall multi-cell stack and then several parametric studies were performed in 2-D. The multi-cell stack consists of ninety six cells stacked in series. They concluded with several important results, one of which is the increased

interconnector thickness results in a linear reduction of the peak temperature difference and also the increase in aspect ratio of a cell results in the decrease of temperature difference on a stack. Also Burt et al. [48] studied the numerical investigation for five cell stack considering the impact of a flow distribution and a heat transfer. Besides this, the influence of the radiative heat transfer, between the PEN and the neighboring separator plates, on the temperature distribution is also considered. They concluded with the result that, the variations in a cell temperature are attributed to the asymmetries in the stack geometry and the non-uniformity in the fuel and air flow rates, which results in the temperature non-uniformities. They recorded that, these temperature non-uniformity is large when only the convection and the conduction heat transfer considered so large variations in the cell performance is recorded. When the radiative heat transfer is included in the mathematical model, it is recorded that the uniformity in the mathematical model is improved thus leading to more uniform cell voltages. Also, the effect of the flow distribution is investigated and compared with the radiation effect. It was found to be, the radiation effect is lower than effect of the flow uniformity, which was also investigated through [43-46]. Effect of the radiation is also investigated by Tanaka et al. [49] and concluded with its effect on the stack cell performance, which agrees with the result obtained by [48].

Besides the theoretical investigations, concerning thermal and performance of stack issues, the experimental methods are also developed. Guan et al. [50] studied the experimental method to measure temperatures of the cells, inside three-cell SOFC stacks, by using K-type thermocouples and self-developed CAS-I sealing materials in which the thermocouple is inserted. The active area of an each cell is $10 \times 10 cm^2$ with the total area of $13 \times 13 cm^2$. The effect of the gas flow rates, the direct-current (DC) discharging and the discharging time on the temperatures of the cell surfaces are investigated. The results show that the discharging DC has more significant impact than the gas flow rate on the temperatures inside the SOFC stacks.

23

In view of life cycle of SOFC operation, the thermal stresses caused by the temperature gradients are almost determinist. Lin et al. [51] aimed in their study to characterize the thermal stress distribution in a planar SOFC stack during various stages in a multiple-cell stack by using a 3D Finite Element Analysis model. The model, in which the temperature profiles are integrated from the thermo-electrochemical model, includes complete components used in a practical SOFC stack. They concluded that, the CTE mismatch between the PEN and the connecting components generated a more significant effect on the thermal stress distribution than did the temperature gradients alone, but the effect of the temperature gradient is significant when CTE's effects are disregarded, that is CTE's of stack components are close to each other.

To conclude literature survey, several brief guidelines can be argued from those studies as summarized in Table 2.1.

Table 2.1 Summary of literature results for cell and stack levels modeling

Conclusions	References
Electrode and electrolyte thicknesses and heterogeneous electrode properties are important on cell performance	[27-29]
Diagonal flow of the electric current is due to the electromotive force	[30]
Air side has higher heat transfer rate	[31-37], [40]
Co-flow has better temperature profile	[33-38]
Geometric simplifications effect the SOFC model results	[38],[39],[48], [43-46]
Increase in contact area decreases the power density and temperature gradient	[40]
Interconnector thickness and aspect ratio of channels effect the temperature gradients in a stack	[47]
Thermal boundary conditions effects SOFC characteristics	[48], [49]
Flow uniformity per cell in a stack effects the performance of SOFC	[43-46]
Discharging DC has more significant effect on the temperatures inside SOFC stacks than the gas flow rate	[50]
CTE mismatch between the PEN and other components has a more significant effect on the thermal stress distribution than did the temperature gradients alone	[51]
Effect of temperature gradient is significant when CTE's of stack components are close to each other.	[51]

CHAPTER 3

SOFC OPERATING PRINCIPLE AND MODELLING

3.1   Operation Principle of SOFC

The SOFC is an electrochemical device for the conversion of a chemical energy of a fuel into the electricity and heat. The following equations are taken from [52]. When hydrogen is used as a fuel, reactions occurring at an SOFC are:

$$\begin{aligned}
&Anode: H_2 + O^{2-} \rightarrow H_2O + 2e^- \\
&Cathode: \tfrac{1}{2}O_2 + 2e^- \rightarrow O^{2-} \\
&Overall: H_2 + \tfrac{1}{2}O_2 \rightarrow H_2O
\end{aligned} \tag{3.1}$$

The oxygen ions produced at the cathode, pass through the electrically insulated electrolyte to the anode side. At the anode, the oxygen ions react with the hydrogen ions to form the water and 2 moles of electrons are released for a 1 mole of the hydrogen. These steps are shown in Figure 3.1.
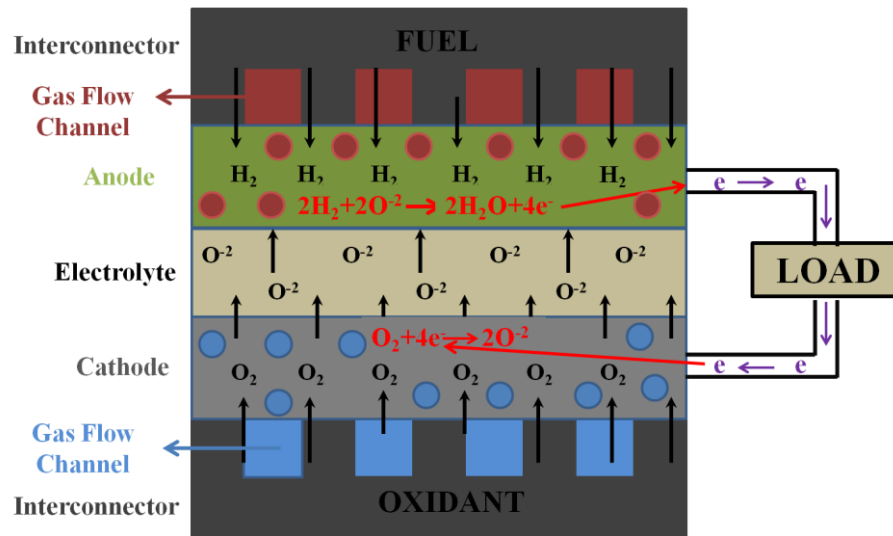
Figure 3.1 SOFC working principle

These electrons are conducted to the cathode through the external circuit with the help of the electrically conducting interconnector material. If these electrons were conducted through the electrolyte, the same overall reaction would occur, but at this time, the power could not be obtained. Therefore, the electrolyte must be electrically insulated otherwise, all would be lost.

3.1.1   Open Circuit Potential

In SOFC, the maximum electrical power obtained is equal to the maximum theoretical work that can be obtained from the overall electrochemical reaction. This maximum theoretical work is equal to the change in the molar Gibbs free energy of equation (3.1):

$$\Delta G = \Delta H - T \times \Delta S \tag{3.2}$$

where ΔH is the enthalpy change or the total energy that can be obtained theoretically, ΔS is the entropy change by the reaction and T is the temperature in Kelvin. Since this change in molar Gibbs free energy is equal to the maximum electrical work, we have:

$$W_{elec}^{max} = \Delta G = V \times I \tag{3.3}$$

26

where V is the potential difference across the cell and I is the current passing through the external circuit.

When equation (3.1) is considered, it is obvious that, for 1 mole of hydrogen 2 moles of electron is released. If the charge obtained by one electron is $-e$, current, I, can be calculated as:

$$I = 2 \times N \times (-e) = -2Ne = -2F \tag{3.4}$$

where N is the Avogadro number and F is the Faraday constant meaning the charge on one mole of an electron.

For equation (3.1), change in molar Gibbs free energy, ΔG, can also be calculated as:

$$\Delta G = \Delta G^0 - R \times T \times \ln\left(\frac{P_{H_2} \times \left(P_{O_2}\right)^{1/2}}{P_{H_2O}}\right) \tag{3.5}$$

where ΔG^0 is the molar Gibbs free energy at the standard pressure and R is the universal gas constant. By substituting the equation (3.4) and (3.5) into the equation (3.3) we obtain:

$$\Delta G = V \times I$$

$$\Delta G^0 - R \times T \times \ln\left(\frac{P_{H_2} \times \left(P_{O_2}\right)^{1/2}}{P_{H_2O}}\right) = V \times (-2F) \tag{3.6}$$

$$V = -\frac{\Delta G^0}{2F} + \frac{R \times T}{2F} \ln\left(\frac{P_{H_2} \times \left(P_{O_2}\right)^{1/2}}{P_{H_2O}}\right)$$

The whole equation (3.6) is called Nernst equation giving the Nernst voltage V and the first term on the right hand side is V^0, known as the electromotive force or the reversible/no loss open circuit voltage (OCV). That is, it is the maximum voltage that can be reached.

3.1.2 Polarization

Due to irreversibilities, fuel cell operates at voltages below that of Nernst potential. These irreversibilities are commonly called the polarizations and are the function of the current density. There exist mainly three dominant polarizations as shown in Figure 3.2, which are the ohmic, activation and concentration/ mass transport polarizations.
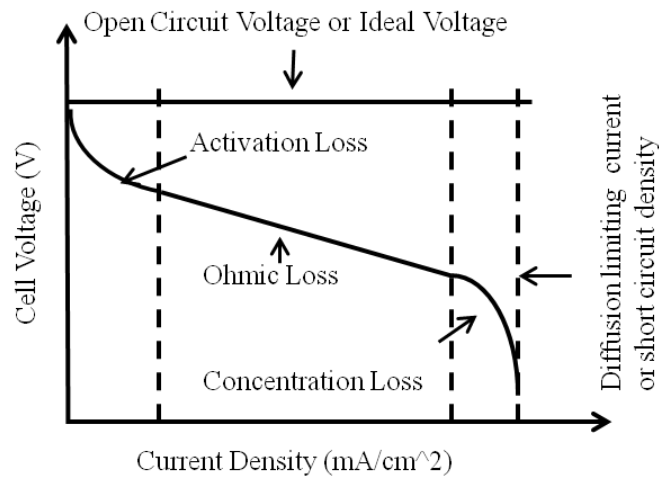
Figure 3.2 Polarization types

3.1.2.1 Ohmic Polarization

The ohmic polarizations/losses occur due to the electronic conduction of the current through the interconnectors and electrodes and the ionic conduction of the oxygen ions through the solid electrolyte. So, the conductivity of materials plays a very important role for the ohmic polarization. The voltage drop, due to the ohmic polarization, can easily be calculated as:

$$\Delta V_{ohm} = I \times R \tag{3.7}$$

where "I" is the current density and "R" is the area specific resistance (ASR) corresponding to 1cm^2 of a cell.

3.1.2.2 Activation Polarization

The activation polarization is the energy lost due to the slowness of the electrochemical reactions at the anode and the cathode electrodes actually at the TPBs. It can also be regarded as an extra energy necessary to overcome the energy barrier created by slowness of the electrochemical reaction. The activation polarization can be calculated as:

$$\Delta V_{act} = \frac{R \times T}{n \times \alpha \times F} \ln\left(\frac{i}{i_{exc}}\right) \tag{3.8}$$

where "i" is the current density, "i_{exc}" is the exchange current density, "α" is the charge/electrochemical transfer coefficient and "n" is the number of electrons transferred, which is equal to 2 for the hydrogen fueled SOFC. The equation (3.8) is the same for the anode and cathode polarizations. Thus we have:

$$\Delta V_{act} = \frac{R \times T}{2 \times \alpha_a \times F} \ln\left(\frac{i}{i_{exc}^{a}}\right) + \frac{R \times T}{2 \times \alpha_c \times F} \ln\left(\frac{i}{i_{exc}^{c}}\right) \tag{3.9}$$

giving the total activation polarization where i_{exc}^{a} and i_{exc}^{c} are the exchange current densities for the anode and cathode respectively and α_a and α_c are the charge transfer coefficients for the anode and the cathode respectively. Both of these parameters are dependent on the materials and electrochemical reactions involved. For the hydrogen fueled fuel cells like SOFC, the anode activation polarization is negligible compared to that of the cathode. Moreover, it becomes less important at high temperatures due to the increase in the electrochemical reaction kinetics.

3.1.2.3 Concentration/Mass Transport Polarization

The concentration polarization is called the reduction in the cell voltage due to the decrease in the partial pressure of the hydrogen and the oxygen. This decrease in the partial pressures is resulted from the consumption of the

hydrogen and oxygen in the direction of the gas flow channels. The total potential loss due to the concentrations polarizations can be written as:

$$\Delta V_{con} = -\frac{R \times T}{n \times F} \left[\frac{1}{2} \ln\left(1 - \frac{i}{i_{\lim}^c}\right) + \ln\left(1 - \frac{i}{i_{\lim}^a}\right) - \ln\left(1 + \frac{P_{H_2} \times i}{P_{H_2O} \times i_{\lim}^a}\right) \right] \tag{3.10}$$

where $i_{\lim}^a$ and $i_{\lim}^c$ are the limited current densities for the anode and the cathode respectively. The anode limited current density is the current density, at which the hydrogen is assumed to be fully consumed and the partial pressure of hydrogen is nearly zero at the anode/electrolyte interface. Similarly, the cathode limited current density is the current density, at which the oxygen is assumed to be fully consumed and the partial pressure of the oxygen is nearly zero at the cathode/electrolyte interface. Both of these parameters are dependent on the electrode microstructures such as the porosity.

3.1.3   Actual Cell Voltage

The actual cell voltage can be found by adding three polarizations and then subtracting this total polarization from the Nernst voltage. That is the actual cell voltage is equal to:

$$V_{cell} = V - \Delta V_{ohm} - \Delta V_{act} - \Delta V_{conc} \tag{3.11}$$

where all the unknowns are explained above.

3.1.4   Cell Efficiency

For SOFC, the maximum energy that can be converted into the electricity is the enthalpy change ΔH, as denoted in equation (3.2). If this was the change, then the theoretical voltage should be:

$$V_{theoretical} = \frac{\Delta G}{2F} \tag{3.12}$$

So the cell efficiency can be written as:

$$\eta_{cell} = \frac{V_{cell}}{V_{theo}} \qquad\qquad (3.13)$$

where V_{cell} is the actual cell voltage. But, when the SOFC is running, all the fuel supplied is not consumed, that is some fuel is unused. So, the fuel utilization factor μ_{fuel}, can be defined as (fuel consumed in a fuel cell)/ (fuel supplied to a fuel cell). Then the SOFC efficiency can be written in terms of μ_{fuel} as:

$$\eta_{cell} = \mu_{fuel} \frac{V_{cell}}{V_{theo}} \qquad\qquad (3.14)$$

3.2   SOFC Modeling

Numerical modeling is formulating the relationships between the process variables and then solving them to predict the behavior of the process for the different sets of input conditions. The main advantages of the numerical modeling are the relatively low cost and high speed. However, experiments are still needed to validate the numerical models. In some cases, it is difficult and expensive to setup an experiment. Therefore, an optimum balance should be maintained between the modeling and experiment.

In a fuel cell, sometimes the experimental setup is difficult and expensive. Also due to the its high working temperatures, it is not possible to obtain some parameters and dispersion of properties at a specified surfaces, so, commercial Computational Fluid Dynamics (CFD) software packages now become an important tool in investigating the fuel cell behavior under the various operating conditions, the effects of various parameters and the performance of a particular design.

3.3   SOFC Mathematical Model

The considered model of an SOFC is shown in Figure 3.3 schematically. The system consist of an SOFC ceramic PEN, a crofer mesh and a nickel porous on

the cathode and the anode sides of the PEN respectively and the current collectors, on which there are the gas flow channels also. The crofer mesh and nickel porous are used as a current collector to improve the capability of collecting the current produced in an SOFC cell.
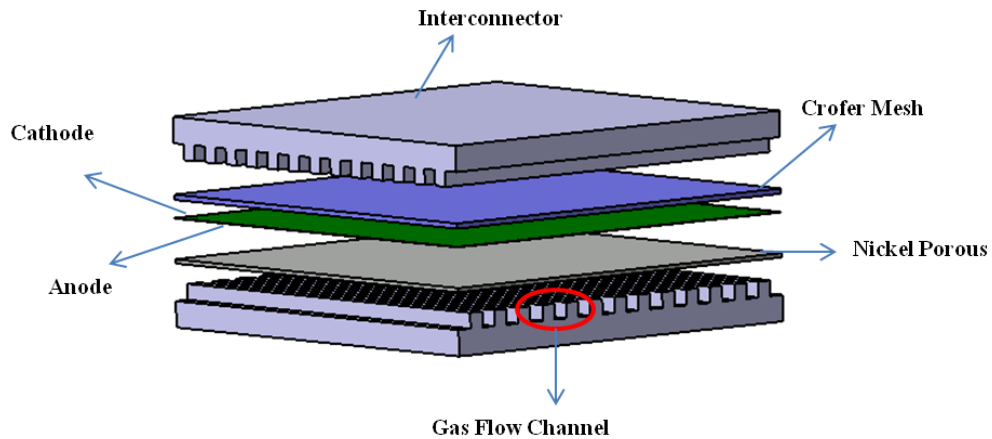

Figure 3.3 Schematic of SOFC

In this study, a commercial product Fluent$^{®}$ with SOFC With Unresolved Electrolyte Model add-on module is used to model the SOFC single cell. In SOFC With Unresolved Electrolyte Model add-on module, the anode and the cathode interlayer and the electrolyte are not actually included in the computational domain. That is, the species and energy sources and sinks due to the electrochemical reactions are added to the adjacent computational cells. More specifically, with this add-on module, the followings are done:

- The fluid flow, the heat transfer and the mass transfer in the flow channels and the porous anode and cathode electrodes are captured,
- The transport of the current and the potential field in the porous electrodes and in the solid conducting regions are modeled,
- The electrochemical reactions that take place at the electrolyte/-electrode-gaseous species interface are modeled.

In Fluent® SOFC With Unresolved Electrolyte Model add-on module, a User Defined Function, UDF, is employed to model the electrochemical reactions particularly, since they involve some electrical principles, which have to be defined in UDF. The UDF solves for the potential developed in the operation, the current distribution and the different over potentials (losses) in the fuel cell operation. The electrical model accounts for the potential field in the conductive layers of the cell. The two electrodes in the model are connected using the potential jump feature in the UDF's, for calculating the potential. The mass diffusion model used in the solver, corrects the effect of the porosity and tortuosity in the porous media using the multi-component diffusion model.

Details of the modeling approaches, equations solved in each domain, parameters and model setup are given below.

3.4 General Governing Equations

Modeling approach and equations solved in each domain are given below. The equations are taken from reference [5] and [53].

3.4.1 The Mass Conservation Equation

The equation for the conservation of a mass or continuity equation for all domains i.e. the anode, the cathode, the current collectors (the crofer mesh and the nickel porous) and the gas channels can be written as follows:

$$\frac{\partial \rho}{\partial t} + \nabla \cdot \left(\rho \vec{v} \right) = S_m \tag{3.15}$$

where ρ is the density, $\vec{v}$ is the velocity vector and S_m is the additional mass source. Density of the mixture can be calculated based on the volumetric ratio species i in the mixture as:

$$\rho = \sum_{i=1}^{N} \rho_i c_i \tag{3.16}$$

where ρ_i and c_i are the density and the concentration of species i in the mixture. On the other hand, density of the species can be calculated from the Ideal Gas Law as:

$$P_i = \rho_i R_i T \tag{3.17}$$

where P is the pressure and R is the ideal gas constant.

3.4.2 The Species Balance

The species balance equation is defined as:

$$\frac{\partial}{\partial t}\left(\rho Y_i\right) + \nabla \cdot \left(\rho \vec{v}\, Y_i\right) = -\nabla \cdot \vec{J}_i + R_i + S_i \tag{3.18}$$

where Y_i is the mass fractions of each species, R_i is the net rate of production of species i by the chemical reactions, S_i is the additional species source and J_i is the diffusion flux of species i, which arises due to the gradients of the concentration and temperature. By default, the mass diffusion due to concentration gradients is modeled using the multicomponent diffusion model. The mass diffusion is obtained from Maxwell-Stefan equations and can be written as:

$$\vec{J}_i = \sum_{j=1}^{N-1} \rho D_{i,j} \nabla Y_j - D_{T,i} \frac{\nabla T}{T} \tag{3.19}$$

where $(N-1)$ is the number of species, N is the total number of fluid phase chemical species present in the system, T is the temperature and $D_{T,i}$ is the thermal diffusion coefficient of species i and $D_{i,j}$ is the diffusion coefficient. For the porous electrodes, an effective binary diffusion coefficient is calculated accounting for the porosity and tortuosity of the electrode structures, which can be calculated as:

$$D_{i,j,eff} = \frac{\varepsilon}{\varsigma} D_{i,j} \qquad (3.20)$$

Where ε is the porosity and ς is the tortuosity, that is the average path length over the actual length. Also, additional species source term, S_i, can be calculated as:

$$S_i = I \frac{M_i}{nF} \qquad (3.21)$$

where M_i is the molecular weight of the species i, I is the current density and n is the number of electrons involved in the electrochemical reaction.

3.4.3   The Momentum Equation

In SOFC, since the velocity of fluids is small and the utilization factor of the fuel is low, the flow is assumed to be laminar. Then momentum equation can be expressed as:

$$\frac{\partial}{\partial t}\left(\rho \vec{v}\right) + \nabla \cdot \left(\rho \vec{v} \vec{v}\right) = -\nabla p + \nabla\left(\vec{\tau}\right) + \rho \vec{g} + \vec{F} \qquad (3.22)$$

where $\rho \vec{g}$ and $\vec{F}$ are the gravitational body force and the external body forces respectively. $\vec{F}$, also contains the model dependent source terms such as the porous media. Also $\vec{\tau}$ is the stress tensor and can be calculated as:

$$\vec{\tau} = \mu\left[\left(\nabla\vec{v} + \nabla\vec{v}^{T}\right) - \frac{2}{3}\nabla\vec{v}\right] \qquad (3.23)$$

where μ is the viscosity obtained similar to the density calculation.

3.4.4   The Charge Balance

The conservation of a charge principle applied to the conductive regions is:

35

$$\nabla \cdot i = 0 \tag{3.24}$$

where:

$$i = -\sigma \nabla \phi \tag{3.25}$$

In above equations, σ is the electrical conductivity and ϕ is the electrical potential. Therefore, the governing equation for the electrical field is the Laplace equation:

$$\nabla \cdot (\sigma \nabla \phi) = 0 \tag{3.26}$$

which also combines the following attributes:

- Ohmic losses in all the conducting materials, including the electrolyte, the electrodes and the current collector
- Contact resistances at the appropriate interfaces
- Ohmic heating through the conduction materials as a result of the ohmic losses and the current density throughout the domain

3.4.5 The Electrochemical Model Equation

As described above, actual cell voltage is less than the open circuit voltage due to the irreversibilities and it is equal to:

$$V_{cell} = V - \Delta V_{ohm} - \Delta V_{act} - \Delta V_{conc} \tag{3.27}$$

The exchange current density should be calculated to be able to calculate the actual cell voltage. It is calculated by Butler-Volmer formulation, which is given below:

$$i = i_0 \left[e^{\frac{\alpha_a n(\phi - \phi_0)F}{RT}} - e^{-\frac{\alpha_c n(\phi - \phi_0)F}{RT}} \right] \tag{3.28}$$

where i_0 is the exchange current density at equilibrium, α_a and α_c are the transfer coefficients of the anode and the cathode respectively and n is the

36

number of electrons that are released. Also, activation loss, η_{act}, can be defined as:

$$\eta_{act} = \phi - \phi_0 \tag{3.29}$$

Using this relation, the Butler-Volmer equation can be written as:

$$i = i_{0,eff} \left[e^{\frac{\alpha_a n \eta_{act} F}{RT}} - e^{-\frac{\alpha_c n \eta_{act} F}{RT}} \right] \tag{3.30}$$

where:

$$i_{0,eff} = i_{0,ref} \left(\frac{\chi_j}{\chi_{j,ref}} \right)^{\gamma_j} \tag{3.31}$$

and $i_{0,ref}$ is the exchange current density at the reference condition, χ_j is the mole fraction and γ_j is the concentration exponent for species j. More specifically at the anode side we have:

$$i_{0,eff}^{anode} = i_{0,ref}^{anode} \left(\frac{\chi_{H_2}}{\chi_{H_2,ref}} \right)^{\gamma_{H_2}} \left(\frac{\chi_{H_2O}}{\chi_{H_2O,ref}} \right)^{\gamma_{H_2O}} \tag{3.32}$$

Likewise at the cathode side we have:

$$i_{0,eff}^{cathode} = i_{0,ref}^{cathode} \left(\frac{\chi_{O_2}}{\chi_{O_2,ref}} \right)^{\gamma_{O_2}} \tag{3.33}$$

The Butler-Volmer equation can be solved using the Newton's method after the initial input values for the model provided. The activation over potentials for the anode and the cathode are calculated using this equation.

3.4.6   The Energy Equation

For an incompressible flow, the energy equation, within the each computational domain is given by the following:

$$\frac{\partial}{\partial t}(\rho E) + \nabla \cdot \left(\vec{v}(\rho E + p) \right) = \nabla \cdot \left(k_{eff} \nabla T - \sum_j h_j \vec{J}_j + \left(\vec{\tau}_{eff} \cdot \vec{v} \right) \right) + S_h \qquad (3.34)$$

where S_h is the volumetric source or sink of an energy where:

$$E = h - \frac{p}{\rho} + \frac{v^2}{2} \qquad (3.35)$$

and:

$$h = \sum_j Y_j h_j \qquad (3.36)$$

where h is the enthalpy. In the all electrically conducting zones, the ohmic heating is added to the energy equation as a source term. In other words:

$$S_h = i^2 . R_{ohmic} \qquad (3.37)$$

In addition, the energy equation needs treatment at the electrode-electrolyte interface to account for the heat generated or lost as a result of the electrochemistry and the over potentials.

The total energy balance on the electrolyte interface is computed by enumerating the enthalpy flux of all species including the heat of formation (sources of the chemical energy entering the system) and then subtracting off the work done (leaving the system), which is simply the local voltage jump multiplied by the local current density. What remains is the waste heat due to the irreversibilities to satisfy the 2nd Law of Thermodynamics. For the hydrogen reaction, the balance should be:

$$\dot{Q}^{\prime\prime} = h^{\prime\prime}_{H_2} + h^{\prime\prime}_{O_2} - h^{\prime\prime}_{H_2O} - i\Delta V \qquad (3.38)$$

where Q is the heat generation and h is the total enthalpy of species composed of the sensible enthalpy in addition to the enthalpy of formation.

The standard enthalpy is:

$$h_{H_2} = \dot{m}_{H_2} \left[\int_{T_{ref}}^{T} C_p dT + h_0 \right]$$ (3.39)

The source term is then added in the cell energy equation by:

$$S_h = \frac{Q}{Volume}$$ (3.40)

One half of this value is applied as a source term to the energy equation of the anode computational cell adjacent to the electrolyte and the other half is applied as a source term to the energy equation for the cathode cell adjacent to the electrolyte. This equal distribution of the heat generation/destruction is purely arbitrary. Note that, by using the work term, the effect from all over the potentials are taken into account.

The ohmic resistance in the conducting region is calculated as:

$$\eta_{ohmic} = i \cdot R$$ (3.41)

3.4.7 Modeling Reactions

The electrochemical reactions at the anode and cathode boundaries are modeled by calculating the rate of species production and destruction, thus calculating the dependence of the concentration of species on the current-voltage characteristics of the cell:

$$S = -\frac{\alpha i}{nF}$$ (3.42)

where α is the stoichiometric coefficient. By convention, the current density is positive when it flows from the electrode into the electrolyte solution i.e., the current densities are positive at the anode and negative at the cathode.

3.4.8 Boundary Conditions

All the external boundary walls are assumed to be adiabatic surfaces and no flux condition is applied to the electric field at the boundaries as:

$$\frac{\partial \phi}{\partial \vec{n}} = 0$$
$$\dot{Q}'' = 0 \qquad (3.43)$$

where $\vec{n}$ is the unit normal vector of the boundary walls. Beside this, internal boundary walls, exposed to fluid flow, are assumed to be impermeable to the species and the no-slip condition is applied to the velocities:

$$\frac{\partial c_i}{\partial \vec{n}} = 0$$
$$\vec{V} = 0 \qquad (3.44)$$

3.5 Numerical Solution Technique

The equations mentioned above, are solved by a commercial CFD code, Fluent®. The finite volume approach is used as the numerical solution technique and the pressure based coupled algorithm is used as the numerical solution technique. In the pressure based coupled algorithm, by solving a pressure equation, the constraint of the mass conservation of the velocity field is obtained. From the continuity and the momentum equations, the pressure equation is derived in such a way that the velocity field, corrected by the pressure, satisfies the continuity. The solution process involves iterations, where entire set of equations are solved repeatedly until the solution converges, because the governing equations are nonlinear. The steps are explained below:

1. Fluid properties are updated (e.g. density, viscosity, specific heat).
2. System of momentum and pressure-based continuity equations are solved simultaneously.
3. Mass flux is updated.
4. Energy, species, turbulence and other scalar equations are solved.
5. Convergence is checked.

If the convergence criterion is achieved, which is $1*10^{-4}$ for the continuity, x, y, and z-velocities and $1*10^{-8}$ for the energy, H_2O, H_2, O_2 and User Defined Scalar equations, then the iteration processes stops, if not, it returns to the first step [53].

3.5.1 General Scalar Transport Equation

Fluent$^®$ converts a general scalar transport equation to an algebraic equation that can be solved numerically. The transport equation is integrated about each control volume, which yields a discrete equation that expresses the conservation law on a control-volume basis. The following equations are taken from [53].

For a scalar quantity, ϕ, which is unity in the continuity equation, $\vec{v}$ in the momentum equation, h in the energy equation and c_i concentration of each species in the species conservation equation, the unsteady conservation equation illustrating the governing equations most easily can be written as follow:

$$\int_v \frac{\partial \rho \phi}{\partial t} dV + \oint \rho \phi \vec{v} \bullet d\vec{A} = \oint \Gamma_\phi \nabla \phi \bullet d\vec{A} + \int_v S_\phi dV \qquad (3.45)$$

where $\vec{v}$ is the velocity vector, $\vec{A}$ is the surface area vector, Γ_ϕ is the diffusion coefficient for ϕ, $\nabla \phi$ is the gradient of ϕ and S_ϕ is the source of ϕ per unit volume. The equation (3.45) is applied to each control volume, or a cell, which is shown in Figure 3.4, in the computational domain.

41
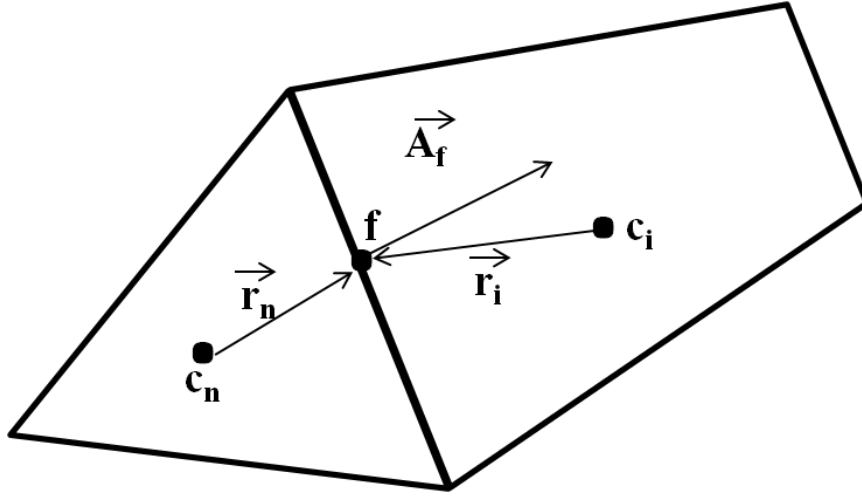
Figure 3.4 Schematic of 2-D control volume [53]

Discretization of the equation (3.45) on a given cell yields:

$$\frac{\partial \rho \phi}{\partial t}V + \sum_{f}^{N_{faces}} \rho_f \, \vec{v}_f \phi_f \bullet \vec{A}_f = \sum_{f}^{N_{faces}} \Gamma_\phi \nabla \phi_f \bullet \vec{A}_f + S_\phi V \qquad (3.46)$$

where N_{faces} is the number of faces enclosing cell, ϕ_f is the value of ϕ

conducted through the face f, $\rho_f \, \vec{v}_f \bullet \vec{A}_f$ is the mass flux through the face

f, $\vec{A}$ is the area of the face and $\nabla \phi$ is the gradient of ϕ at the face f.

3.5.2   Spatial Discretization

Fluent$^{\circledR}$ stores the scalar of ϕ at the cell centers default. But, ϕ_f values are

required for the convection terms in equation (3.46) and must be interpolated

from the cell center values. This is accomplished by using an upwind scheme,

which means that ϕ_f is obtained from quantities in the cell upstream, or

"upwind" relative to the direction of the normal velocity, v, in the equation

(3.46). Among the different types of the upwind schemes available for the

pressure based coupled algorithm, the second order upwind scheme is used in

this study, which is the most accurate and reliable one. In this scheme, all the

quantities at the cell faces are computed using a multidimensional linear

42

reconstruction approach, in which the higher order accuracy is achieved through the Taylor series expansion of the cell centered solution about the cell center. So, the face value of ϕ_f is obtained by:

$$\phi_f = \phi + \nabla\phi \bullet \vec{r} \qquad\qquad (3.47)$$

where ϕ and ϕ_f are the cell centered values and its gradient in the upstream and $\vec{r}$ is the displacement vector from the upstream cell center to the face center.

CHAPTER 4

SOFC MODEL VALIDATION AND VERIFICATION

In order to start numerical analysis of SOFC parameters with a validated model, an experimental setup is prepared and the data obtained from the setup is used for validation and verification.

4.1   Description of Experimental Setup and Results

The experiments are done at Vestel Defense Industries Laboratories using its instruments necessary for the experiment. Since the experiment is done at high temperatures, there is no chance to repair any mistakes in the experimental setup. That is, the gas sealing and the electrical contact between the PEN and the current collectors must be in a good condition before starting the experiment. So, an extra care is given to prepare experimental setup.

The experimental procedure starts with production of interconnector, on which the gas flow channels are machined. Cross-Flow arrangement is selected for the experiments. Interconnectors are sent to surface grinding to ensure the flatness of the surface. Crofer-22 Apu is selected for interconnector material since it has a good electrical conductivity and a high corrosion resistance at the high temperatures. Detailed description of the geometry, used in the experimental setup, is given in Table 4.1.

Table 4.1 Details of geometry used in experimental setup

Parameter	Value
Number of air/fuel channels	14
Active area (mm × mm)	43.5 × 43.5
Total interconnect thickness (mm)	2.5
Height and width of fuel and air channels (mm)	1.5

A 2 meter long pipe is curled from stainless steel AISI 310 to be able to supply the fuel and air to a stack and heat them up to 1073 K, which is the working temperature of SOFC [55], [56]. The pipe is welded to the interconnectors, as shown in Figure 4.1. Also, two probes are welded on the pipes to measure the voltage and current during experiment.
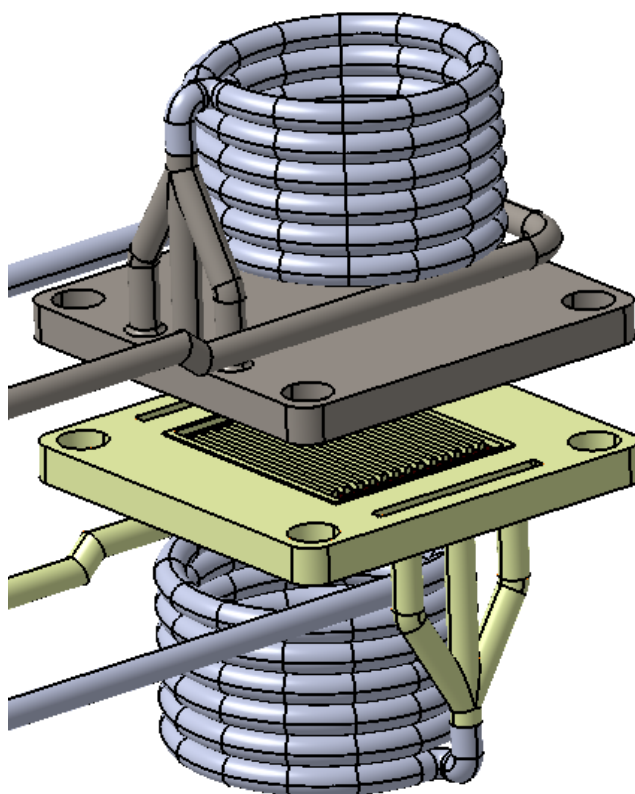
Figure 4.1 Interconnector and pipes

After the interconnectors are ready, the seal material is placed on both of the interconnectors. Then, the nickel porous and crofer mesh as current collectors

are cut in the dimensions of a cell and also placed on the interconnectors above the flow channels. After that, SOFC membrane, as shown in Figure 4.2 (a.1) and (a.2), is placed and squeezed between the interconnectors by facing the green part (anode) and the nickel porous, as shown in Figure 4.2 (b), to form the SOFC single cell stack.
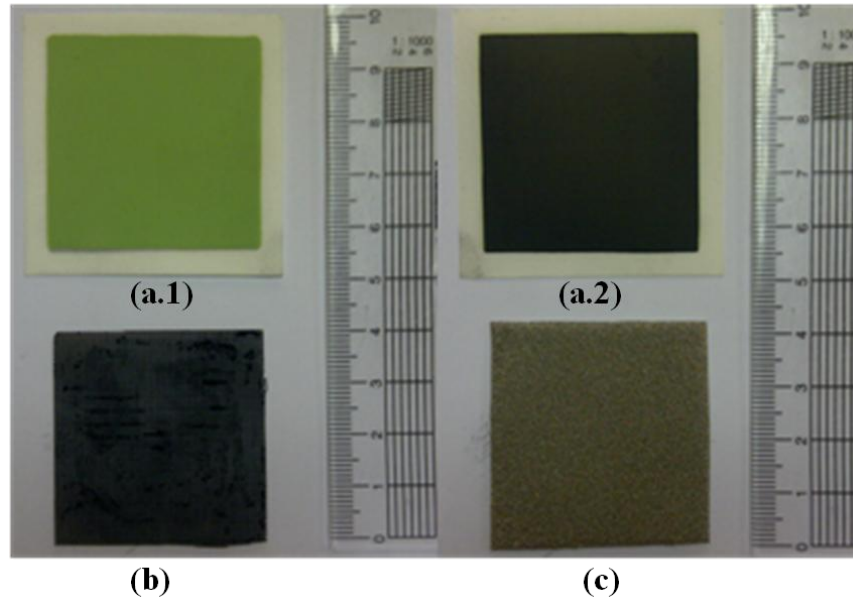
Figure 4.2 (a.1) and (a.2) SOFC membrane (b) crofer mesh (c) nickel porous

The dimensions of the nickel porous, crofer mesh and membrane are given in Table 4.2.

Table 4.2 Dimension of the nickel porous, crofer mesh and membrane

Parameter	Value
Anode thickness (μm)	15
Electrolyte thickness (μm)	200
Cathode thickness (μm)	20
Thickness of Nickel Porous and Crofer Mesh (mm)	0.4
Active area (mm × mm)	43.5 × 43.5

This single cell is then is placed in an electrical furnace at the temperature of $800^{o}C$, which is controlled by electronic controller. The temperature is

increased by 1°C/minute. Then, the probes on the pipes are connected to DC-Load to determine the current-voltage characteristic at several voltages.

After that, the flow-meter shown in Figure 4.3, is connected to the fuel and air inlet and outlet of the cell to measure the flow rates in milliliter per minute (ml/min) with a sensitivity of 10 ml/min.

Figure 4.3 Flow-meter

During experiments, within the limitations of the available equipment, all possible measurements are taken to be able to verify the mathematical model. Some parameters are impossible to measure with today's technology and some measurements are very expensive such as the temperature and current distribution at the PEN surface. The power output of the stack and flow rates of the air and fuel are easy to measure, which are used in this study in verification. Schematic of the experimental setup is shown in Figure 4.4.
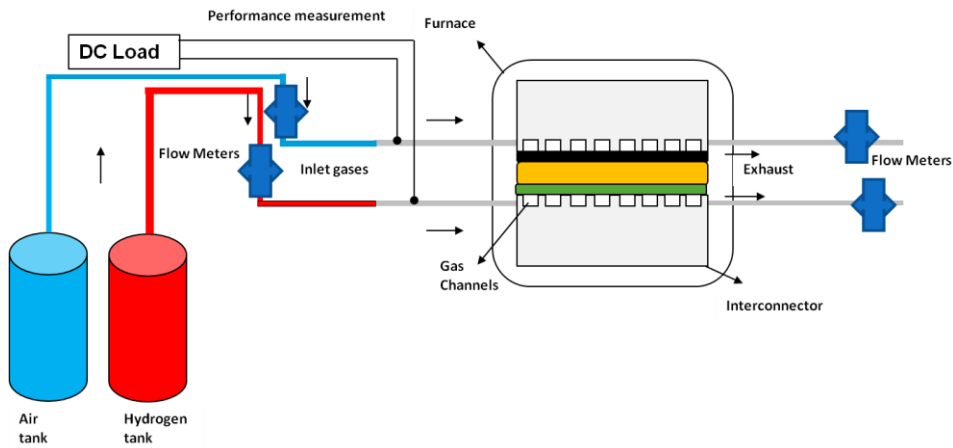
Figure 4.4 Schematic of experimental setup

4.1.1 Gas Leak Test

Sealing is one of the most important problems of a SOFC stack. It is hard to find or develop a sealing material at high temperatures. If good sealing is not achieved, then there is a risk of explosion of the hydrogen or hydrogen will just burn, which will reduce the efficiency. So, before starting experiment, gas leak test should be done to avoid any misleading results in experiment. The gas leak test schematic is shown in Figure 4.5.

A-Anode side, C-Cathode side, M – Manometer, V - Vane
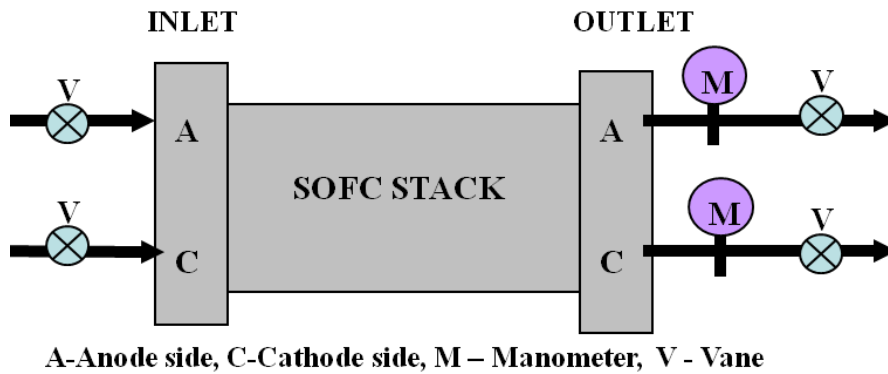
Figure 4.5 Gas leak test schematic

The gas leak test is done by using helium gas to prevent any accidents according to the US Fuel Cell Council standards [57]. Test is done at the anode

side first by closing the vanes at the anode side and opening the vanes at the cathode side at the SOFC working temperature of 1073 K. Then the vane at the anode inlet is opened slowly to pressurize the anode side up to 100 mbar and then vane is closed. Then after 10 minutes, the manometer is read. The same procedure is applied to the cathode side and it is observed in both of the experiments that there is no change in manometer readings, so it can be said that no gas leakage is observed for both the anode and cathode sides. As a result, the experimental setup is ready to be used for further studies.

4.1.2 SOFC Performance Test

The performance test is done after the gas leak test. The test starts with supplying 99% pure hydrogen at 250 ml/min and air at 320 ml/min to the anode and the cathode sides, respectively. These flow rates are taken from studies done at Vestel Defense Industries. It is assumed that, the hydrogen gas mixture carries 1% mass fraction of water vapor in it. Then after an hour, the experimental data collection is started at several voltages, which are possible working voltages of the SOFC. For a voltage change from one value to another, at least 10 minutes of waiting period is required for the system to reach equilibrium. The voltage of a cell is controlled with DC-Load and the obtained current-voltage characteristic curve is given in Figure 4.6.
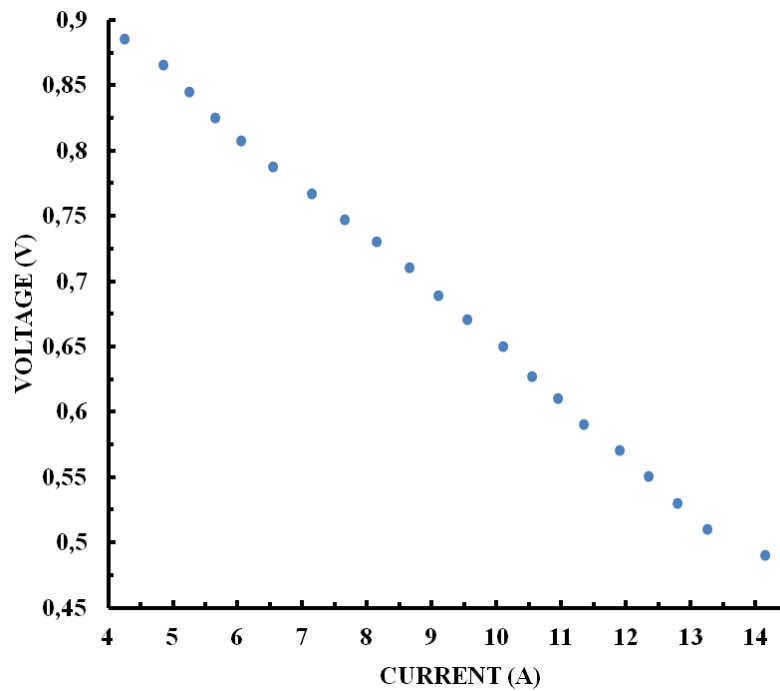
Figure 4.6 Current-voltage characteristic of the SOFC single cell

4.1.3 Flow Rate Measurements

After current-voltage characteristics are obtained, the flow rates are measured for the inlet and the outlet of the fuel and the air under different the load conditions by waiting at least 10 minutes between the different loads. Results are given in Table 4.3.

Table 4.3 Fuel flow rate at outlet from experiment

	INLET	OUTLET (±0.005 Volt)				
		0.9 V	0.8 V	0.7 V	0.6 V	0.5 V
H$_2$ Flow Rate (ml/min) (±10 ml/min)	250	210	190	170	160	150
Air Flow Rate (ml/min) (±10 ml/min)	320	300	280	270	260	250

It is observed that, as the operating voltage decreases, more current is drawn from the cell and also the outlet flow rates decreases. This is caused by the fact that, more electrochemical reactions is occurring to supply the load.

4.2 Experimental Uncertainty

No physical quantity can be measured exactly and one can only know its value with a certain range of uncertainty. This uncertainty is dependent on the calibration of the instrument. Also, the resolution of the instrument is important, since it must capture the changes in the physical value correctly.

In experiments, all of the instruments used were calibrated. When calibration forms are checked, it is observed that the error for the flow meter is -0.77% and +0.3% for the hydrogen and the air flow meters respectively. This is a very low uncertainty but the resolution of the flow meter is quite insufficient since it has a low sensitivity of 10 ml/min. Therefore, in order to capture the flow rates more accurately, flow meters with higher sensitivity should be used. Also, the flow rate of the air at the cathode outlet is measured with a flow meter for air, but, since the oxygen in the air is used in a fuel cell, the measured value contains some error. But this error is acceptable because the density of the air is close to the density of the oxygen so consumption of the oxygen will cause a small error in the measured values.

Beside flow meters, DC-load used in the experiments, has measurement inaccuracy for the voltage and current as +0.05% and +0.001%, respectively, as given in its calibration form. Also electrical furnace has uncertainty of $\pm0.4^{o}C$ at $800^{o}C$.

4.3 SOFC Model Setup

After experiment with a single cell is concluded, the SOFC numerical model with Fluent$^{®}$ commercial program is setup. This model is verified and validated with the experimental data to show the reliability of the model. Thus, a reference case is formed for further studies. Also, with the developed model, one gets a chance to investigate the several parameters, which are impossible to obtain from experiments. This is the most important advantage of CFD simulation.

In Fluent®, the SOFC model setup is divided the solution domain into control volumes. The related governing equations are integrated over each control volume numerically.

The model setup needs various parameters as input in mainly 5 distinct steps. The steps are the selection of the physical model and material properties, assigning cell zone conditions and boundary conditions and selecting numerical solution method.

4.3.1 Physical Model

The SOFC model setup consists of the physics of flow, energy, species transport and reactions and the SOFC electrochemistry. The model consists of the anode/cathode interconnector, anode/cathode gas flow channels, crofer mesh, nickel porous, anode and cathode. The electrolyte is not actually included in the solution domain, which is the species and energy sources and sinks due to the electrochemical reactions added to the adjacent computational cells [5].

For the model to work properly, the electrical and electrochemical parameters must be defined correctly. The necessary parameters are taken from Vestel Defense Industries and are given in Table 4.4.

Table 4.4 Electrical and electrochemical properties in the SOFC [17]

Property	Value
Current Under Relaxation Factor	3
Total System Voltage (V)	0.6
Electrolyte Thickness(m)	0.002
Electrolyte Resistivity (ohm-m)	0.16
Anode Exchange Current Density (Amp/m^2)	15500
Cathode Exchange Current Density (Amp/m^2)	2675
Mole Fraction Reference Values for H_2, O_2 and H_2O	1
Concentration Exponents for H_2, O_2 and H_2O	0.5
Anodic and Cathodic Transfer Coefficient for Anode and Cathode Reactions	0.5
Anode and Cathode Tortuosity	3
Anode Conductivity (1/ohm-m)	100000
Cathode Conductivity (1/ohm-m)	7700
Anode Contact Resistance (ohm-m^2)	$1*10^{-7}$
Crofer Mesh Conductivity (1/ohm-m)	1460
Nickel Porous Conductivity (1/ohm-m)	100000
Cathode Contact Resistance (ohm-m^2)	$1*10^{-8}$

4.3.2 Material Properties

For different cell zones and boundary conditions, appropriate material properties must be applied. The properties are given in Table 4.5.

Table 4.5 Material properties [17]

	Anode	Cathode	Electrolyte	Interconnector	Crofer Mesh	Nickel Porous
Material	Ni-Doped YSZ	LSM	YSZ	Crofer-22 Apu	Crofer-22 Apu	Nickel
Density (kg/m^3)	6220	6180	5820	7700	7700	8900
Thermal Conductivity (W/m-K)	6.23	11	2.7	25	25	Temperature Dependent
Specific heat (J/kg-K)	450	600	480	650	650	Temperature Dependent

These parameters are also taken from Vestel Defense Industries. Some of those parameters are determined from experiments and some of them are taken from manufacturer.

4.3.3 Cell Zone Conditions

At the model, the anode and cathode interconnectors are defined as solid regions whereas other regions are defined as fluid zones. But the gas channels, anode/cathode electrodes and current collectors are different type of fluid zones where the anode/cathode electrodes and the current collectors are the porous zones. The porosities and viscous resistances for porosity definition are given in Table 4.6.

Table 4.6 Porosities of zones [17]

	Anode	Cathode	Electrolyte Material	Interconnector	Crofer Mesh	Nickel Porous
Porosity (ε)	0.4	0.5	Impermeable	Impermeable	0.5	0.5
Viscous Resistance ($1/m^2$)	$1*10^{13}$	$1*10^{13}$	-	-	$1*10^9$	$1*10^9$

4.3.4 Boundary Conditions

In the model, a mass flow inlet boundary condition is defined for the anode and cathode inlet. For the outlets, the pressure outlet boundary condition is applied. The outlet pressures are assumed to be atmospheric.

The conjugate heat transfer is solved between the flow zones (flow channels, electrodes and current collectors) and solid regions (interconnectors), while the zero velocity is assumed at the walls for the laminar flow. The model is also solved with the turbulence model of "Spalart-Allmaras" for the fluid flow equations, in order to see the effect of the fluid flow model type on the results and the effect of the wall roughness on the cell performance. The wall

roughness height of 0.00001m is taken from the manufacturer of the interconnector.

For the wall boundary conditions, appropriate material types are selected. The boundary condition parameters are given in Table 4.7.

Table 4.7 Operating and boundary conditions

Operating and Boundary Conditions		Reference
Fuel Flow Rate (kg/s)	$3.4466*10^{-7}$	Vestel Defense Industries
Air Flow Rate (kg/s)	$6.1941*10^{-6}$	Vestel Defense Industries
Fuel Inlet Temperature (K)	1073	Vestel Defense Industries, [35]
Air Inlet Temperature (K)	1073	Vestel Defense Industries, [58]
Operating Pressure (Pa)	101325	Vestel Defense Industries, [32]
Mass Fraction of H_2	0.99	Vestel Defense Industries
Mass Fraction of H_2O	0.01	Vestel Defense Industries
Mass Fraction of O_2	0.23	Vestel Defense Industries
Wall Roughness Height (m)	0.00001	Vestel Defense Industries
External Walls	Insulated	[32],[35]

4.3.5 Numerical Solution Method

For the solution of the governing equations, a commercial CFD code, Fluent$^®$, is used. The numerical solution technique of Fluent$^®$ is based on the Finite Volume Method, in which the solution domain is divided into the smaller control volumes. The equations are then numerically integrated over these control volumes, within which the value of any quantity is given by its value at the center of the control volume or the cell. Since, this solving technique is an iterative process, errors due to the truncation and round-off become more important as the iteration progresses, so the discretization method used in solving Finite Difference Equation (FDE) is very important. Among the discretization methods, Second Order Upwind with Coupled Pressure-Velocity Coupling scheme, which is used in this study, gives the more accurate results compared to others.

4.4 Verification and Validation of the Model

After developing any physical model with the numerical technique, model must be verified and validated. Two conditions must be satisfied, which are checking the model, if it is solving the model correctly and checking the solution, if it represents the reality or not, to verify and validate the model. Generally, the former is called verification and latter is called validation.

Verification and validation of a model is usually done by comparing the model results with the ones from experiments or from other models with the same operating and boundary conditions. In SOFCs, verification of a model is very difficult and sometimes impossible to compare a model results with experiments because of their high working temperature. The high working temperature of an SOFC makes it impossible or very expensive to collect or measure some properties during an experiment and also, it is hard to find suitable numerical results in the literature. Because of this reason, to verify SOFC model with an experimental setup, quantity of the output power of SOFC at the certain voltages of 0.5 V, 0.6 V, 0.7 V, 0.8 V and 0.9 V will be compared. Also, with the certain air and fuel flow rates supplied to the SOFC stack, the outflow rates will be compared. Also, tendency and distribution of some results will be compared with the model results found in the literature to validate the model. Also, different SOFC single cell models are formed differing in mesh density to show mesh independence.

In verifying the SOFC model with experimental results and determining optimum grid type, Cross-Flow arrangement of the SOFC single cell, as shown schematically in Figure 4.7, is used.
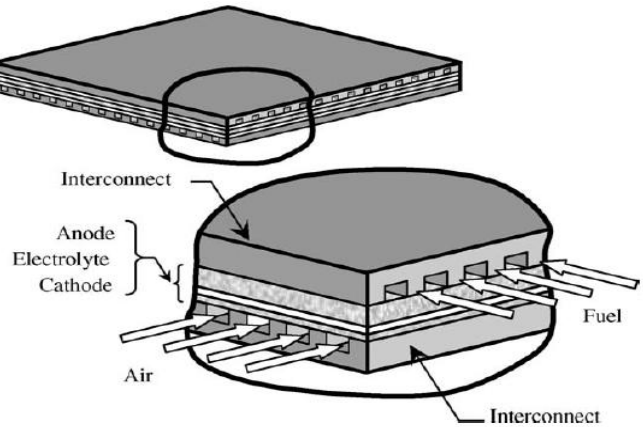
Figure 4.7 SOFC single cell Cross-Flow arrangements [54]

4.4.1 Verification of the Numerical Model

For most of the studies to verify the model, comparing the output power from the experiment and model should be sufficient but more data should be used for comparison to obtain a better model. For this reason, beside output power, the gas flow rates at the outlets will also be used in verification of model.

To verify model with the experiment, all of the parts used in the experiment, is meshed with four different mesh densities to show the grid independence. All of the four different grids are structured type with the highest quality in terms of orthogonal quality.

The model is solved for steady state operation. Using these results, an I-V (current-voltage) curve, which is the characteristics of the SOFC performance, is plotted and the results are compared with the results obtained from the experiments. The comparison is shown in Figure 4.8.
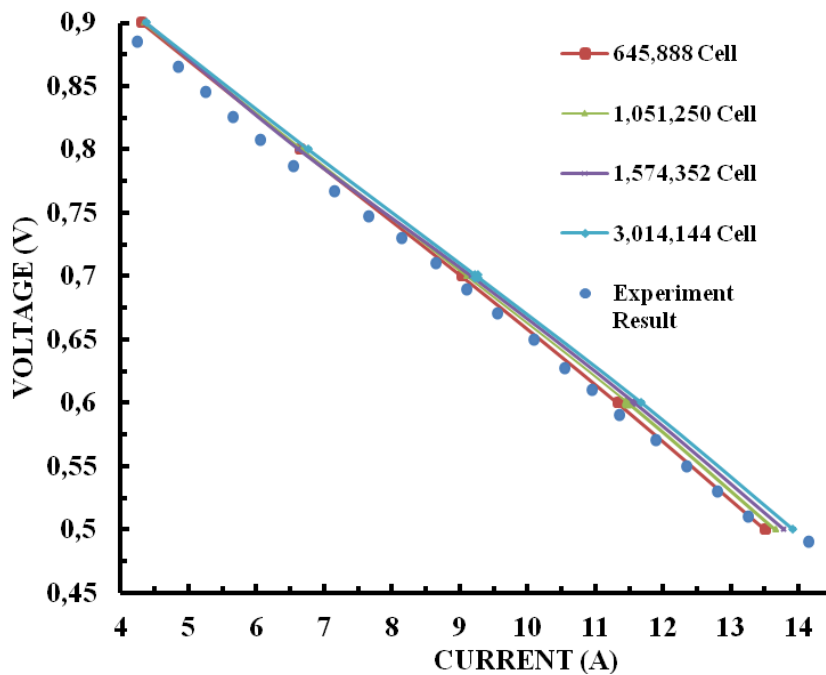
Figure 4.8 Comparison of the model and experimental results for different cell numbers

As can be observed from the graph, the model and experimental results are very close to each other for all cell numbers. Also at Table 4.8, the error in the current obtained from the models is shown.

Table 4.8 Error in the current obtained from the models and experiment

Operating Voltage (V)	Errors for Different Number of Cell			
	645,888	1,051,250	1,574,352	3,014,144
0.5	1.4%	0.3%	-0.6%	-1.6%
0.6	-1.6%	-2.9%	-3.8%	-4.7%
0.7	-1.8%	-2.6%	-3.3%	-4.2%
0.8	-5.2%	-6.1%	-5.1%	-7.4%
0.9	-6.5%	-7.3%	-7.6%	-7.9%

The small difference between the model and experiment should be attributed to the uncertainties in instruments and unexpected losses at the experiment such as the electrical losses at cables. Also, note that, the experimental voltage points do not correspond to the model voltage points exactly, because of DC-load uncertainty. So, if they were the same, then the difference between results

should be less, because the current decreases as the voltage increases and vice versa. With a detailed investigation, it is observed that by this arrangement results become closer.

Beside current-voltage characteristics, more data are compared at 0.6 V to determine the optimum number of cells for further studies. The comparison is done at the anode outlet side for a single outlet channel in the middle as shown in Figure 4.9 and the average H_2 and O_2 mole fractions at outlets.
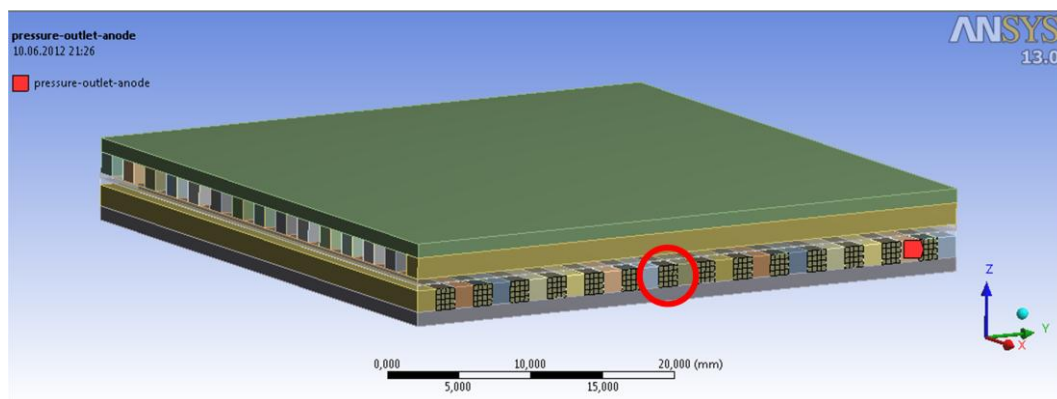
Figure 4.9 The anode outlet used for verification

At the shown single anode outlet channel in Figure 4.9, various parameters are compared such as the mass flow rate, average temperature and H_2 mole fraction. The results are given in Table 4.9. Note that, the errors for all of the parameters are calculated with respect to the model with 3,014,144 number of cell.

From Table 4.9, it is observed that the error decreases as the number of the cells increases. But it is observed that, maximum error is -1.31% for 1,051,250 number of cell for mass flow rate. Since this error is quite low and to decrease the solution time for further models, a model with 1,051,250 is selected as a reference for further studies.

Table 4.9 Parameters at the selected single anode outlet for the different models

Parameters at 0.6V	Number of Cell			
	645,888	1,051,250	1,574,352	3,014,144
Mass Flow Rate*10^8 (kg/s)	8.9	9.1	9.1	9.2
Error	-2.23%	-1.31%	-0.68%	-
H_2 Mole Fraction	0.662	0.658	0.655	0.652
Error	1.64%	0.96%	0.50%	-
Average Temperature (Kelvin)	1241.63	1230.18	1223.08	1214.36
Error	2.25%	1.30%	0.72%	-

Also, in Table 4.10 the flow rates in (kg/s) for the model and in (ml/min) for the model and the experiment are given. Please note that, the volumetric flow rates for the model results at the outlet are calculated from the model mass flow rate results at the outlet.

Table 4.10 Outlet flow rates from the experiment and models with 1,051,250 cells

		OUTLET				
		0.9 V	0.8 V	0.7 V	0.6 V	0.5 V
H_2 Mass Flow Rate (kg/s)*10^7	Model	2.9	2.7	2.5	2.2	1.9
H_2 Flow Rate (ml/min)	Model	216.8	198.9	180.4	162.3	145.5
	Experiment	210	190	170	160	150
Error		-3.2%	-4.7%	-6.1%	-1.4%	3%
Air Mass Flow Rate (kg/s)*10^6	Model	5.8	5.6	5.4	5.2	5.1
Air Flow Rate (ml/min)	Model	301.4	291.4	280.9	270.9	261.4
	Experiment	300	280	270	260	250
Error		-0.5%	-4.1%	-4.1%	-4.2%	-4.5%

As can be observed from the results, a model with 1,051,250 numbers of cells gives very close results to the experiment for output power and outlet flow rates, from which it can be concluded that the model captures the experimental case setup correctly. Furthermore, since as the number of cells increases, the

time needed for the model to be solved increase, so the grid types similar to the model with the number of cells 1,051,250 are used in further studies.

4.4.2 Validation of the Numerical Model

To validate the model, it is sufficient to investigate some results. In Figure 4.10, scaled residuals are shown for Cross-Flow arrangement. Scaled residuals show the convergence of the selected equations. In this study, an absolute convergence criterion of $1*10^{-4}$ is selected for the continuity, x, y, and z-velocities and an absolute criterion of $1*10^{-8}$ is selected for the energy, H_2O, H_2, O_2 and User Defined Scalar equations. From the figure, it is observed that a convergence criterion is reached for the selected equations and there is no need for more iteration.
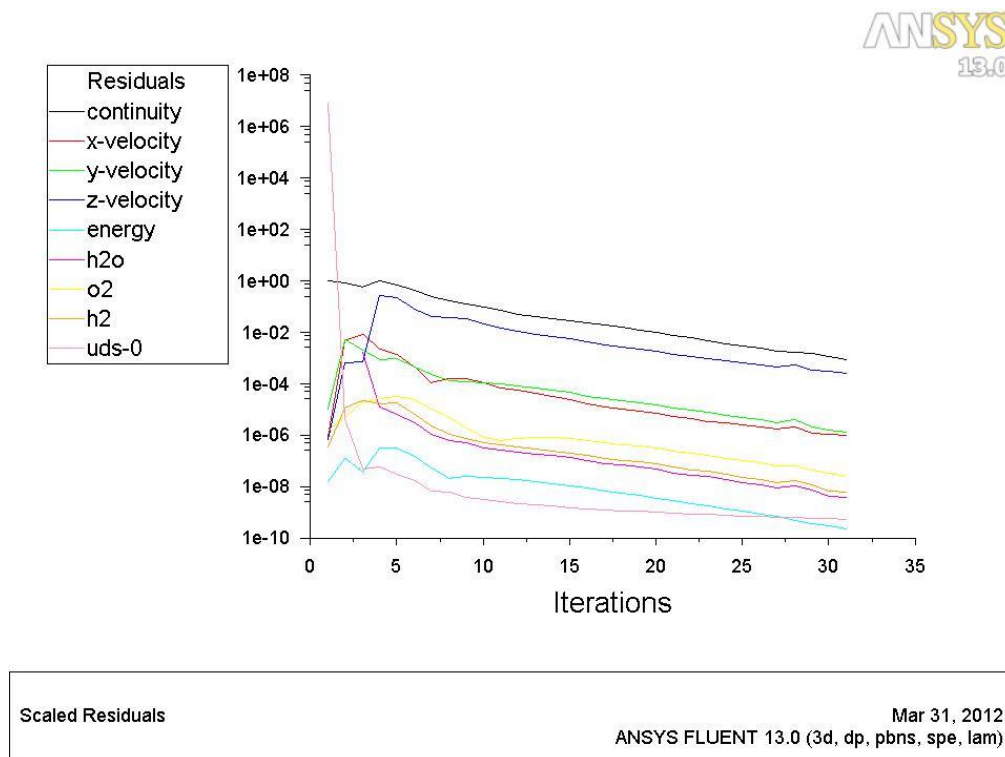
Figure 4.10 Scaled residuals for the selected equations

In Figures 4.11-4.15, some results for the model with 1051250 cells are shown. In Figure 4.11, temperature distribution is shown at the anode/cathode-

electrolyte surface when the cell is at 0.6 V. It is observed that, the temperature difference is increasing along the diagonal of the geometry when Cross-Flow arrangement used. The reason for this difference is the electro-chemical reactions occurring at the anode/cathode-electrolyte surface, which is exothermic. Similar results are also reported by [33-36], which are mainly attributed to different flow rates of the air and fuel. The flow rate of the air is as much as 9 times of the fuel flow rate in [33-36], whereas in this study, it is about 1.3 times, thus here the difference in the region of maximum temperature is reasonable.

In Figures 4.12-4.14, for Cross-Flow case, contours of the mole fraction of H_2O and H_2 at the anode-electrolyte surface and the mole fraction of O_2 at the cathode-electrolyte surface are shown respectively. Note that, ripples in Figures 4.12-4.14, correspond to the flow channels, in which the cathode side flow is from the top to the bottom and the anode side flow is from the left to the right. From the figures, it can be observed that, the mole fraction of H_2O increases as the mole fraction of H_2 decreases. Moreover, the mole fractions of H_2 and O_2 decrease to the end of gas-flow channels perpendicular to each other.
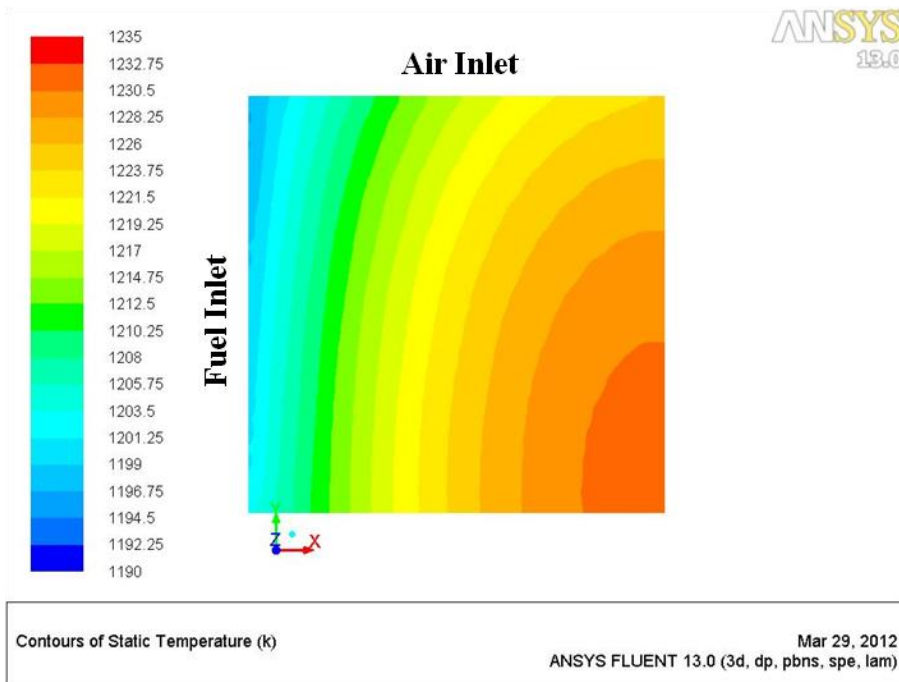
Figure 4.11 Contours of temperature at the anode/cathode-electrolyte surface
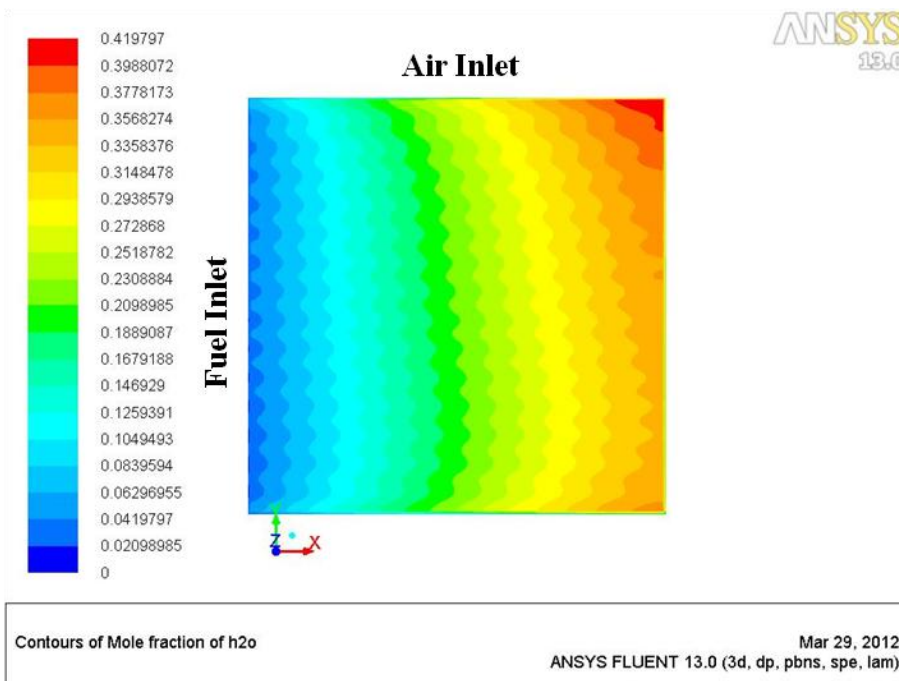
Figure 4.12 Contours of mole fraction of H_2O at the anode-electrolyte surface
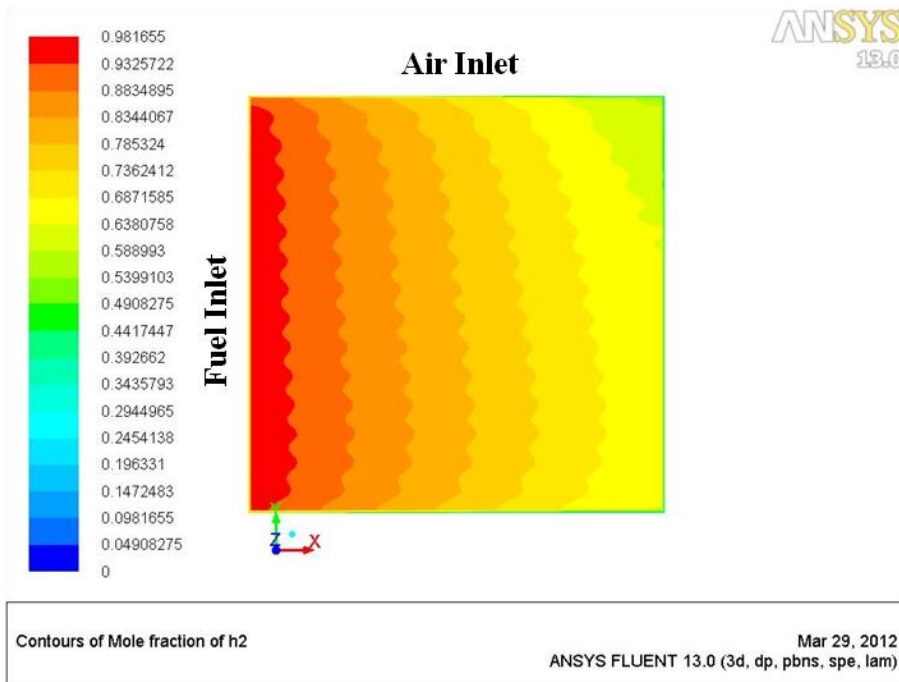
Figure 4.13 Contours of mole fraction of H_2 at the anode-electrolyte surface
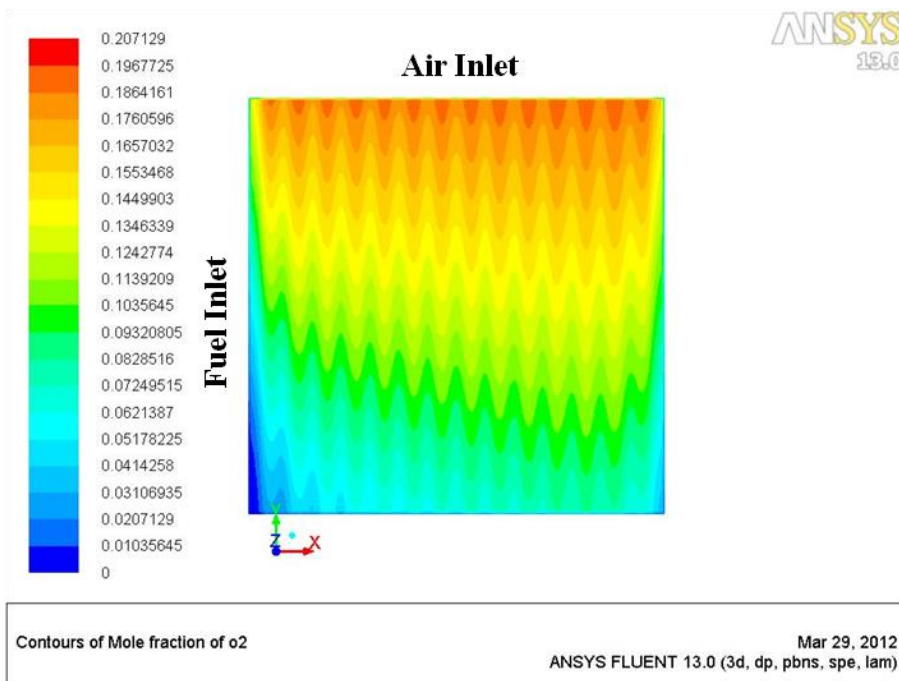
Figure 4.14 Contours of mole fraction of O_2 at the cathode-electrolyte surface

Interface current density is another important result to be checked at the anode/cathode-electrolyte surface, which is shown in Figure 4.15. From the figure, it is observed that higher current density is achieved at the first meeting region for the fuel and air flows with a decrease along the diagonal through the end of the channels, because there are higher mole fractions of gases at the first meeting region, which results in a higher electro-chemical reaction rate. These results are almost similar with the ones obtained in [33-36]. Also, when Figure 4.12 and Figure 4.13 are compared with Figure 4.15, it is observed that the mole fraction of H_2O is the highest and the mole fraction of H_2 is the lowest at upper right corner, which is the end of the uppermost gas flow channel.
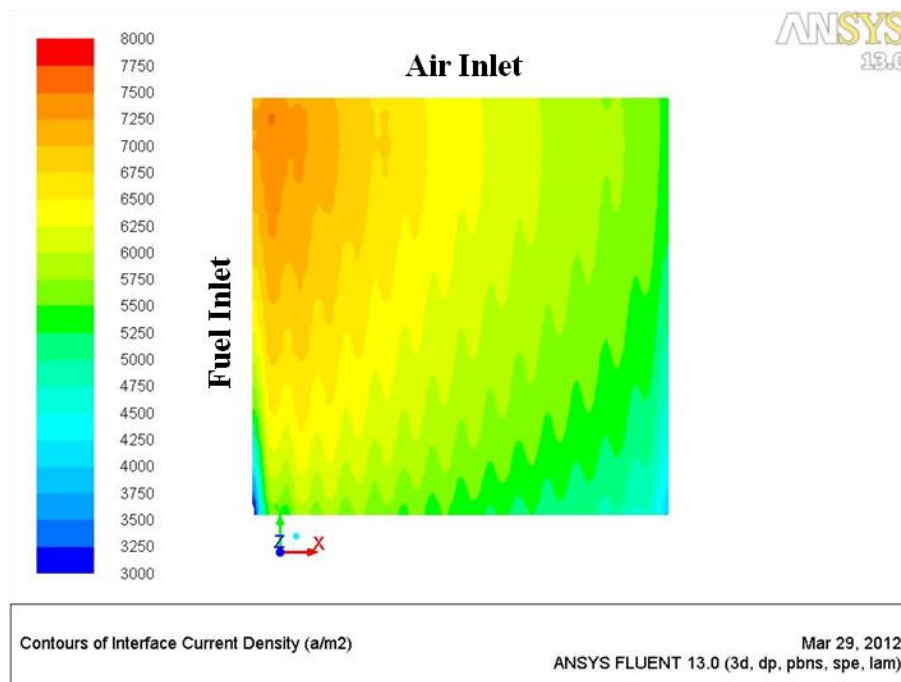
Figure 4.15 Contours of interface current density at the anode/cathode-electrolyte surface

In Table 4.11, the mole fractions of species at the inlet and the outlet are given. There is a recorded increase in the mole fraction of H_2O, whereas a decrease in the mole fraction of H_2 and O_2. With a detailed investigation, it is observed that, the observed changes in the species mole fractions are proportional to

overall chemical reaction constants given in equation (3.1). So, these results show that the model's predictions are reasonable.

Table 4.11 Species mole fraction at the inlet and the outlet

Species	Mole Fraction at the Inlet	Mole Fraction at the Outlet
H_2O	0.02	0.35
H_2	0.98	0.65
O_2	0.21	0.08

CHAPTER 5

EFFECT OF FLOW ARRANGEMENT

In this study, several interconnector geometries determining the fuel and air flow directions are developed and compared with the traditional ones by mathematical modeling. The aim of developing the new interconnector designs is to minimize the temperature gradient, which can cause the thermal stresses. These thermal stresses results in a fracture of the PEN, which decreases the lifetime of the SOFC stack. This is the most important problem of the SOFCs. Other parameters, that effect performance of an SOFC must also be checked, while optimizing the geometry for the temperature gradient. The results obtained from the previous chapters, are going to be used as a reference case for the models discussed in this chapter.

Traditional and the newly developed fuel and air flow directions studied in this work, are shown schematically in Figure 5.1. Traditional designs are the most popular ones because of their simplicity in forming an SOFC stacks and ease of manufacturing.
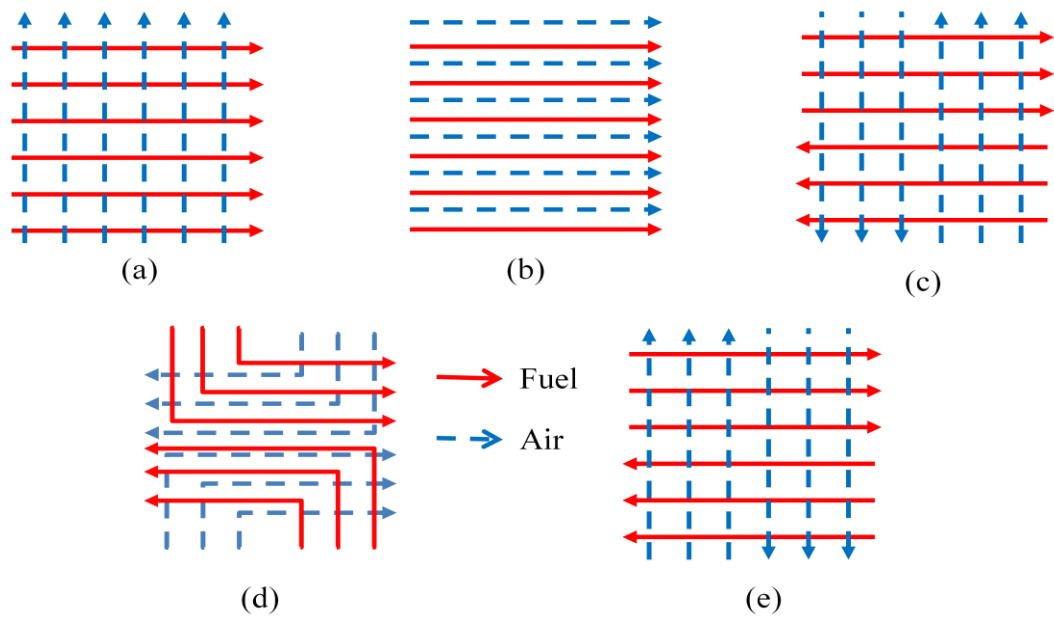
Figure 5.1 Traditional [(a) and (b)] and developed geometries [(c), (d) and (e)]:
(a) Cross-Flow, (b) Co-Flow, (c) G-1, (d) G-2, (e) G-3

In Figure 5.1, only the fuel and air flow directions are shown schematically. However, it must also be shown that, it is possible to manufacture a complete interconnector for the newly developed fuel and air flow arrangements. The proposed complete interconnector geometries are designed with Catia-V5 [59] and they are shown in Figure 5.2.
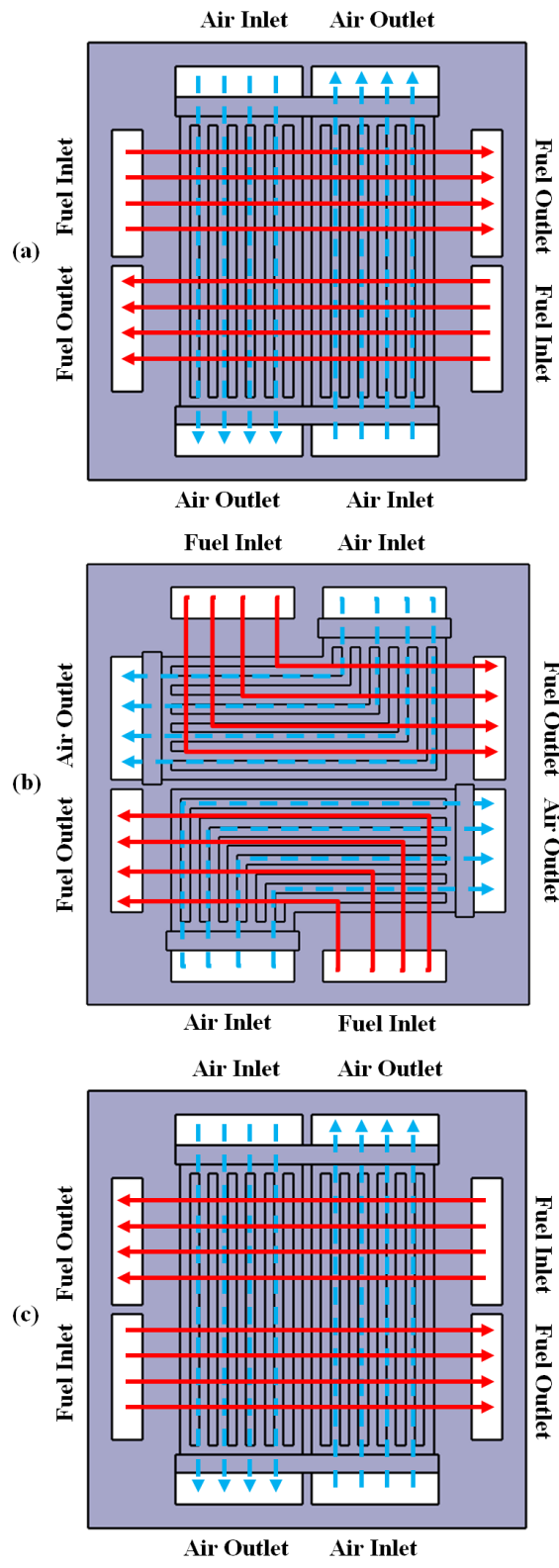
Figure 5.2 Interconnector designs for developed flow arrangements: (a) G-1, (b) G-2, (c) G-3

5.1 Results for Different Configurations

5.1.1 Results with Laminar Flow Model

Five different flow arrangements, as shown in Figure 5.1, are modeled with the same electro-chemical parameters, boundary conditions and type of grid in order to offer a new interconnector design, which improves the thermal stability of the SOFC stack.

Several parameters must be investigated, when comparing results for different geometries because it is not acceptable, while optimizing the one parameter, to cause another parameter to go worse. Also, one should note that, the results are evaluated at the same voltage, 0.6 V, which is a possible working voltage.

In order to observe the improvement in the thermal management of the SOFC stack, temperature profiles at the PEM anode/cathode-electrolyte surfaces are plotted for the five different gas flow channels arrangements. In Figures 5.3-5.7, temperature profiles at the PEN anode/cathode-electrolyte surface for Co-Flow, Cross-Flow, G-1, G-2 and G-3 stack designs are shown. In these figures, the same temperature scales are used in order to make the comparison easy.

From these figures, it can be said that, the traditional designs have darker and lighter colors representing the temperatures at the selected surfaces than the newly developed ones. Moreover, G-3 has better distribution of the temperature, which is observed from Figure 5.7. So, it can be said that, the newly developed interconnector designs have more uniform temperature profiles at the selected surfaces than the traditional ones. Also, note that for all of the designs, temperature increases at the end of the channel, which is the result of the heat generation.
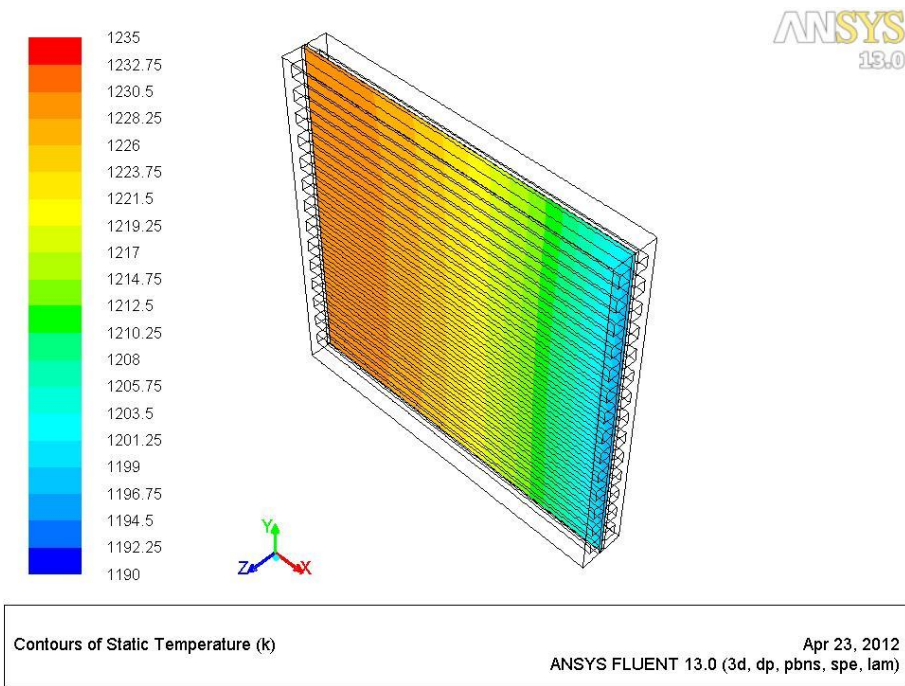
Figure 5.3 Temperature profile at the anode/cathode-electrolyte surface of Co-Flow design
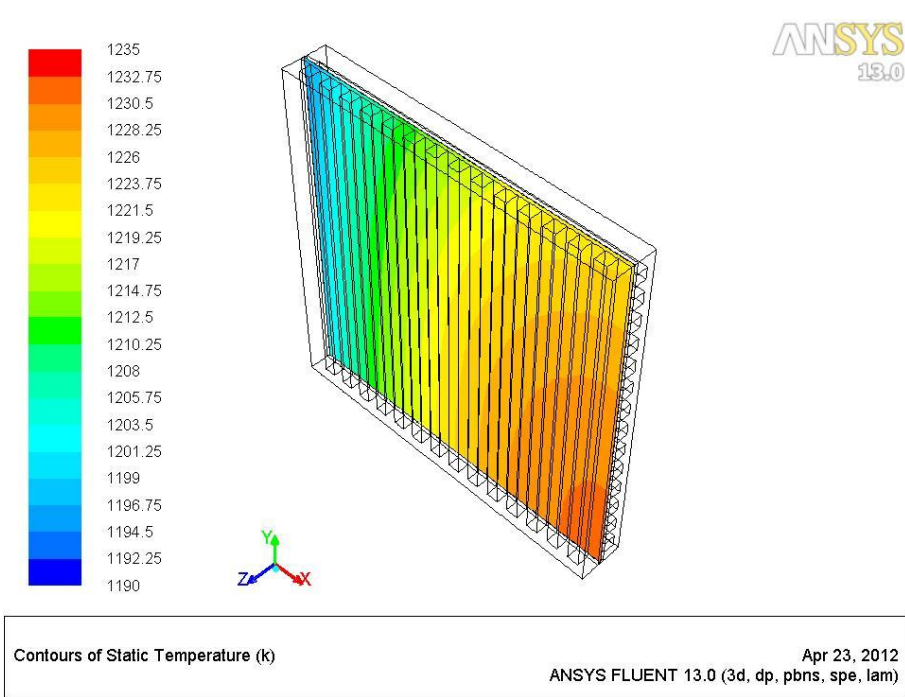
Figure 5.4 Temperature profile at the anode/cathode-electrolyte surface of Cross-Flow design

71
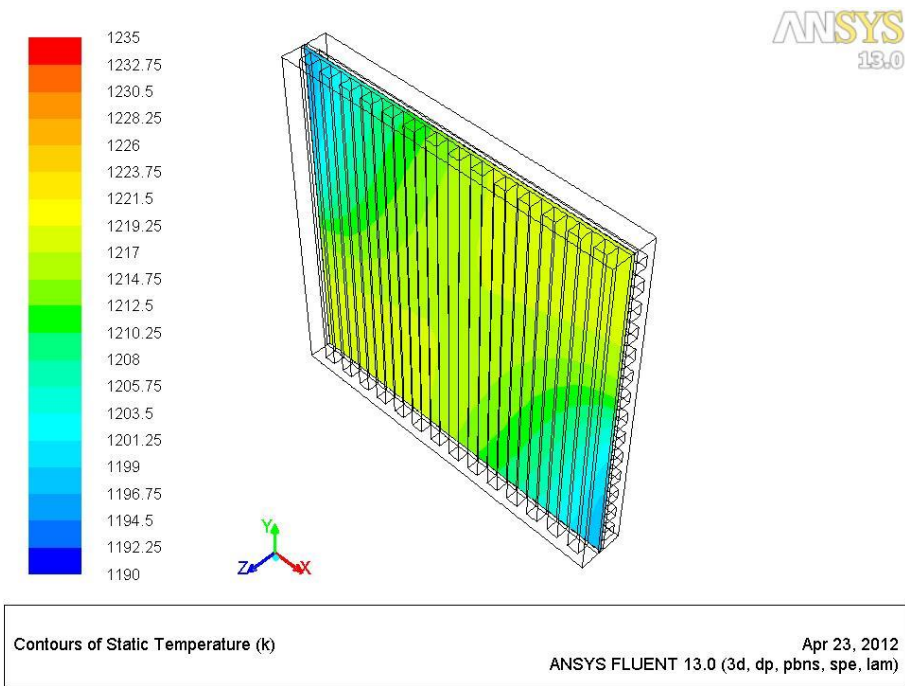
Figure 5.5 Temperature profile at the anode/cathode-electrolyte surface of G-1 design
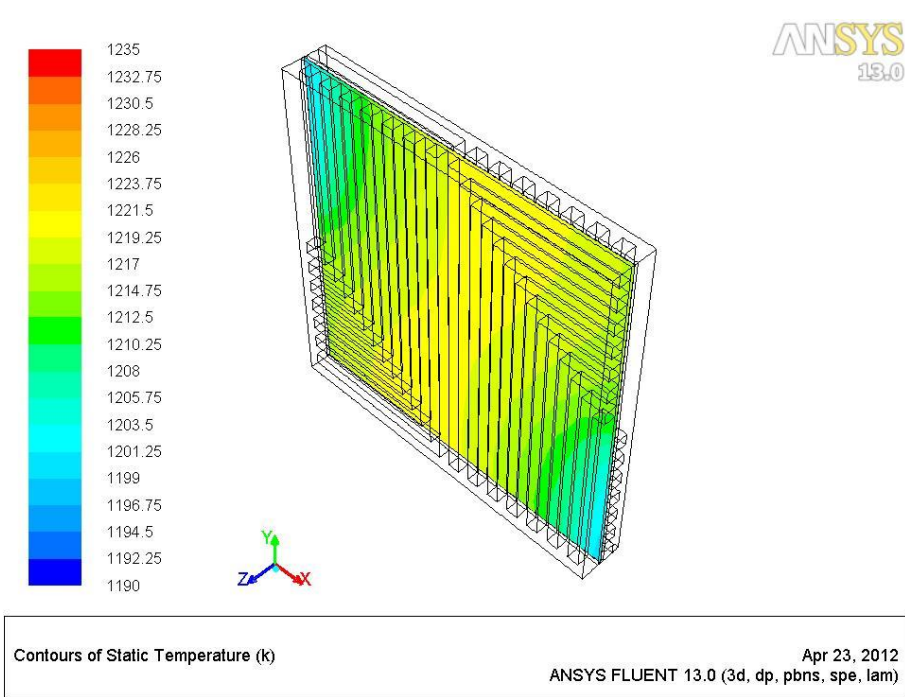
Figure 5.6 Temperature profile at the anode/cathode-electrolyte surface of G-2 design
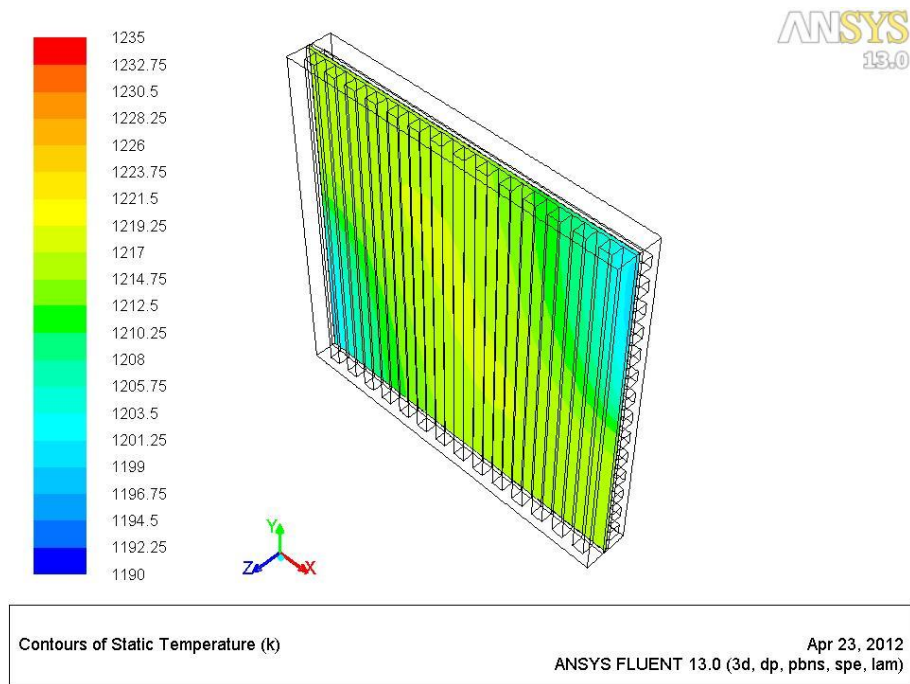
Figure 5.7 Temperature profile at the anode/cathode-electrolyte surface of G-3 design

Scalar temperature values must be compared, to make the temperature comparison for the five different designs more reliable.

In Table 5.1, temperature scalar values are given. For the traditional designs, it is observed that the minimum and maximum temperature values are lower and higher respectively than the newly developed ones, which results in the higher temperature difference. Also, the area weighted averages of the temperature is higher. This increases the possibility of occurrence of the problems caused by the high temperature gradient and the high temperature. So, it can be concluded that, the newly developed designs are advantageous than the traditional ones in terms of the temperature gradient and the maximum temperature that occurs at selected surfaces. Also, note that when Co-Flow and Cross-Flow results are compared, it is observed that, Co-Flow design is advantageous, which is the same result obtained by [33-35].

Table 5.1 Scalar values of temperature results at the anode/cathode-electrolyte surface

Design Configuration	T_{min} at Electrolyte Surface (Kelvin)	T_{max} at Electrolyte Surface (Kelvin)	ΔT at Electrolyte Surface (Kelvin)	T_{ave} at Electrolyte Surface (Kelvin)
Cross-Flow	1195.9	1230.9	34.9	1216.5
Co-Flow	1196.2	1230.1	33.9	1219.8
G-1	1196.5	1219.1	22.6	1213.4
G-2	1199.2	1220.4	21.2	1216.1
G-3	1199.8	1217.2	17.5	1213.8

Besides the temperature, uniform distribution of the temperature at the selected surfaces is also important and must be included in the comparison. This can be observed by obtaining standard deviation values of the temperature at these surfaces, which is the variation or dispersion of the selected values from the average. The higher standard deviation value means, the data is spread over a larger range with respect to average. In Table 5.2, the standard deviation of the temperature at the selected surfaces is given. It is observed that, for the traditional designs, the standard deviation is higher, whereas for the newly developed designs it is lower. This result gives weight to the idea that, the new designs have more uniform temperature profile at the selected surfaces than the traditional ones. This development decreases the probability of occurrence of the problems caused by the high temperature gradient.

When these results, minimum temperature T_{min}, maximum temperature T_{max}, temperature difference ΔT and the standard deviation at selected surfaces are investigated in detail, it can be said that, besides the five designs, G-3 is more advantageous than the other four.

Table 5.2 Standard deviation of temperature

Design Configuration	Standard Deviation of Temperature at the Selected Surface
Cross-Flow	9.1
Co-Flow	9.5
G-1	5.2
G-2	4.5
G-3	3.9

One must be aware of the fact that, these increases in the temperature during SOFC operation are a result of occurring electro-chemical reactions. As a result of the reactions, an electric power and a heat are generated. The power obtained and the heat generated are dependent on each other linearly. That is, when power obtained is high, more heat is generated. Also, please note that, the anode/cathode-electrolyte surface is the center of the heat/electricity generation. So, it is observed that, there must be a relationship between the temperature distribution and the current density at the anode/cathode-electrolyte surface. This relationship can be investigated from Figures 5.3-5.7 and from Figures 5.8-5.12 respectively. From comparison, it is observed that, at the anode/cathode-electrolyte surface, the temperature and the current density values are inversely proportional to each other. That is, at any point on the anode/cathode-electrolyte surface, when the temperature is high then the current density is low and vice versa. This again can be explained by the fact that, heat generated in electrochemical reactions is carried through the outlet, where the maximum temperature occurs, but the maximum current density occurs at different regions depending on the mole fractions of hydrogen and oxygen. Also, from Figures 5.8-5.12, it is observed that, G-3 has more uniform current density distribution than the others, which is important in the lifetime of the PEN.
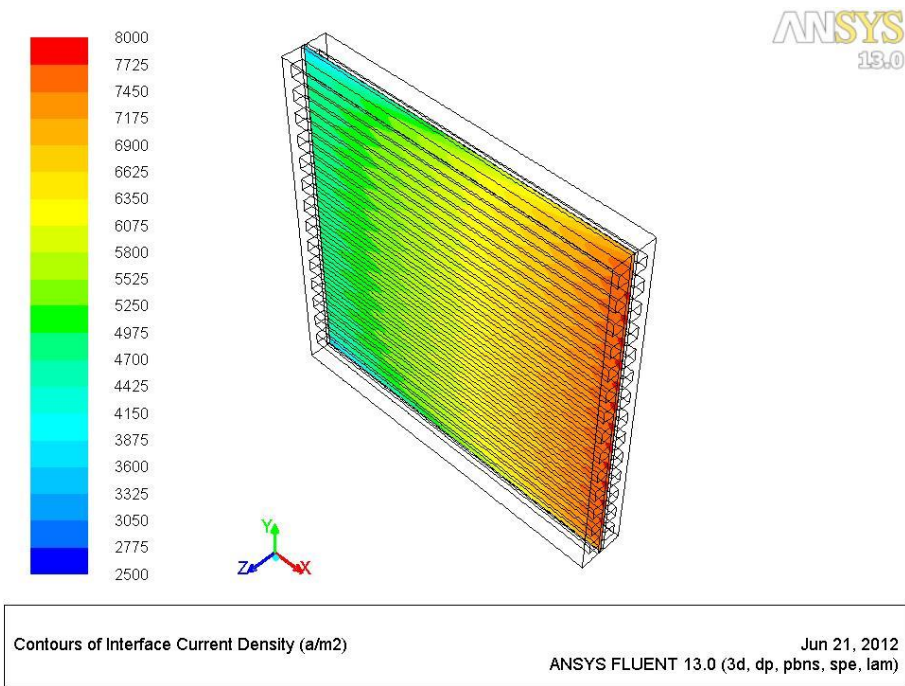
Figure 5.8 Interface current density at the anode/cathode-electrolyte surface for Co-Flow design
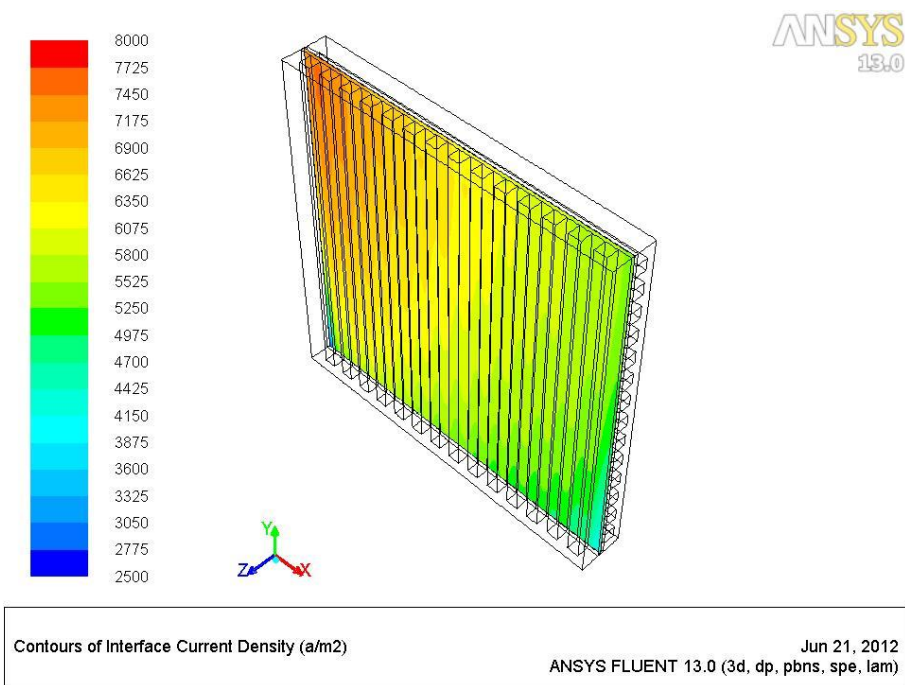
Figure 5.9 Interface current density at the anode/cathode-electrolyte surface for Cross-Flow design
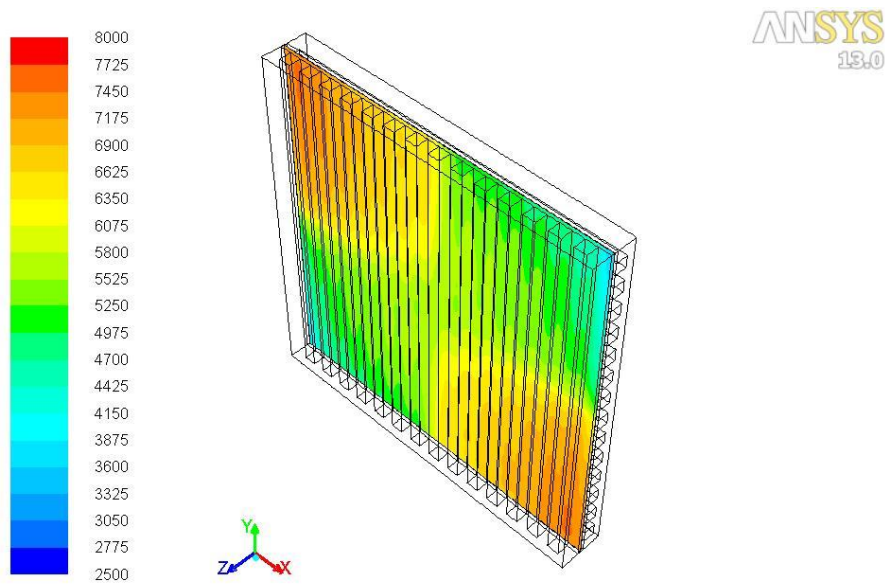
Figure 5.10 Interface current density at the anode/cathode-electrolyte surface
for G-1 design
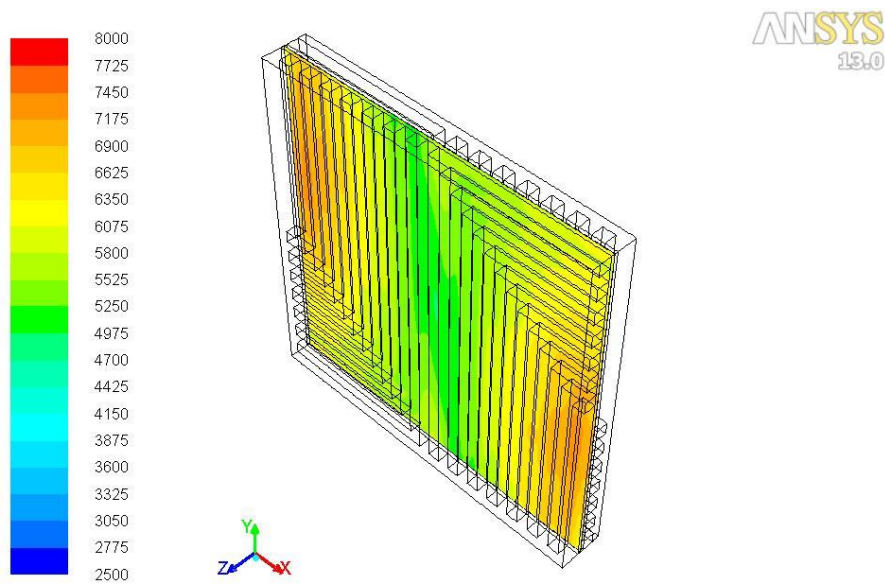
Figure 5.11 Interface current density at the anode/cathode-electrolyte surface
for G-2 design
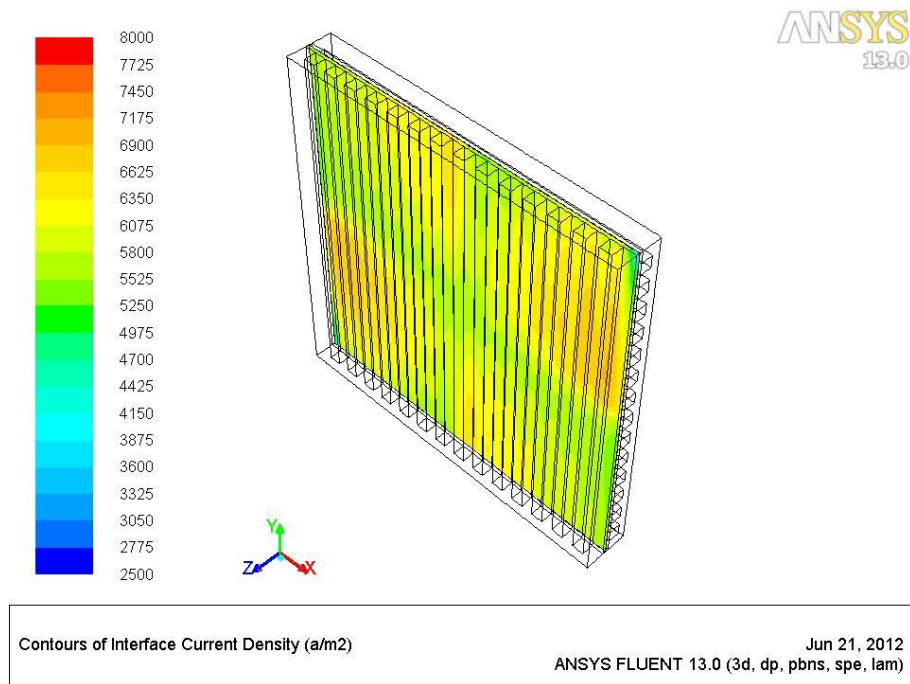
Figure 5.12 Interface current density at the anode/cathode-electrolyte surface
for G-3 design

When dealing with temperature problems with the aim of developments in designs, the SOFC stack power must also be compared for different designs. In Table 5.3, the power and current obtained from the five SOFC stack designs under 0.6 V is given. It is observed that, under the same operating conditions, Cross-Flow design and G-3, have the maximum output power. In fact, Cross-Flow design has the maximum output power with only 0.15% higher than G-3. But, when the advantages of G-3 in terms of temperature are considered, this 0.15% output power difference is acceptable.

Table 5.3 Power output for different geometries

Design Configuration	Current at 0.6 Volt (Ampere)	Power (Watt)
Cross-Flow	11.49	6.89
Co-Flow	11.41	6.85
G-1	11.35	6.81
G-2	11.40	6.84
G-3	11.46	6.88

Besides the power obtained from any design, the species concentrations should also be compared, because it is another indication of the efficiency in design. For the same power output, lower fuel and air utilizations mean better design. As shown in Table 5.4, the species concentrations are very close to each other. So, it can be concluded that, with the newly develop designs, good thermo-structural ability with the similar power output is achieved with the similar fuel and air utilization ratios.

Table 5.4 Species concentrations at the outlets

Design Configuration	Mole fraction of H_2 at outlet	Mole fraction of O_2 at outlet
Cross-Flow	0.6478	0.0795
Co-Flow	0.6501	0.0807
G-1	0.6486	0.0813
G-2	0.6506	0.0802
G-3	0.6448	0.0798

To operate an SOFC stack more efficiently, the power consumed during operation of the SOFC stack must also be considered and must be as low as possible. The major power used to operate the SOFC stack is consumed in heating the SOFC to the operating temperatures and pumping the fuel and oxidant to the SOFC stack. After the SOFC stack starts to generate power, it also starts to generate the heat so the energy need for the heating vanishes. But the pumping power need for the fuel and oxidant supply goes on as long as the SOFC stack runs.

The power consumed, in supplying the fuel and oxidant, mainly depends on the pressure drops at the interconnectors. So, this situation must also be taken into account in developing new interconnector designs.

In Table 5.5, the pressure losses at the anode and cathode gas flow channels are given. From the results, it is observed that, G-3 has another important advantage over the other designs, which is the lowest pressure loss at the anode gas flow channels.

Table 5.5 Pressure loss at the anode and cathode flow channels

Design Configuration	ΔP_{anode} (Pascal)	$\Delta P_{cathode}$ (Pascal)
Cross-Flow	7.86	13.38
Co-Flow	7.95	13.34
G-1	7.39	12.85
G-2	7.58	13.23
G-3	7.29	12.93

5.1.2 Results with Turbulence Model

The same models for all of the designs are also solved with a turbulence model, to show the result independency on the flow model and see the effect of the wall roughness on the cell performance. Also, the turbulence model results should reveal the existence of the turbulence, if any. From Table 5.6, the results related to the temperature are given for the laminar and turbulence models. It is observed that, the results only differ after the second digit after the floating point so, it can be said that, the two models give very close answers to each other.

Table 5.6 Temperature results from the laminar and the turbulence models

Design Configuration		T_{min} at Electrolyte Surfaces (Kelvin)	T_{max} at Electrolyte Surfaces (Kelvin)	T_{ave} at Electrolyte Surfaces (Kelvin)	Standard Deviation of Temperature
Cross-Flow	Laminar	1195.982	1230.945	1216.496	9.10384
	Turbulence	1195.974	1230.940	1218.878	9.10381
Co-Flow	Laminar	1196.238	1230.144	1219.791	9.45826
	Turbulence	1196.230	1230.137	1219.784	9.45825
T_1	Laminar	1196.483	1219.091	1213.434	5.20091
	Turbulence	1196.472	1219.080	1213.422	5.20067
T_2	Laminar	1199.215	1220.393	1216.099	4.46543
	Turbulence	1199.207	1220.384	1216.090	4.46512
T_3	Laminar	1199.748	1217.233	1213.781	3.94745
	Turbulence	1199.738	1217.221	1213.769	3.94695

When power outputs are compared, it is also observed that, results are very close to each other, as shown in Table 5.7.

Table 5.7 Power from the laminar and the turbulence models

Design Configuration		Current at 0.6 V (Ampere)	Power (Watt)
Cross-Flow	Laminar	11.48847	6.89308
	Turbulence	11.48883	6.89330
Co-Flow	Laminar	11.40823	6.84494
	Turbulence	11.40821	6.84493
T_1	Laminar	11.34580	6.80748
	Turbulence	11.34589	6.80753
T_2	Laminar	11.39881	6.83929
	Turbulence	11.39889	6.83933
T_3	Laminar	11.46280	6.87768
	Turbulence	11.46291	6.87775

Also, the species concentrations at the outlets must be compared. The results are shown in Table 5.8. It is observed that, results are very close to each other.

Table 5.8 Species concentrations from the laminar and the turbulence models

Design Configuration		Mole fraction of H_2 at outlet	Mole fraction of O_2 at outlet
Cross-Flow	Laminar	0.647777	0.079502
	Turbulence	0.647704	0.079467
Co-Flow	Laminar	0.650078	0.080680
	Turbulence	0.650077	0.080677
T_1	Laminar	0.648579	0.081304
	Turbulence	0.648577	0.081300
T_2	Laminar	0.650587	0.080162
	Turbulence	0.650584	0.080157
T_3	Laminar	0.644788	0.079772
	Turbulence	0.644785	0.079768

Also, when pressure drop for two models are compared, again it is observed that, the results are nearly the same, as shown in Table 5.9.

Table 5.9 Pressure drop results from the laminar and the turbulence models

Design Configuration		ΔP_{anode} (Pascal)	$\Delta P_{cathode}$ (Pascal)
Cross-Flow	Laminar	7.8623	13.37461
	Turbulence	7.8608	13.36746
Co-Flow	Laminar	7.9527	13.33069
	Turbulence	7.9498	13.32364
T_1	Laminar	7.3865	12.85229
	Turbulence	7.3838	12.84548
T_2	Laminar	7.5768	13.22874
	Turbulence	7.5723	13.21718
T_3	Laminar	7.2929	12.93313
	Turbulence	7.2903	12.92632

From those comparisons for the laminar and turbulence models, it can be said that, the results are nearly the same. So, there is no turbulence in those designs. Also, it can be observed from this study that, the performance of the cell is not dependent on the wall roughness.

5.2 Anode Gas Recycle

Besides the temperature gradient, low fuel utilization ratio is another problem for the SOFC systems. Large amount of energy is consumed to generate the hydrogen. Generally in the SOFC systems, the reformer units are used to generate the hydrogen, which needs hydrocarbon fuel, water and sometimes heat for the endothermic reforming reactions. There is a need for energy in pumping fuel and water to a reformer unit, in addition to the heat necessary for the reforming reactions. Lots of electricity generated in the SOFC system is consumed in pumping the fuel and water because large pressure drops occur in a vaporization process of the fuel and water and in the reformer unit during reforming process. The recycling of the anode gas is a good solution to decrease this demand in energy. So, the recycling technique is also suggested in this study for the newly developed designs as well as the traditional designs. Numerical models are developed for each design and the results are compared.

In Figure 5.13, the mass flow inlets and the pressure outlets for those different designs are shown. For those designs, only the anode outlet is recycled because the cathode recycling is not efficient. As can be seen from the Figure 5.13, there are two mass flow inlets and two pressure outlets corresponding to the mass flow inlets. The total mass flow rate of the hydrogen for recycling is half of the original case that is supplied to mass flow Inlet-1. The outlet from mass flow Inlet-1, which is called pressure Outlet-1, is fed to mass flow Inlet-2. By doing so, the temperature, the species concentrations and the mass flow rates for Inlet-2 are compared with the model results for original case for each design.
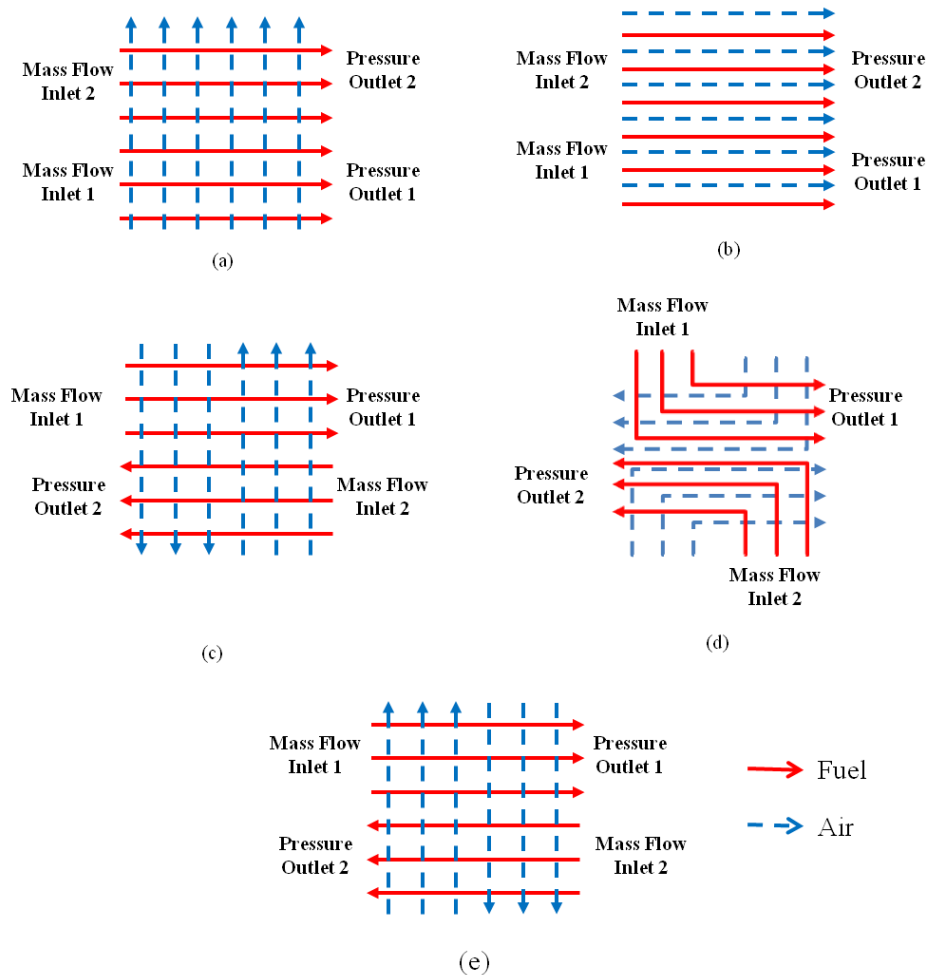
Figure 5.13 Traditional and developed geometries for recycling: (a) Cross-Flow, (b) Co-Flow, (c) G-1, (d) G-2, (e) G-3

For all of the designs, other than Cross-Flow, there is only one possible configuration but for Cross-Flow there are two possibilities that are feeding Outlet-1 to the Inlet-2 or feeding Outlet-2 to the Inlet-1, which make two different gas flow configurations, so the different results are obtained. The first configuration is referred to as Cross-Flow-1 and the second referred to as Cross-Flow-2. But for other design configurations, it does not make any difference because they are symmetric.

From Figures 5.14-5.19, the temperature profiles at the anode/cathode-electrolyte surface for different designs are shown. In these figures, the temperature scale is the same for ease of comparison. It is observed from the figures that, G-3 has the best temperature profile at the anode/cathode-electrolyte surface, which is the most important region in the SOFC also for the recycling case.

Also, please note the difference between the two different arrangements for Cross-Flow design. In Figure 5.15 and Figure 5.16, it is observed that the coldest region is different for the two different Cross-Flows recycling, which is observed at the original inlet not at the recycled inlet, because the recycled gas temperature is higher than the original one.
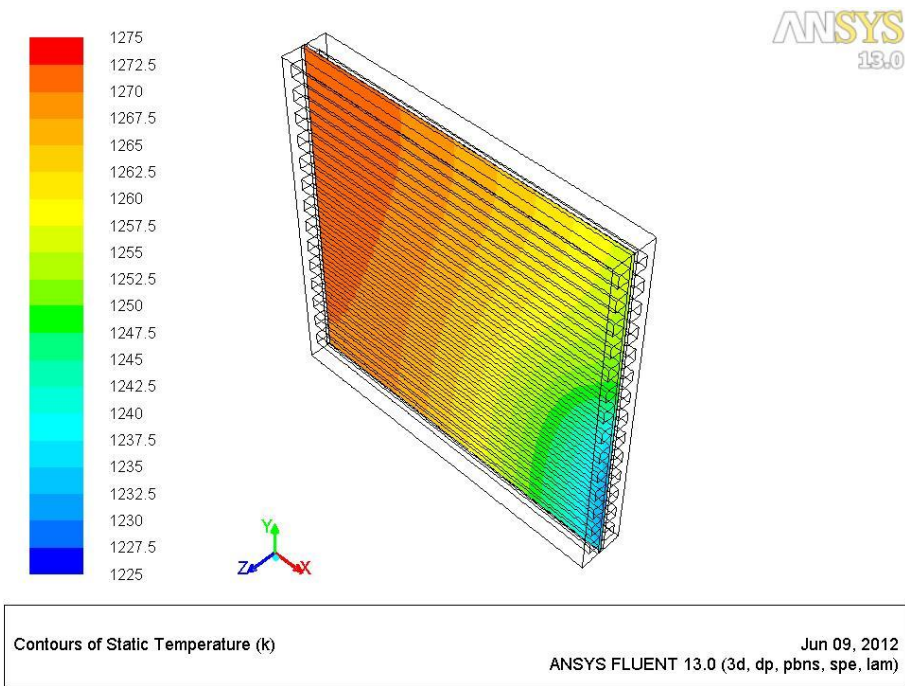
Figure 5.14 Temperature profile at the anode/cathode-electrolyte surface of Co-Flow stack design with recycling
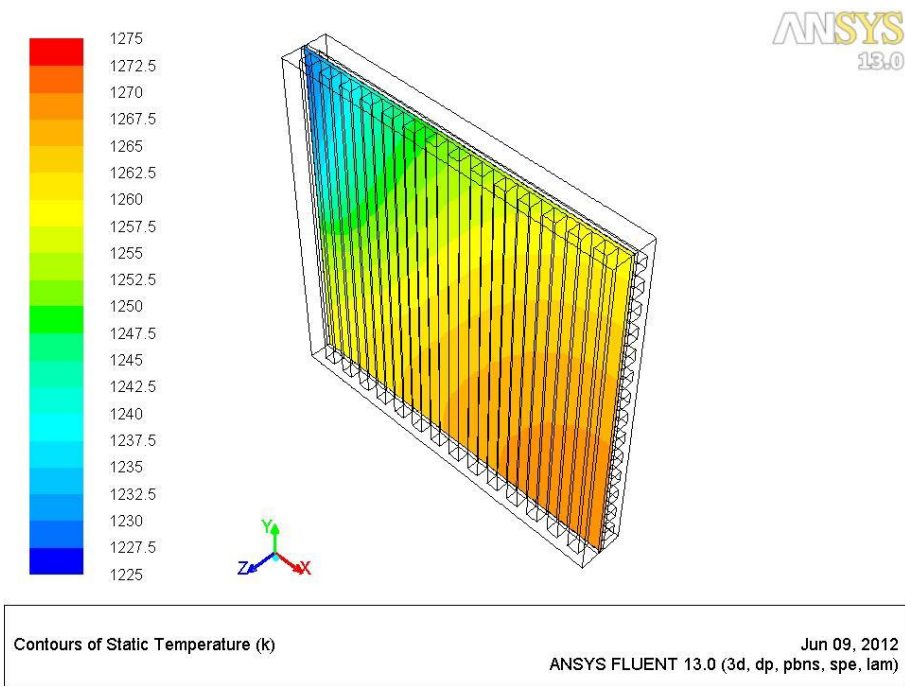
Figure 5.15 Temperature profile at the anode/cathode-electrolyte surface of Cross-Flow-1 stack design with recycling
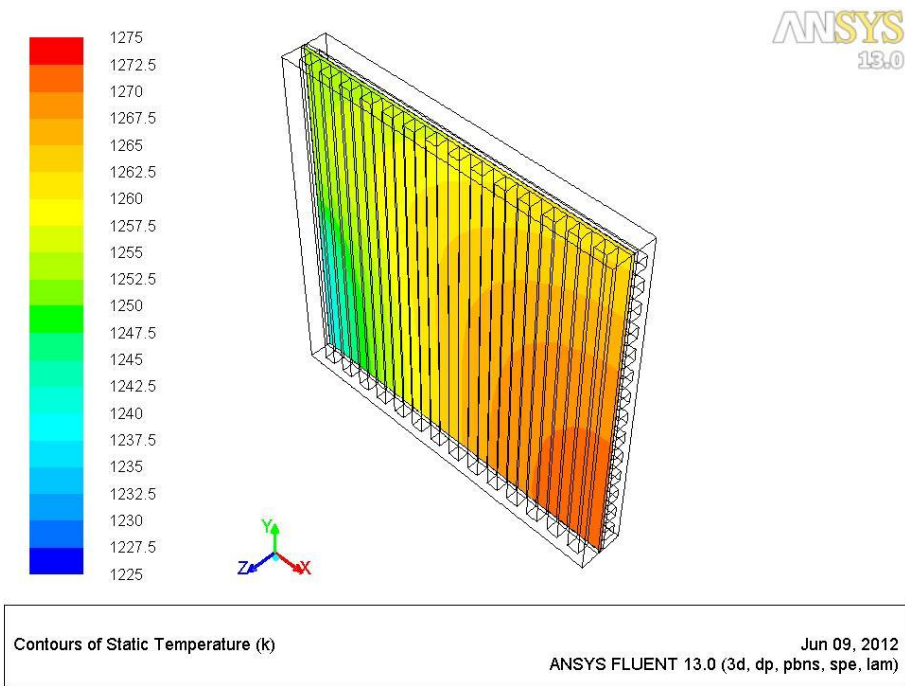
Figure 5.16 Temperature profile at the anode/cathode-electrolyte surface of Cross-Flow-2 stack design with recycling
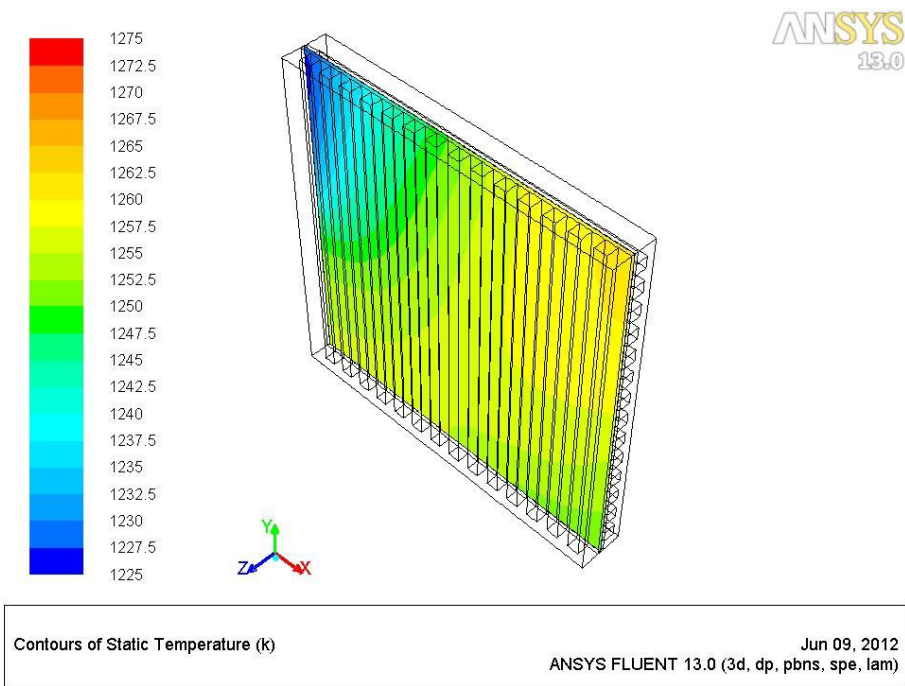
Figure 5.17 Temperature profile at the anode/cathode-electrolyte surface of G-1 stack design with recycling
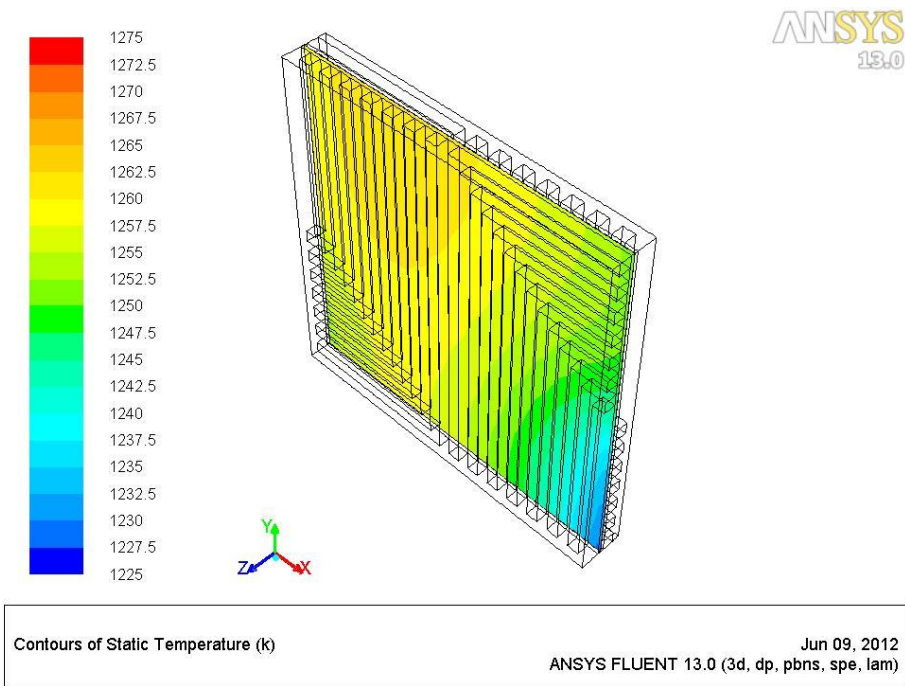
Figure 5.18 Temperature profile at the anode/cathode-electrolyte surface of G-2 stack design with recycling
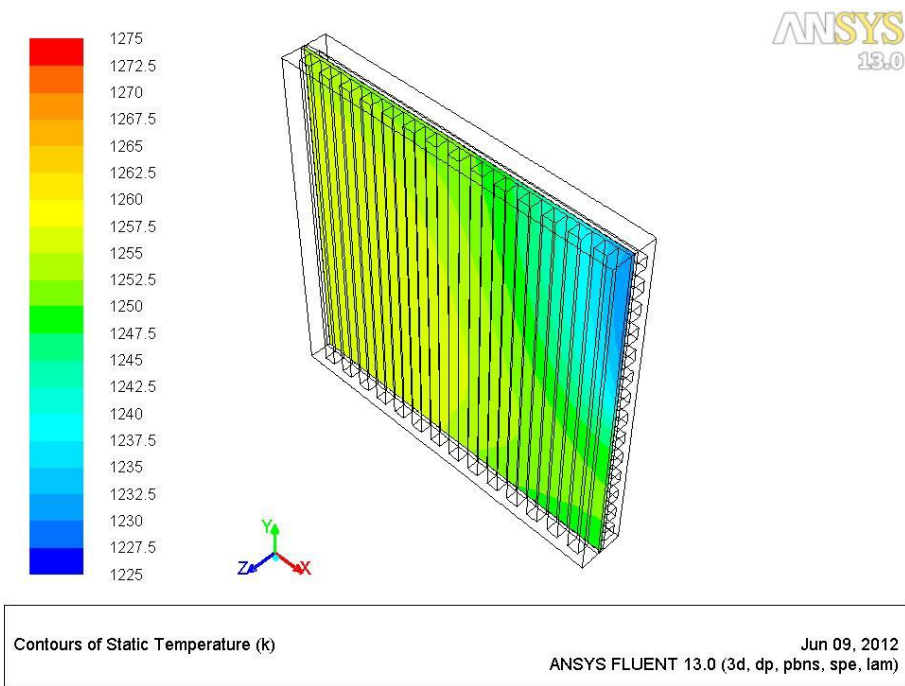
Figure 5.19 Temperature profile at the anode/cathode-electrolyte surface of G-3 stack design with recycling

Besides the temperature profiles figures, in Table 5.10, scalar values of the temperature results at the anode/cathode-electrolyte surface with the recycling are shown. As can be observed from Cross-Flow results, there is a distinct difference between the two different arrangements.

Also, when Table 5.1 and Table 5.10 are compared, it is observed that the minimum and the maximum temperatures and the standard deviations are higher for the recycling case. This is caused by the higher inlet temperature than the original for the recycled fuel. Temperature of the fuel increases until reaching the outlet, which is then recycled to the second inlet.

When Table 5.10 is investigated for temperature differences at the anode/cathode-electrolyte surface, it is observed that, G-3 has the lower temperature difference at the anode/cathode-electrolyte surface than the other designs. Also, again G-3 has the lowest standard deviation value. From the results obtained for the original case, these two results, the temperature difference and the standard deviation, are also the lowest for G-3 as can be observed from Table 5.1. So, it can be said that G-3 has the best temperature characteristics for the fuel recycling as well for the original conditions.

Table 5.10 Scalar values of temperature result at the anode/cathode-electrolyte surface with recycling

Design	T_{min} at Electrolyte Surface (Kelvin)	T_{max} at Electrolyte Surface (Kelvin)	ΔT at Electrolyte Surface (Kelvin)	T_{ave} at Electrolyte Surface (Kelvin)	Standard Deviation of Temperature
Co-Flow	1230.9	1271.9	41.0	1262.2	9.0
Cross-Flow	1228.6	1269.2	40.6	1258.6	8.6
	1237.4	1271.3	33.9	1261.1	7.1
G-1	1226.0	1260.2	34.2	1252.8	6.6
G-2	1228.8	1261.5	32.8	1255.4	6.1
G-3	1229.5	1257.3	27.8	1252.0	5.6

Besides the temperature comparison, other parameters should also be compared. In Table 5.11, the pressure losses with recycling are shown. From the table, it is observed that, the anode side pressure drop is the lowest for G-3

while the cathode side pressure drop is the lowest for G-1. These two results are also obtained for the original case as can be observed from Table 5.5. The results, with recycling, are slightly higher than the original case. This can be explained by the increased inlet temperature for the recycled inlet. It increases both the minimum and the maximum temperatures, which can be argued from Table 5.1 and Table 5.10 and pressure losses at flow channels. As a result, there will be less energy need for pumping the air and fuel with G-1 and G-3 respectively with recycling case also, which is an important advantage.

When the recycling and the original cases are compared, although the results for recycling are higher, recycling is the advantage of lower pumping power because there should be less pressure drop during the vaporization of the fuel, which is very high compared to the pressure drop in the flow channels.

Table 5.11 Pressure loss at the anode and cathode flow channels with recycling

Design Configuration		ΔP_{anode} (Pascal)	$\Delta P_{cathode}$ (Pascal)	Average ΔP_{anode} (Pascal)	Average $\Delta P_{cathode}$ (Pascal)
Co-flow	Inlet 1	8.11	14.12	9.84	14.28
	Inlet 2	11.57	14.44		
Cross-Flow	Inlet 1	8.05	11.62	9.84	14.21
	Inlet 2	14.03	14.38		
	Inlet 1	12.10	14.21	10.07	14.36
	Inlet 2	8.04	14.52		
G-1	Inlet 1	7.55	13.56	9.17	13.71
	Inlet 2	10.78	13.86		
G-2	Inlet 1	7.74	13.94	9.43	14.10
	Inlet 2	11.12	14.26		
G-3	Inlet 1	7.47	13.80	9.11	13.76
	Inlet 2	10.76	13.73		

Besides the pumping power, heat is also needed because of the endothermic reforming reactions. As discussed above, by recycling, the mass flow rate is half of the original case, so the energy needed for the reforming is also halved. In Table 5.12, the species concentrations at the outlet with the recycling are

shown. In that table, the mole fraction of H_2 at the outlets are given for the two outlets but the value at Outlet-2 for all design cases except Cross-Flow arrangement represents the final hydrogen concentration to be discharged. Also for Cross-Flow arrangement, the smallest value for the mole fraction of H_2 at the outlets represents the final hydrogen concentration to be discharged. When Table 5.4 and Table 5.12 are compared, it is observed that, the mole fraction of H_2 at the outlets is smaller for the recycling case. So, by taking into account that the fuel flow rate is halved, it can be said that, the fuel utilization is increased.

Table 5.12 Species concentrations at the outlets with recycling

Design Configuration		Mole Fraction of H_2 at Outlets	Mole Fraction of O_2 at Outlets	Average Mole Fraction of O_2 at Outlets
Co-Flow	Outlet 1	0.6224	0.0897	0.1007
	Outlet 2	0.4361	0.1117	
Cross-Flow	Outlet 1	0.6037	0.0929	0.1005
	Outlet 2	0.4374	0.1081	
	Outlet 1	0.4439	0.0908	0.0987
	Outlet 2	0.6298	0.1065	
G-1	Outlet 1	0.6027	0.0984	0.1006
	Outlet 2	0.4478	0.1030	
G-2	Outlet 1	0.6173	0.0879	0.0998
	Outlet 2	0.4402	0.1117	
G-3	Outlet 1	0.6004	0.1037	0.0996
	Outlet 2	0.4418	0.0954	

When Table 5.12 is compared with Table 5.4, for the average mole fraction of O_2 at the outlets, it is observed that, the mole fraction of O_2 is higher for the recycling case. This can be explained by the decrease in the H_2 mass flow rate and concentration due to the recycling. So as a result of this, a decrease in the power output is also expected. The power output for recycling and its comparison with the original cases are given in Table 5.13. From this table, it is observed that, there is a decrease in the output power. Total amount of decrease in the power needed for the fuel pumping and the energy needed for

the endothermic reforming reactions, is higher than the decrease in the output power. So, the recycling of the anode gas should be preferable.

Table 5.13 Comparison of the output power for the recycling and the original cases

Design Configuration	Current at 0.6 V (Ampere)		Power (Watt)		Percent Decrease In Power Output
	With Recycling	Original Case	With Recycling	Original Case	
Co-Flow	9.81	11.49	5.88	6.89	14.63%
Cross-Flow	9.83	11.41	5.90	6.84	13.85%
	9.97		5.98		
G-1	9.81	11.35	5.89	6.81	13.54%
G-2	9.83	11.40	5.90	6.84	13.72%
G-3	9.89	11.46	5.94	6.88	13.70%

CHAPTER 6

CONCLUSION AND FUTURE STUDIES

In this thesis, a planar Solid Oxide Fuel Cell stack mathematical model including the fluid flow, heat and mass transfer and electro-chemical reactions is developed. In this model, all of the components in the SOFC stack, which are the solid interconnector, anode and cathode current collector, anode and cathode gas flow channels and Positive Electrode-Electrolyte-Negative Electrode (PEN), are considered. The model is formed using Fluent$^{®}$ commercial product. The model is verified and validated with the experiments considering the single SOFC cell. The validated case is used as a reference for further studies. The electrochemical parameters, operating conditions and boundary conditions are optimized using the experiments performed at Vestel Defense Industries.

6.1   Conclusion

The aim of this study is, to offer a new flow arrangement to minimize the problems caused by the heat generation during the operation of the SOFC stack and to offer a recycling technique to increase the fuel utilization. Three different designs are developed. Developed designs are compared with the traditional ones to see the improvements.

The mathematical model results show several improvements. The major ones are listed below:

   a) The developed interconnector designs gives lower maximum temperature over the PEN surface, which decreases the possibility of

failure of the SOFC stack components such as the sealing material, due to the high temperature.

b) When an SOFC stack is formed, the components are assumed to be bonded together. Lower thermal stresses will occur with the achievement of a lower maximum temperature.

c) The newly developed interconnector designs also show lower temperature differences and standard deviations in the most important component of the SOFC, PEN. This improvement decreases the thermal stress formed as a result of temperature gradients, which may cause the SOFC PEN to break down.

d) The lower temperature difference and standard deviation also results in the more uniform power generation from the PEN, which is also advantageous considering the long time operation of the SOFC stack.

e) With G-3, the lower pressure losses in the anode and the cathode gas flow channels are achieved with only 0.15% difference in the power compared to the traditional Cross-Flow design. This increases the efficiency of the SOFC stack since lower pumping powers for the fuel and air are needed.

f) The anode gas recycling techniques are offered for all of the considered designs. The fuel utilization is increased with an acceptable decrease in the power output.

g) With the recycling case, it is also obvious that, G-3, is advantageous than the traditional and newly developed ones in terms of their temperature characteristics.

6.2 Future Work Suggestions

By its nature, the mathematical modeling includes several assumptions and simplifications. Several assumptions and simplifications are done in this study also. These assumptions and simplifications affect the reliability of the mathematical model. Therefore, the following studies are planned for further

studies to improve the mathematical model and to improve the thermal stability of the SOFC stack:

- The temperature dependent exchange current densities are going to be evaluated.
- The experimental setup is going to be devised for the developed designs to validate the mathematical models.
- The mathematical model will be improved by including the furnace in the model to account for the heat transfer caused by the convection and radiation at the external surfaces of the SOFC stack.
- The mathematical model will be improved by including the gas feed headers/manifolds in the model geometry to increase the reliability of the mathematical models.
- Optimization of parameters such as the anode and cathode gas flow rates and the concentrations is going to be modeled and verified with experiments.
- The PEN with a higher active area is going to be modeled and verified.

REFERENCES

[1] A. B. Stambouli, E. Traversa, Solid Oxide Fuel Cells (SOFCs), "A review of an environmentally clean and efficient source of energy", Renewable and Sustainable Energy Reviews 6 (2002) 433–455.

[2] S. R. Pakalapati, "A new reduced order model for solid oxide fuel cells", Ph.D. Dissertation, College of Engineering and Mineral Resources at West Virginia University, Morgantown, West Virginia (2006).

[3] K. C. Pulagam, "Optimization of solid oxide fuel cell interconnector design", M.S. Thesis, University of Nevada, Las Vegas (2009).

[4] O. Yamamoto, "Solid oxide fuel cells: fundamental aspects and prospects", Electrochimica Acta 45 (2000) 2423–2435.

[5] Ansys Fluent Fuel Cell Modules Manual, Release 13.0, November 2010.

[6] B. Timurkutluk, "Performance analysis of an intermediate temperature solid oxide fuel cell" , M.S. Thesis, Middle East Technical University Graduate School of Natural and Applied Sciences, Ankara, (2007).

[7] D. Bhattacharyya, R. Rengaswamy, C. Finnerty, "Isothermal models for anode-supported tubular solid oxide fuel cells", Chemical Engineering Science 62 (2007) 4250 – 4267.

[8] H. Chen, S. Yang, S. Huang, Y.P. Chyou , "A paraffin fueled SOFC system design and integration", Journal of the Chinese Institute of Chemical Engineers, 38 (2007) 185-190.

[9] T. Seitarides, C. Athanasiou, A. Zabaniotou, "Modular biomass gasification based solid oxide fuel cells (SOFC) for sustainable development" , Renewable and Sustainable Energy Reviews, 12 (2008) 1251-1276.

[10] D. L. Cresswell, I. S. Metcalfe, "Energy integration strategies for solid oxide fuel cell systems", Solid State Ionics 177 (2006) 1905–1910.

[11] M. L. Ferrari, A. Traverso, L. Magistri, A. F. Massardo, "Influence of the anodic recirculation transient behavior on the SOFC hybrid system performance" , Journal of Power Sources 149 (2005) 22–32.

[12] P.F. Oosterkamp, "Critical issues in heat transfer for fuel cell systems", Energy Conversion and Management 47 (2006) 3552–3561.

[13] S. Murthy, A. G. Fedorov, "Radiation heat transfer analysis of the monolith type solid oxide fuel cell", Journal of Power Sources 124 (2003) 453–458.

[14] S. C. Singhal, "Advances in solid oxide fuel cell technology", Solid State Ionics 135 (2000) 305–313.

[15] R. Bove, S. Ubertini, "Modeling solid oxide fuel cell operation: Approaches, techniques and results", Journal of Power Sources 159 (2006) 543-559.

[16] S. C. Singhal, K. Kendall, "High Temperature Solid Oxide Fuel Cells: Fundamentals, Design and Applications (2003)", Elsevier Advanced Technology, The Boulevard, Langford Lane, Kidlington Oxford OX5 lGB, UK, p 205.

[17] S. Aksongur, "Farklı Çalışma Parametrelerinde Katı Oksit Yakıt Pillerinin Sayısal Analizi" , M.S. Thesis, Gazi University Graduate School of Natural and Applied Sciences, Ankara, (2012).

[18] C. Lee, J. Bae, "Fabrication and characterization of metal-supported solid oxide fuel cells", Journal of Power Sources 176 (2008) 62–69.

[19] I. Antepara, I. Villarreal, L. M. Rodriguez-Martıınez, N. Lecanda, U. Castro, A. Laresgoiti, "Evaluation of ferritic steels for use as interconnects andporous metal supports in IT-SOFCs", Journal of Power Sources 151 (2005) 103–107.

[20] S. H. Chan, K. A. Khor, Z. T. Xia, "A complete polarization model of a solid oxide fuel cell and its sensitivity to the change of cell component thickness", Journal of Power Sources 93 (2001) 130-140.

[21] S. Molin, B. Kusz, M. Gazda, P. Jasinski, "Evaluation of porous 430L stainless steel for SOFC operation at intermediate temperatures" , Journal of Power Sources 181 (2008) 31–37.

[22] S. Hui, D. Yang, Z. Wang, S. Yick, C. Deces-Petit, W. Qua, A. Tuck, R. Maric, D. Ghosh, "Metal-supported solid oxide fuel cell operated at 400–600 ^{o}C", Journal of Power Sources 167 (2007) 336–339.

[23] Y. B. Matus, L. C. De Jonghe, C. P. Jacobson, S. J. Visco, "Metal-supported solid oxide fuel cell membranes for rapid thermal cycling", Solid State Ionics 176 (2005) 443–449.

[24] Z. Wang, J. O. Berghaus, S. Yick, C. Deces-Petit, W. Qu, R. Hui, R. Maric, D. Ghosh, "Dynamic evaluation of low-temperature metal-supported solid oxide fuel cell oriented to auxiliary power units", Journal of Power Sources 176 (2008) 90–95.

[25] A. C. Burt, 2005, "Refinement of numerical models and parametric study of sofc stack performance", Ph.D. Dissertation, West Virginia University, Morgantown (2005).

[26] R. Bovea, P. Lunghia, N. M. Sammes, "SOFC mathematic model for systems simulations. Part one: from a micro-detailed to macro-black-box model" , International Journal of Hydrogen Energy 30 (2005) 181 – 187.

[27] R. Bovea, P. Lunghia, N. M. Sammes, "SOFC mathematic model for systems simulations. Part 2: definition of an analytical model" , International Journal of Hydrogen Energy 30 (2005) 189 – 200.

[28] B. Zitouni, H. B. Moussa, K. Oulmi, S. Saighi, K. Chetehouna, "Temperature field, H_2 and H_2O mass transfer in SOFC single cell: Electrode and electrolyte thickness effects", International Journal of Hydrogen Energy 34 (2009) 5032-5039.

[29] J. Shi, X. Xue, "CFD analysis of a symmetrical planar SOFC with heterogeneous electrode properties" , Electrochimica Acta 55 (2010) 5263-5273.

[30] H. Yakabe, T. Sakurai, "3D simulation on the current path in planar SOFCs" , Solid State Ionics 174 (2004) 295–302.

[31] Y. Yang, G. Wang, H. Zhang, W. Xia, "Computational analysis of thermo-fluid and electrochemical characteristics of MOLB-type SOFC stacks", Journal of Power Sources 173 (2007) 233–239.

[32] Z. Qu, P. V. Aravind, S. Z. Boksteen, N. J. J. Dekker, A. H. H. Janssen, N. Woudstra, A. H. M. Verkooijen, "Three-dimensional computational fluid dynamics modeling of anode-supported planar SOFC" , International Journal of Hydrogen Energy 36 (2011) 10209-10220.

[33] K. P. Recknagle, R. E. Williford, L. A. Chick, D. R. Rector, M. A. Khaleel, "Three-dimensional thermo-fluid electrochemical modeling of planar SOFC stacks", Journal of Power Sources 113 (2003) 109-114.

[34] E. Achenbach, "Three-dimensional and time-dependent simulation of a planar solid oxide fuel cell stack", Journal of Power Sources 49 (1994) 333-348.

[35] M. Iwata, T. Hikosaka, M. Morita, T. Iwanari, K. Ito, K. Onda, Y. Esaki, Y. Sakaki, S. Nagata, "Performance analysis of planar-type unit SOFC considering current and temperature distributions", Solid State Ionics 132 (2000) 297-308.

[36] C. Stiller, B. Thorud, S. Seljebø, Ø. Mathisen, "Finite-volume modeling and hybrid-cycle performance of planar and tubular solid oxide fuel cells", Journal of Power Sources 141 (2005) 227-240.

[37] Y. Wang, F. Yoshiba, T. Watanabe, S. Weng, "Numerical analysis of electrochemical characteristics and heat/ species transport for planar porous-electrode-supported SOFC" , Journal of Power Sources 170 (2007) 101–110.

[38] H. Liu, P. Li, J. V. Lew, "CFD study on flow distribution uniformity in fuel distributors having multiple structural bifurcations of flow channels", International Journal of Hydrogen Energy 35 (2010) 9186-9198.

[39] C. M. Huang, S. S. Shy, C. H. Lee, "On flow uniformity in various interconnects and its influence to cell performance of planar SOFC", Journal of Power Sources 183 (2008) 205-213.

[40] D. Grondin, J. Deseure, M. Zahid, M. J. Garcia, Y. Bultel, "Optimization of SOFC Interconnect Design Using Multiphysic Computation", Computer Aided Chemical Engineering Volume 25, 2008, Pages 841–846.

[41] M. Lockett, M. J. H. Simmons, K. Kendall, "CFD to predict temperature profile for scale up of micro-tubular SOFC stacks", Journal of Power Sources 131 (2004) 243–246.

[42] W. He, Q. Chen, "Three-dimensional simulation of a molten carbonate fuel cell stack under transient conditions" , Journal of Power Sources 73 (1998) 182–192.

[43] R. J. Boersma, N. M. Sammes, "Distribution of gas flow in internally manifolded solid oxide fuel-cell stacks", Journal of Power Sources 66 (1997) 41-45.

[44] H. Hirata, M. Hori, "Gas-flow uniformity and cell performance in a molten carbonate fuel cell stack", Journal of Power Sources 63 (1996) 115-I20.

[45] J. Park, J. Bae, "Characterization of electrochemical reaction and thermo-fluid flow in metal-supported solid oxide fuel cell stacks with various manifold designs", International Journal of Hydrogen Energy 37 (2012) 1717-1730.

[46] W. Bi, D. Chen, Z. Lin, "A key geometric parameter for the flow uniformity in planar solid oxide fuel cell stacks", International Journal of Hydrogen Energy 34 (2009) 3873-3884.

[47] B. J. Koeppel, K. Lai, M. A. Khaleel, "Effect of geometry and operating parameters on simulated sofc stack temperature uniformity", FuelCell2011-54803 pp. 475-484.

[48] A. C. Burt , I. B. Celik, R. S. Gemmen, A.V. Smirnov, "A numerical study of cell-to-cell variations in a SOFC stack", Journal of Power Sources 126 (2004) 76-87.

[49] T. Tanaka, Y. Inui, A. Urata, T. Kanno, "Three dimensional analysis of planar solid oxide fuel cell stack considering radiation" , Energy Conservation and Management 48 (2007) 1491-1498.

[50] W. B. Guan, H. J. Zhai, L. Jin, C. Xu, W. G.Wang, "Temperature Measurement and Distribution Inside Planar SOFC Stacks", Fuel Cells DOI: 10.1002/fuce.201100127.

[51] C. Lin, T. Chen, Y. Chyou, L. Chiang, "Thermal stress analysis of a planar SOFC stack", Journal of Power Sources 164 (2007) 238–251.

[52] R. O. Hayre, S. Cha, W. Collela, F. B. Prinz (2009), Fuel Cell Fundamentals, 2nd edition, John Wiley & Sons Ltd.

[53] Ansys Fluent theory Guide, Release 13.0, November 2010.

[54] K. J. Daun, S. B. Beale, F. Liu, G. J. Smallwood, "Radiation heat transfer in planar SOFC electrolytes", Journal of Power Sources 157 (2006) 302-310.

[55] M. Ni, M. K. H. Leung, D. Y. C Leung, "Parametric study of solid oxide fuel cell performance", Energy Conversion and Management 48 (2007) 1525-1535.

[56] B. Timurkutluk, S. Celik, C. Timurkutluk, M. D. Mat, Y. Kaplan, "Novel structured electrolytes for solid oxide fuel cells", Journal of Power Sources 213 (2012) 47-54.

[57] USFCC Materials and Components Working Group, "Fuel Cell Leak Testing Requirements and Procedure", US Fuel Cell Council, 04-070A May 1, 2006.

[58] S. Campanari, P. Iora, "Comparison of Finite Volume SOFC Models for the Simulation of a Planar Cell Geometry" , Fuel Cells 2005, 5, No.1.

[59] Catia-V5 R17.

A   SOFC MODEL SETUP PROCEDURES FOR FLUENT®

Fluent® developed the SOFC Unresolved Electrolyte Module for the modeling and simulating 3-D SOFC designs. A separate license is needed for this module. The following steps illustrate how the SOFC model is setup with Fluent®.

i.   **Start Fluent® and Import the Mesh**

- Start Fluent® 13.0 with 3-D and double precision.
- Import the mesh file (File → Read → Mesh).
- Scale the mesh if necessary (General → Mesh → Scale).
- Check the mesh (General → Mesh →Check).
- Select the solver type (General → Solver → Type → Pressure-Based).
- Determine the velocity formulation (General → Solver → Velocity Formulation → Absolute).
- Select the time formulation (General → Solver → Time → Steady).

ii. **Start SOFC Module**

- Via text user interface (TUI) write the followings in the order and press "enter" after each command; "define → models → addon-module".
- A list of Fluent® addon-modules will be displayed as shown below:

Fluent® Addon Modules:

    0. None

1. MHD Model

2. Fiber Model

3. Fuel Cell and Electrolysis Model

4. SOFC Model with Unresolved Electrolyte

5. Population Balance Model

Enter Module Number: [0]

- Write "4" and press "enter"

iii. **Model Setup for the Fluid Flow, Heat Transfer and Species Transport**

- Turn on the energy equation (Problem Setup → Models → Energy) as shown in Figure A.1.
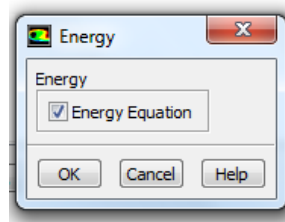
Figure A.1 A screen shot for turning on energy equation

- Determine the flow characteristic (Problem Setup → Models → Viscous) as shown in Figure A.2.
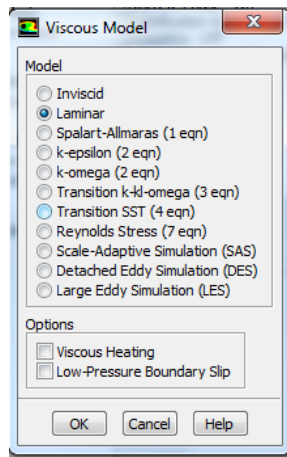
Figure A.2 A screen shot for determining the flow characteristic

- Determine the species transport and the reaction model as shown in Figure A.3.
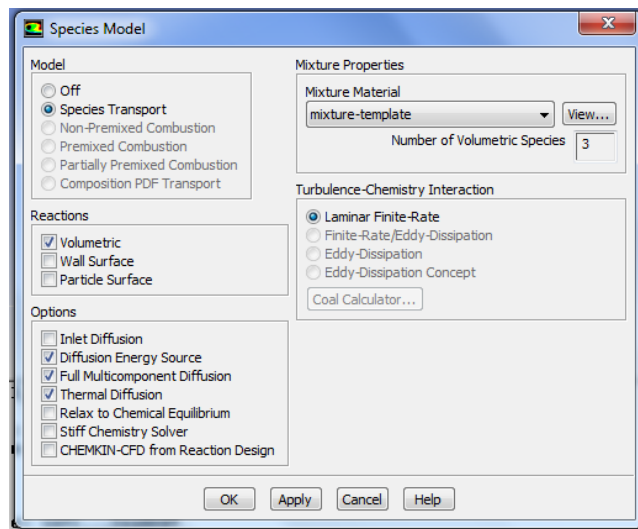
Figure A.3 A screen shot for determining the species transport and reaction model

iv. Model Setup for the SOFC Electro-Chemical Parameters

In this section, the parameter scalar values shown in the figures are an example for a planar SOFC.

- Turn on the SOFC Model (Problem Setup → Models → SOFC (Unresolved Electrolyte)) and edit the parameters shown in the red bracket under the "Model Parameters" tab as shown in Figure A.4.
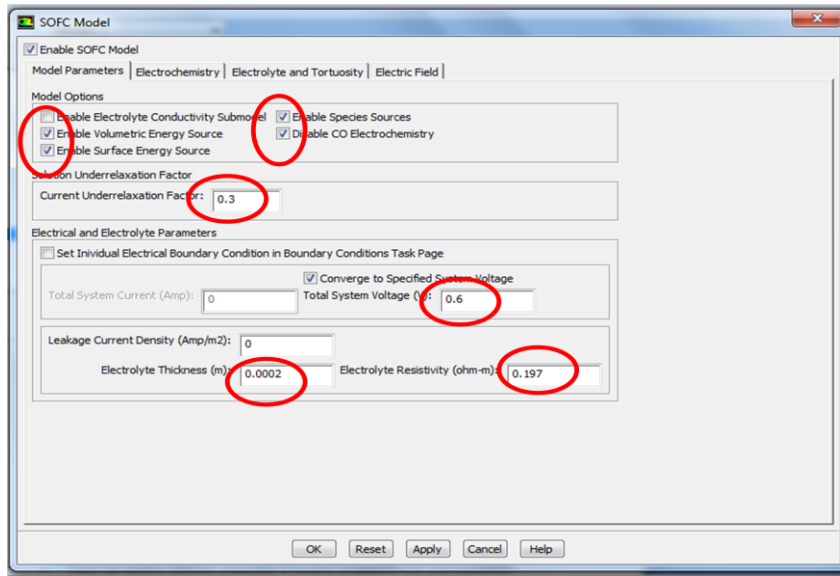
Figure A.4 A screen shot for turning on the SOFC model

- Edit the parameters shown in the red bracket under the "Electrochemistry" tab as shown in Figure A.5.
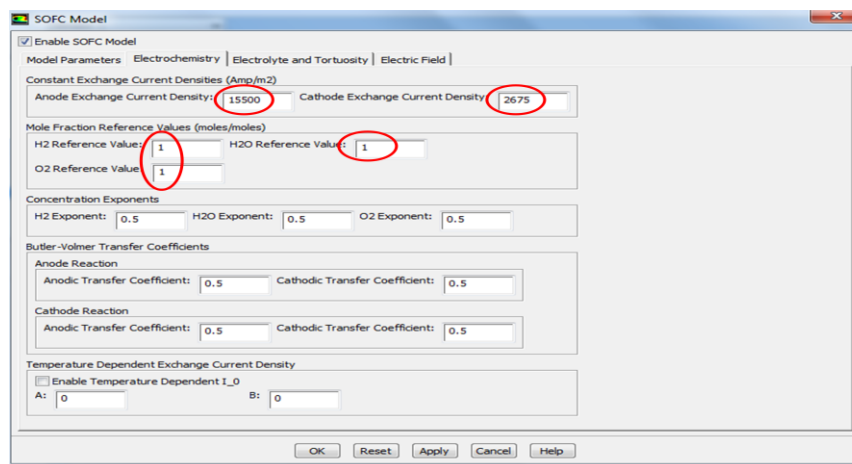
Figure A.5 A screen shot for editing the electrochemistry parameters

- Under "Electrolyte and Tortuosity" tab, define the tortuosity value for the anode and the cathode and determine the anode and cathode interfaces of the PEN as shown in Figure A.6.
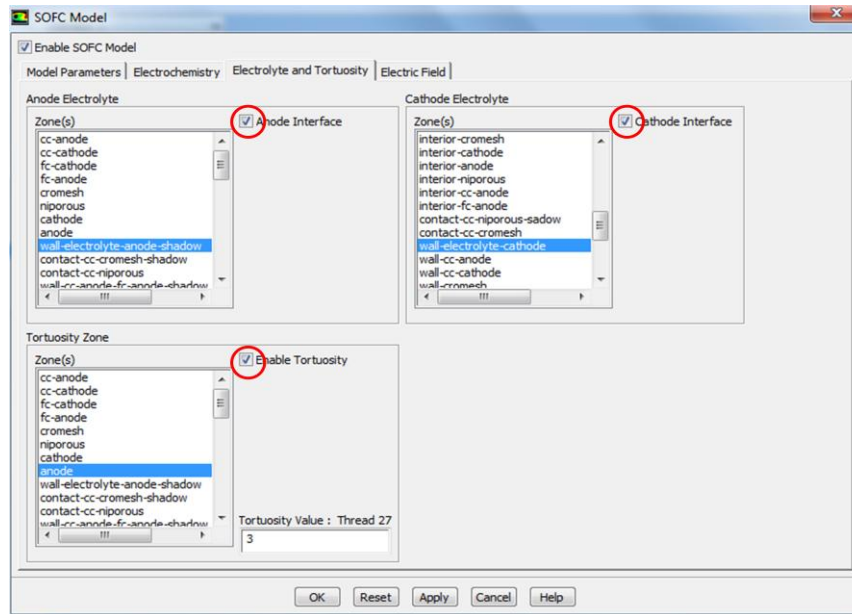
Figure A.6 A screen shot for defining the PEN properties

- Define the electrical parameters under "Electric Field" tab as shown in Figure A.7.
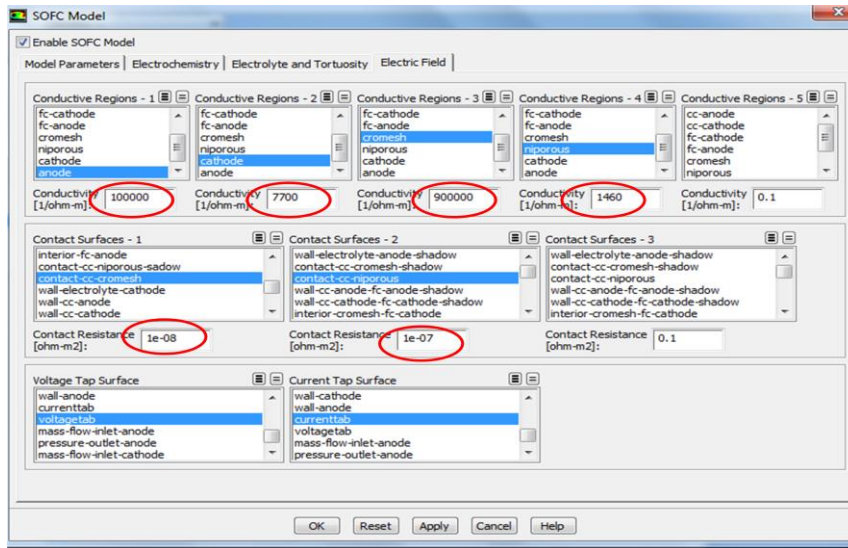
Figure A.7 A screen shot for defining the electrical parameters

v.   Specify the Material Properties

- Define a User-defined scalar. Chang the Number of User-Defined scalars to 1 and indicate node as the Flux Function (Define → User-Defined → Scalars).

- Define 14 User-Defined Memory Locations (Define → User-Defined → Memory).

- Define User-Defined Function Hooks. Change the Adjust function to adjust_function (Define → User-Defined → Function Hooks).

- Create or re-define the new solid materials as appropriate for the electrodes and the electrolyte according to the problem specifications.

- Edit the mixture template by specifying the mixture species names (Problem Setup → Materials → Mixture). Change the names in the order same with the screen shot as shown in Figure A.8.

107
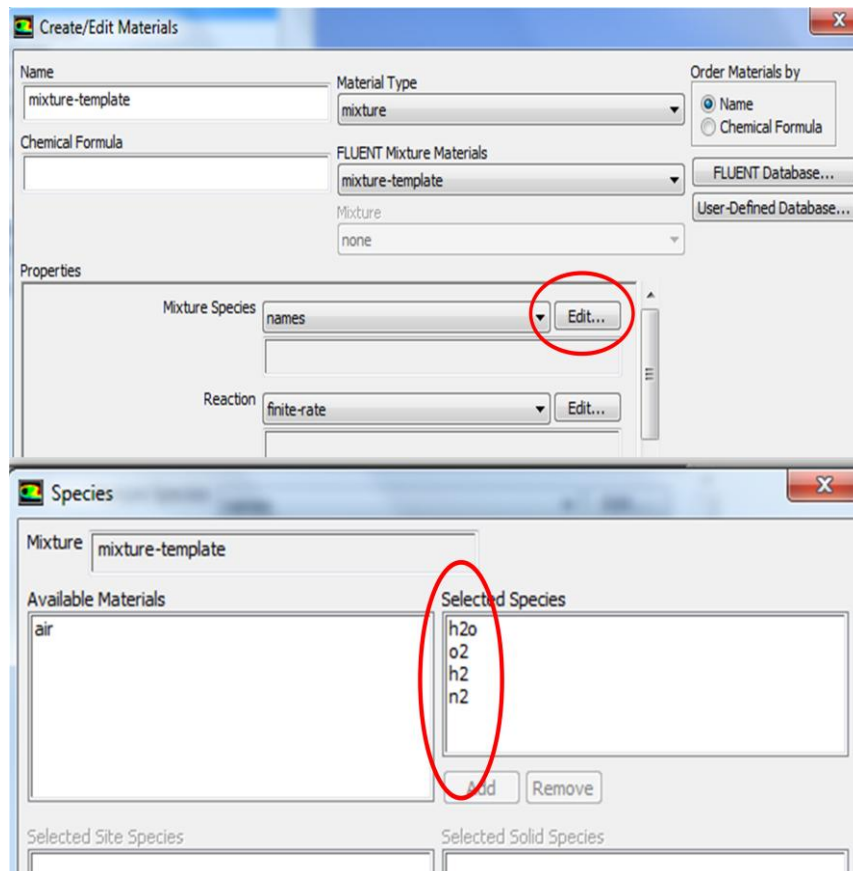
Figure A.8 A screen shot for editing the mixture template

- Change density to the incompressible-ideal-gas, C_p to the mixing law, thermal conductivity and viscosity to the ideal-gas mixing law, Mass Diffusivity to User-Defined and select diffusivity::SOFC, the UDS Diffusivity to User-Defined and select E_Conductivity::SOFC.

vi. **Operating and Boundary Conditions**

- There is no need to make change in the operating condition unless otherwise specified (Problem Setup → Cell Zone Conditions → Operating Conditions).

- Define Cell Zone Conditions for the each component of an SOFC separately with their corresponding values as shown in Figure A.9 and as shown in Figure A.10.
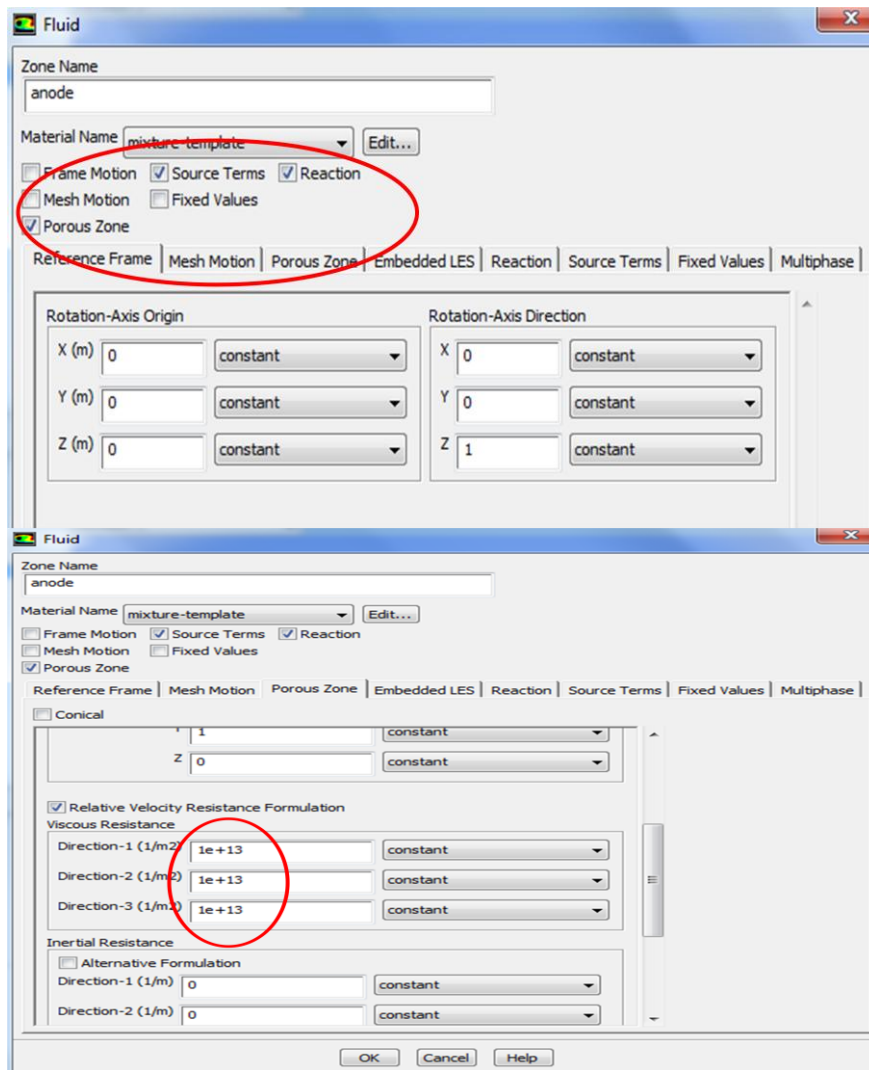
Figure A.9 A screen shot for defining the cell zone conditions-1
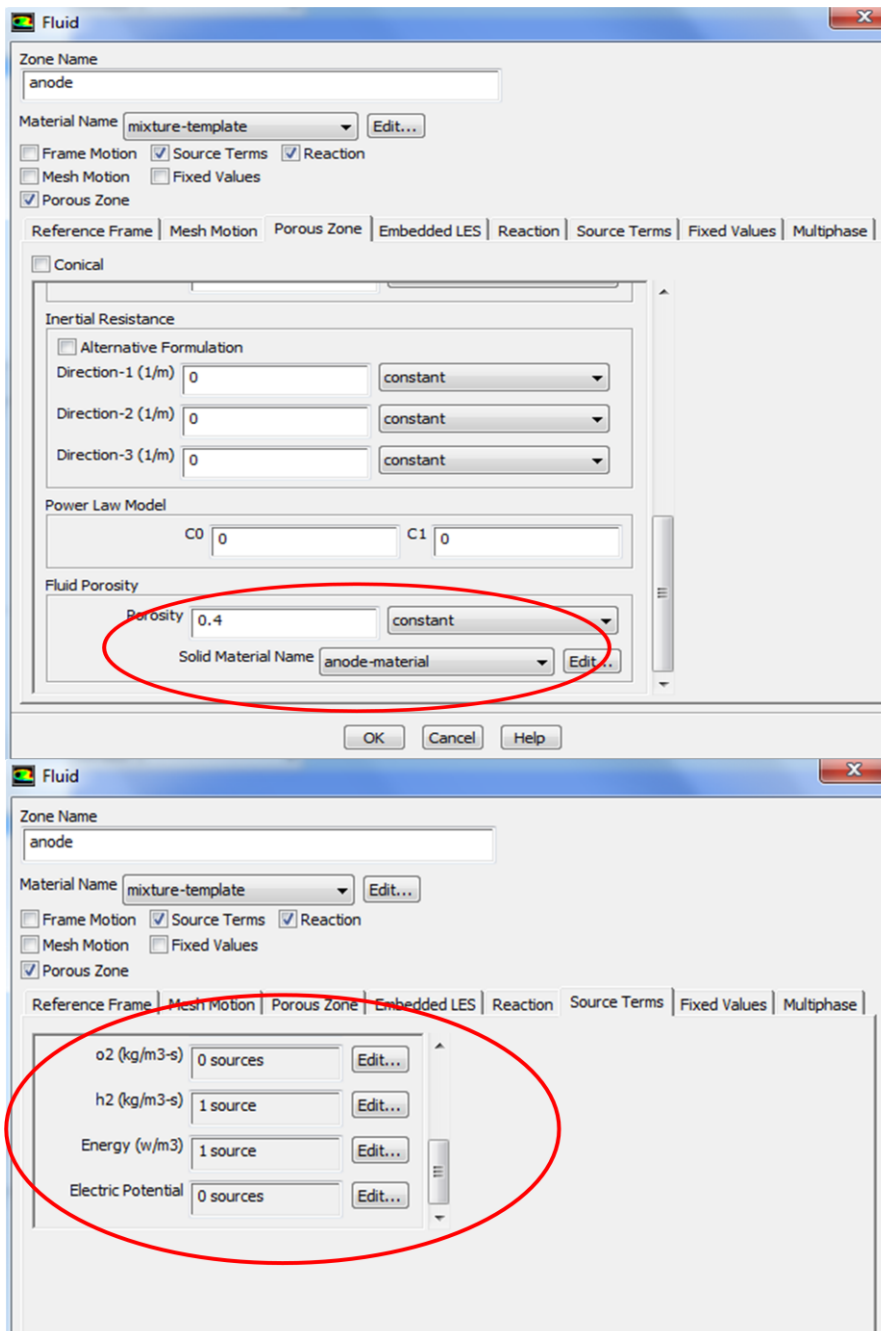
Figure A.10 A screen shot for defining the cell zone condition-2

- For the inlet boundary conditions enter the mass flow rate, inlet temperature of fluids and species mole fractions as described in the screen shot as shown in Figure A.11.
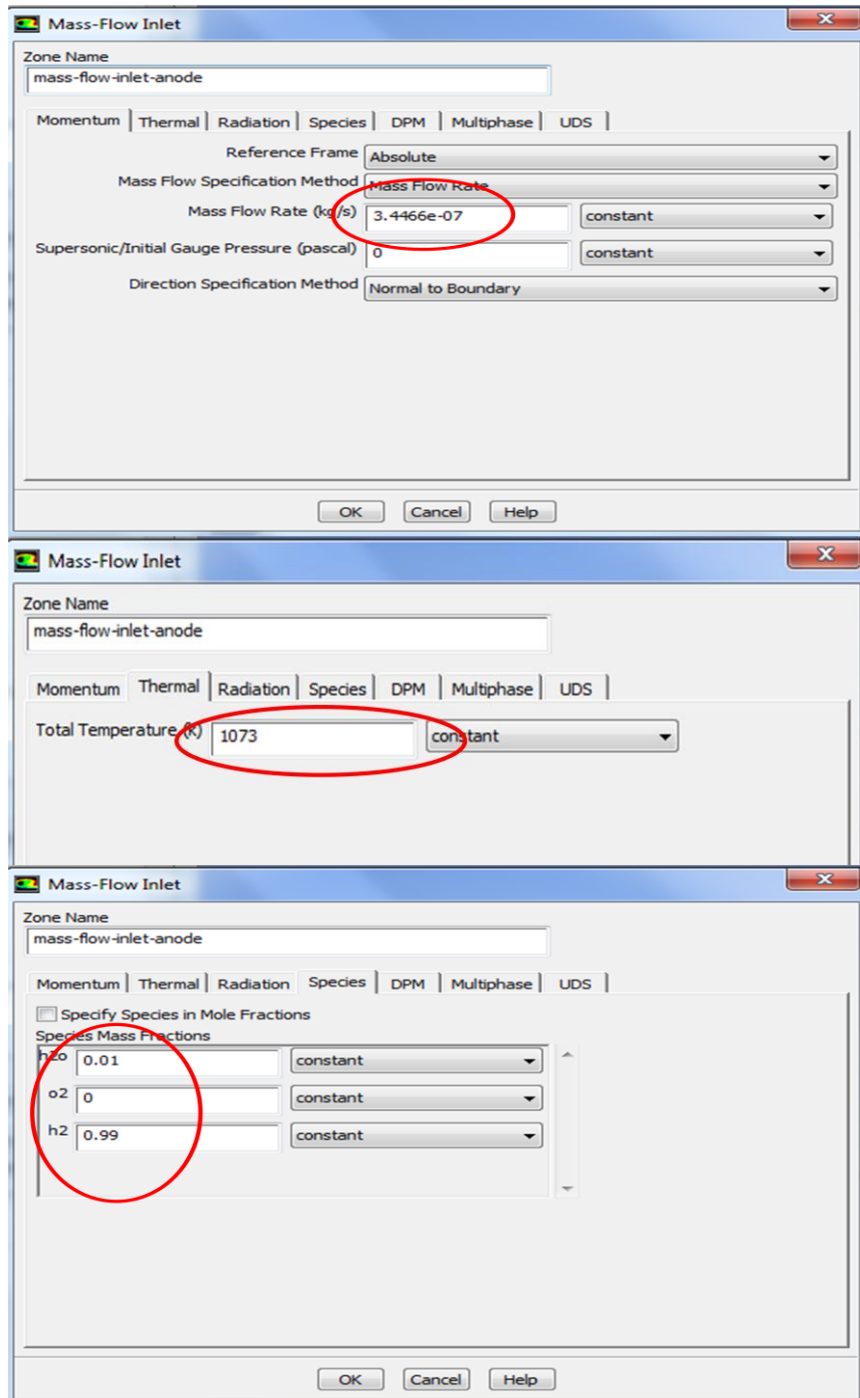
Figure A.11 A screen shot for defining the inlet boundary conditions

- There is no need to enter any data for the outlet boundaries.

- Determine the external wall thermal conditions and write the corresponding values as shown in Figure A.12.

Figure A.12 A screen shot for determining the external wall thermal conditions

- For the PEN anode/cathode-electrolyte surface, which is defined as a wall and wall-shadow surface, change the material name to the PEN material as defined in the materials step as shown in Figure A.13.
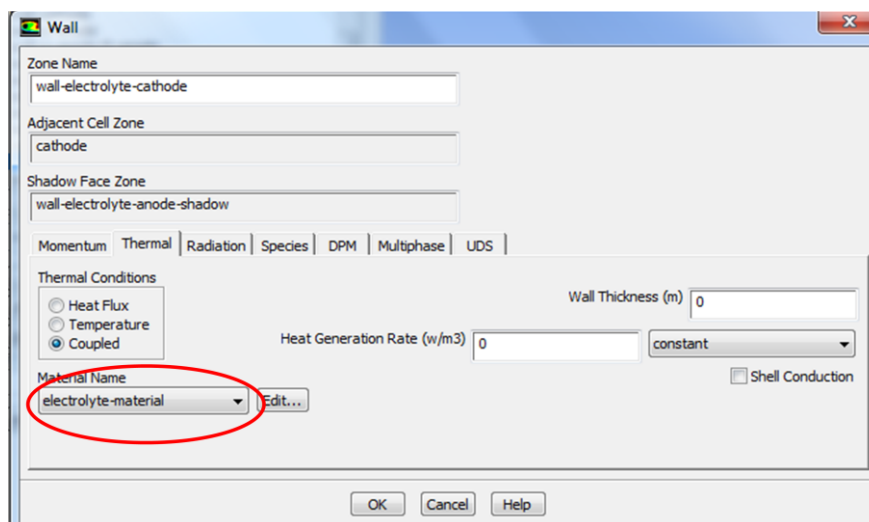
Figure A.13 A screen shot for defining the PEN wall boundary conditions

vii.   **Solution Methods**

- Select Pressure-Velocity Coupling Scheme as "Coupled" (Solution Methods → Pressure-Velocity Coupling → Scheme).

- For Spatial Discretization select Green-Gauss Node Based for Gradient, Second Order for Pressure and Second Order Upwind for all others (Solution Methods → Spatial Discretization).

viii.   **Solution Controls**

- Under Solution Controls Tab press "Advanced" (Solution Controls → Advanced). Change cycle types to F-Cycle and Termination to 0.001 as shown in Figure A.14.
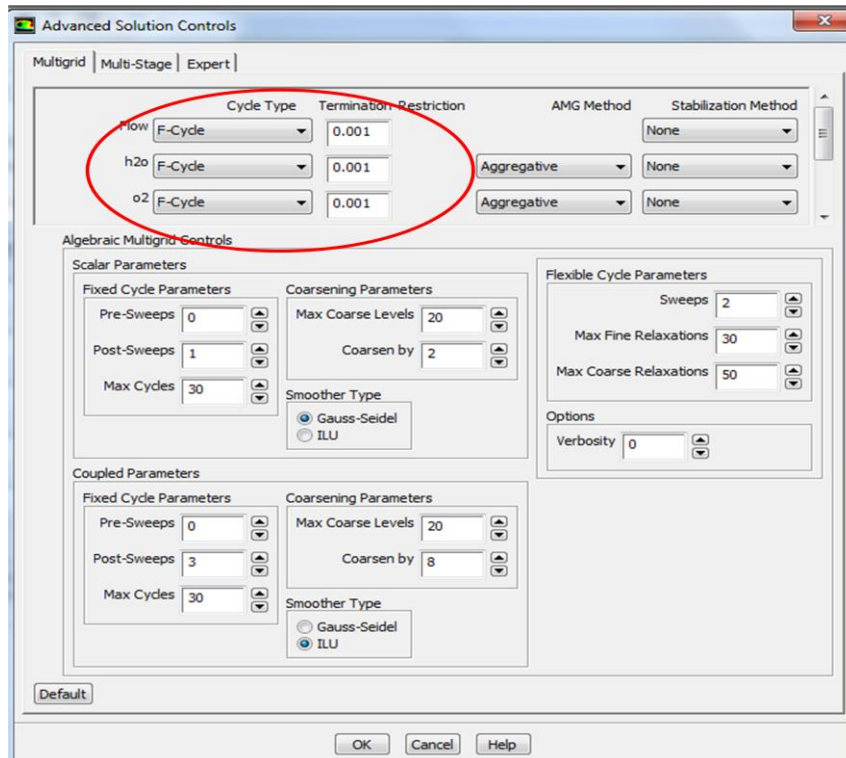
Figure A.14 A screen shot for defining the cycles

ix.   **Monitoring the Solution**

- Turn on the residual monitors and set the convergence criteria as 0.0001 for the continuity and x, y, z-velocities and 1e-08 for all others as shown in Figure A.15.

113
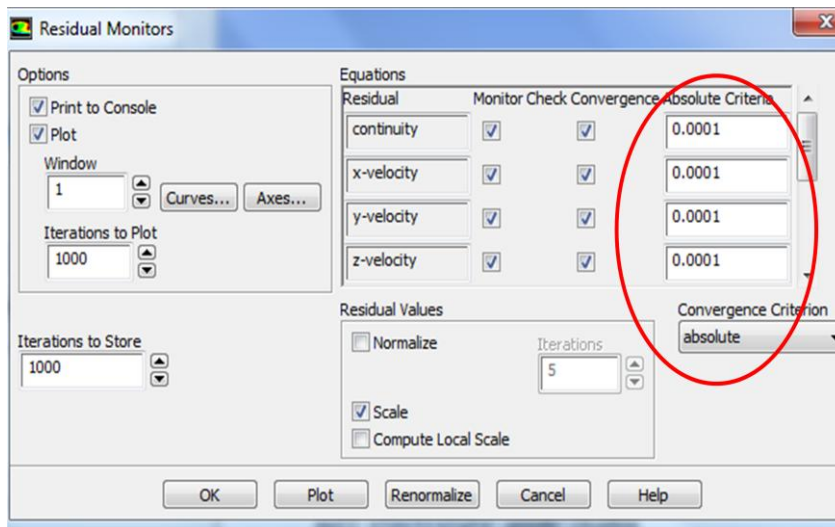
Figure A.15 A screen shot for determining the residuals

x. **Initializing the Solution**

- Initialize the flow field for all zones with the temperature set to "1073" (Solution → Solution Initialization → Initialize).